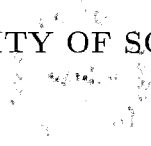# UNIVERSITY OF SOUTHAMPTON

FACULTY OF ENGINEERING, SCIENCE AND MATHEMATICS

School of Mathematics

Semiclassical Analysis of Vibroacoustic Systems

by

Barry Alan Welch

Thesis for the degree of Doctor of Philosophy

September 2005

UNIVERSITY OF SOUTHAMPTON

ABSTRACT

FACULTY OF ENGINEERING, SCIENCE AND MATHEMATICS

SCHOOL OF MATHEMATICS

Doctor of Philosophy

SEMICLASSICAL ANALYSIS OF VIBROACOUSTIC SYSTEMS

by Barry Alan Welch

In this thesis we present the development of semiclassical techniques and
apply these techniques with the aim of investigating elastic plate systems.
For the circular plate the eigenvalues and numerical error in comparison to
established results are calculated by an altered version of Gutzwiller's Trace
Formula. In addition this formula is applied to the square plate to find that
the free edge boundary condition produces less accurate results than other
cases.

The transfer matrix method of Bogomolny to calculate semiclassical phase
correction terms is followed for the free edge boundary condition and a phase
correction is found that improves in accuracy on the previously thought value
and includes contributions from lower order wavenumber and boundary cur-
vature terms.

A system with a diffractive centre is looked at by applying a quantum
scattering technique and we find that in the case of the elastic plate that a
diffraction coefficient cannot be determined without neglecting lower order
terms and so the effects of these terms are still in question. By looking at the
diffractive problems as a star graph model we found that the statistical prop-
erties follow those of the quantum billiard and that the model is applicable
to plate systems.

Contents

List of Figures

Acknowledgements

Without all of the people below I would never have survived the time it took me to complete this thesis so it is with no constraint that I wholeheartedly thank all of my family and friends.

Mum and Dad, Mike and Jas, My Grandparents, Tina and Courtney, Russ, Harvey and Smudge, Phil, Anton, Rob, Javi, Jimmy Angles, Mikey, Jack, 'The Procedure', James O, Andy H, Andy C, Ewan, CJ, Sarah, Rob Hobbit's and Phil Lennnon's, The funktacular music of Lo*chine and everyone else who has been part of my life up until now, I wouldn't be me without you all.

Chapter 1

Introduction

It can be seen that it is possible for classical systems to exhibit chaotic behavior where there is a sensitive dependence on initial conditions, such that a small discrepancy can develop into a large difference. Even the slightest error in initial conditions can then greatly effect the result of the calculation. These systems, difficult to describe in a classical framework, can instead be linked to a probabilistic quantum description by using *quantum chaos*, the study of the quantum wave-like behavior of classically chaotic systems. Describing the eigenvalue spectrum of a vibroacoustic system can be approached in several different ways, but it is the approach based upon semiclassical approximation that we are interested in.

It is the aim of this thesis to investigate the application of semiclassical methods to elastic plate problems. In doing so we hope to develop alterations to these methods that would allow them to be used for chaotic as well as integrable systems. By using these techniques to study numerical errors of semiclassical approximations we hope to identify relevant factors that when considered in greater detail will provide an improvement on current techniques. In order to do this, presenting the development of such tech-

niques becomes necessary, so that we understand their application to elastic systems.

In investigating these systems, it would seem that the *semiclassical limit*, where $\hbar \rightarrow 0$ would reduce the Schrödinger equation

$$-\frac{\hbar}{i}\frac{\partial \Psi}{\partial t} = -\frac{\hbar^2}{2m}\frac{\partial^2 \Psi}{dx^2} + V(x)\Psi \qquad (1.1)$$

to a classical form. However, setting Planck's constant to zero will result in a singular perturbation due to the divergence of this formula, and the quantum formulae will not match their classical counterparts. Instead, the semiclassical region is investigated with asymptotic approximations which have been developed in order to deal with this limit.

A *billiard* is defined as a dynamical system given by the motion of a particle with constant speed inside a compact domain with elastic reflections at the boundary. The boundary is assumed to consist of n smooth components, the geometrical and reflective properties of these components will determine the behavior of the billiard. Given certain boundary interactions *periodic orbits* can arise, where the particle returns to its initial position and momentum after a finite time. These orbits will play a large role in determining the physical behavior of the billiard. The analysis of billiards and the numerical accuracy involved has been looked at using a variety of methods [1] [2], and it is generally considered that semiclassical methods provide a good approximation to exact billiard spectra [3]. In this thesis we shall investigate the use of a variety of these methods in approximating eigenvalue spectra and their statistical behavior when applied to elastic plates, which can be approximated to billiards in simple cases.

Billiards are highly useful in the study of quantum chaos, their periodic orbits are an integral part of the trace formula which acts as a bridge between quantum chaos and classical dynamics due to the fact that the trace formula

itself arises from quantum mechanical path integral representations. By representing the level density of a system in terms of a Fourier decomposition of the oscillating density, solutions can be extracted. This oscillating density is dependent on several 'easily' measured properties of the system being studied, specifically the periodic orbits and associated factors. We shall also need to consider the effects of diffraction on systems we study, as this will allow us to observe how obstacles in the plate interact with the periodic orbits to affect the eigenvalues.

In our consideration of semiclassical methods the effects of boundaries will also become important, we hope to isolate elements of these boundary interactions that would then allow us to focus our attention on changes affecting the semiclassical methods we are looking at. To do this we shall look at the origin of the conditions studied in the hope of complementing our original aims. Having looked at the effects of boundaries we aim to include any vital factors into established semiclassical methods with the goal of increasing their accuracy in both simple cases and in those with more complicated boundaries.

It is also an aim to explore additional effects that are introduced into elastic systems by diffraction. Would it be possible to modify the solution methods we are investigating to take these effects into account and would these effects be restricted to the local area surrounding the diffractive center? We hope to look at this problem as part of our ongoing goal to model elastic plates using semiclassical techniques.

The problem of diffraction itself is very closely linked to the study of optics, where Keller's geometrical approach [4],[5] points us toward a solution. This has been extended to the context of the semiclassical trace formula [6] with the problem being approached by considering the quantum effects

produced in the region of any singularities, and combining this with the classical behavior away from the effects. In doing so, important semiclassical quantities such as the trace formula can be found. Much work has been done in this area of study, looking at many variations such as considering the diffractive effects of a wedge [7], point scatterer [8] [9] or magnetic flux line [9] [10] being just a few examples of what is a well studied problem in semiclassical analysis. Why is this? Well problems such as these are some of the most relevant due to the fact that the investigation of diffractive corrections can help explain important effects with reasonable accuracy.

As part of our our investigation into diffractive effects we also shall look at an alternative model for diffraction in star graphs, could we then utilise this to model the elastic plate? We aim to consider the statistical properties of such a model in order to determine its relevancy to such a case. The extra avenues of investigation that such a model could cover are widespread, and its application of quantum technology to the theory of frames and structures grants credence to our investigation of its use in elastic plate problems.

Looking at the wider picture, much work has been conducted in applying periodic orbit theory to acoustics. Söndergaard [11] uses the WKB-expansion to formulate an isotropic acoustic determinant formula which links well with the work of Gutzwiller. Quantum chaos can also be applied to find details on the fluctuations of eigenvalue spectra by studying the framework of random matrix theory. The experimental comparisons can found in the work of Bertlesen [12] and Schaadt [13] Such investigation is important, because the application of these ideas and others such as Vergini [14] allows for the eigenmodes of physical systems to 'easily' be approximated. These approximations are accurate enough to be able to be used in such ways as the placement of actuators on flat panel speakers and other vibroacoustic devices. This can

then be extended to high frequency analysis, which is more difficult when using more conventional methods. Practical work in the area has been undertaken with some success, Schaadt et al [15] look at the results of plates vibrated by ultrasound resonances. These experiments explore the validity of random matrix theory and the effect of mode mixing on such systems.

The outline of this thesis is as follows. In chapter 2 we look at the basic models of integrable systems, the principles of torus quantization and then relate this to the EBK solution methods. We then introduce the plate equation and the background to solution methods that we will be using in later chapters.

In chapter 3 we consider the use of the semiclassical trace formula in determining the eigenvalues of systems modeled using quantum billiards, verifying current results and then going on to use Poisson summation to investigate the same quantum billiards. We then investigate the calculation of a transfer matrix in chapter 4 in order to model the interactions with a free edge boundary and consider the accuracy of such an approach given various assumptions.

In chapter 5 we look at adding diffractive terms to quantum billiards and the effects that axisymmetric orbits have in comparison to EBK solution methods. We calculate an additional term for the semiclassical trace formula as looked at in chapter 3 that calculates eigenvalues introduced by an extra diffractive term. We then attempt to model this problem by calculating a diffraction coefficient to add into the trace formula by modeling the billiard as an annulus.

In chapter 6 we again look at diffractive systems, this time by means of star graphs. We compare models for a diffractive system governed by Schrödinger to one governed by the plate equation, investigating the vibra-

tions of a plate as introduced in chapter 2. The statistical properties of these two models are then calculated and contrasted. We then finish in chapter 7 by summarising the work of previous chapters and presenting our conclusions.

Chapter 2

Background

In this chapter we shall be covering a range of quantum chaos methods that can be applied to some basic elastic systems at a later point. These approaches will all modified or used for a more complicated problem in later chapters, so the development of these approaches will be presented here in order to put any changes to the basic problem, that of applying such methods to elastic systems, in context. Firstly, in order to establish the viability of using quantum mechanics to investigate classical problems, we need to establish the correspondence between the quantum and classical approaches to a similar problem [16]. First let us consider the Hamilton Jacobi equation for classical motion under the action $S(x, t)$

$$\frac{\partial S}{\partial t} + H(x, \nabla S) = 0 \tag{2.1}$$
$$x \in \mathbb{R}^3, t \in \mathbb{R}.$$

Where

$$H(x, p) = \frac{|p|^2}{2m} + U(x), \tag{2.2}$$

with p being the classical momentum under the displacement x, leading $H(x, p)$ to be equivalent to the sum of energies for the system. The solution

to this equation can then be linked to the classical trajectories as follows; let $S_0 = S$ at $t = 0$ and $p_0 = \nabla S_0(x_0)$, where $x_0 \in \mathbb{R}^3$. The classical trajectory that starts at x_0, p_0 is $x(t)$, $p(t)$, so by considering ∇H,

$$\dot{x} = \frac{p}{m} \tag{2.3}$$

$$\dot{p} = -\nabla U. \tag{2.4}$$

Then $\nabla S(t, x(t)) = p(t)$, so the "waves of action" that are defined by constant action will then sweep out the classical trajectories. If we consider a classical statistical state represented by an initial probability function ρ_c on $\mathbb{R}^3$, this would then evolve by flowing along the trajectories. This is described by the equation of continuity

$$\frac{\partial \rho_c}{\partial t} + \underline{\nabla}. \left(\rho_c \frac{\nabla S}{m} \right) = 0. \tag{2.5}$$

Hence (2.1) and (2.5) can be thought of as a way to describe the propagation of a probability density ρ via classical trajectories with initial momenta ∇S_0. Now to examine the quantum case, consider a solution, $\Psi(t, x)$ of Schrödinger's equation

$$\frac{\hbar}{i} \frac{\partial \Psi}{\partial t} = \frac{\hbar^2}{2m} \nabla^2 \Psi + U(x) \Psi \tag{2.6}$$

If we write $\Psi = \sqrt{\rho_q} \exp\left(i \frac{S}{\hbar} \right)$ with ρ a probability measure on $\mathbb{R}^3$, from (2.6) we can write

$$\frac{\hbar^2}{2m} \nabla^2 \sqrt{\rho_q} + \frac{\partial S}{\partial t} + \frac{1}{2m} (\nabla S)^2 + U = 0 \tag{2.7}$$

$$\frac{\partial \rho_q}{\partial t} + \underline{\nabla}. \left[\rho_q \frac{\nabla S}{m} \right] = 0. \tag{2.8}$$

As $\hbar \to 0$ it appears that (2.7) and (2.8) tend to (2.1) and (2.5), however equation (2.7) is non-linear and involves $\hbar$ in the highest order terms, so such a conclusion cannot be immediately drawn. However, given such a similarity of structure between the Hamilton-Jacobi and Schrödinger equations it

2

certainly strongly suggests a link as $\hbar \to 0$, and in the next section we shall briefly examine this and see how it leads to the WKB approximation.

2.1 Integrable Systems

An integrable system is defined as one with N constants of motion which are all independent of each other and in involution, allowing an exact solution to be found. In these cases the solutions are positioned on an N-dimensional torus which is determined by the system. In this section the development of semiclassical quantum mechanics is presented in order to understand the methods utilized later in this work.

2.1.1 The WKB Approximation

We have just seen that there was a strong suggestion of a link between the classical physics approach of Hamilton-Jacobi to that of Schrödinger's quantum mechanical approach. Considering that Schrödinger was influenced by the HJ equation in the development of his work [17] this is of little surprise. Take the one-dimensional Schrödinger equation

$$-\frac{\hbar^2}{2m}\frac{d^2\psi}{dx^2} + V(x)\psi = E\psi \qquad (2.9)$$

where the potential energy function $V(x)$ has the condition $V(0) = 0$, with $x = 0$ a global minimum value of V. A classical particle moving with energy E will move with periodic motion between two turning points which can be obtained [18] by solving the case where $V(x) = E$. Using the wave number k

$$k(x) = \sqrt{\frac{2m}{\hbar^2}\left(E - V(x)\right)} \qquad (2.10)$$

3

allows (2.9) to be written as

$$\frac{d^2\psi}{dx^2} + k^2(x)\psi = 0. \tag{2.11}$$

Solving this gives a solution for ψ

$$\psi(x) = A(x)\exp\left(\frac{i}{\hbar}S(x)\right) \tag{2.12}$$

where A and S are real functions of x. Substituting (2.12) into (2.9) and separating the real and imaginary parts gives us two equations which are equivalent to the original Scrödinger equation,

$$A\left(\frac{dS}{dx}\right)^2 = Ap^2 + \hbar^2\frac{d^2A}{dx^2} \tag{2.13}$$

$$\frac{d^2S}{dx^2}A + 2\frac{dS}{dx}\frac{dA}{dx} = 0, \tag{2.14}$$

using the value for momentum $p(x) = \hbar k(x)$. Up until now this has just been standard manipulation of (2.9), to proceed to the semiclassical approximation for ψ we neglect the term $\hbar^2\frac{d^2A}{dx^2}$ in this approximation, it is small enough to not be considered. From there, (2.13) and (2.14) are integrated,

$$S(x) = \int_{x_0}^{x} p(x)\,dx \tag{2.15}$$

$$A(x) = \frac{\psi_0}{\sqrt{|p(x)|}} \tag{2.16}$$

with $S(x)$ corresponding to the classical action and ψ_0 being the constant of integration for that case. Inserting these values into (2.12) gives

$$\psi(x) = \frac{\psi_0}{\sqrt{|p(x)|}}\exp\left(\frac{i}{\hbar}\int_{x_0}^{x} p(x)\,dx\right). \tag{2.17}$$

This is the WKB approximation for ψ in one dimension, valid for most cases, except in particular for $p(x) = 0$ which corresponds to the original classical turning points. From the information derived in the one dimensional case,

4
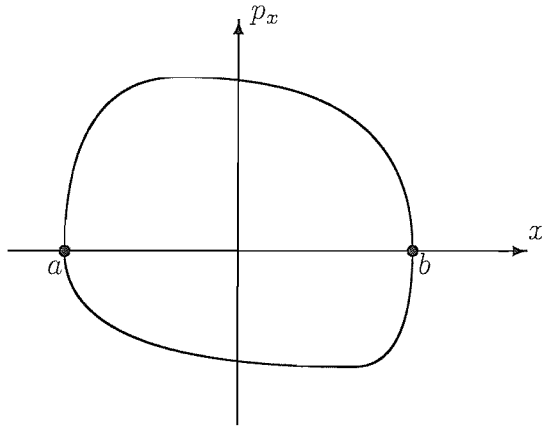
Figure 2.1: Phase branches of momentum meeting at turning points a and b

the classical action S (2.15) which is increasing both with increasing and decreasing x, is hence doubled valued, with the values equal at the classical turning points a and b. This is also true of the derivative of S, allowing the WKB approximation to be written in the form

$$
\psi(x) = \frac{1}{\sqrt{p(x)}} \left(A \exp\left[\frac{i}{\hbar} \int_x^{x_{max}} p(x')\, dx' \right] \right.
$$
$$
\left. + B \exp\left[-\frac{i}{\hbar} \int_x^{x_{max}} p(x')\, dx' \right] \right). \tag{2.18}
$$

This multi-valued nature can be thought of by considering two branches of momentum $p_1(x)$ and $p_2(x)$ as shown in figure 2.1. These branches correspond to two functions, both of action, which vary with x. The points a and b denote the positions at which these branches are equal, creating a closed curve in phase space; these points mark the turning points of the system and hence the points at which any phase changes will occur. At these turning points the wavefunction has to remain single valued and hence also single

5

valued after a complete cycle, we can describe the semiclassical wavefunction over this closed curve as

$$\psi(x, E) = A \exp\left(\frac{i}{\hbar} S(x, E)\right)$$

$$= \frac{1}{\sqrt{2\pi\hbar}} \left|\frac{\partial^2 S(x, E)}{\partial E \partial x}\right|^{\frac{1}{2}} \exp\left(\frac{i}{\hbar} S(x, E)\right). \qquad (2.19)$$

Over one cycle, the action S will have changed by an amount given by ΔS,, meaning that a phase change of $\frac{\Delta S}{\hbar}$ will have been introduced. There will be additional phase changes introduced at the turning points a and b, where the momentum changes sign. Due to this sign change, and the fact that $\exp(i\pi) = -1$, we can then consider each turning point as introducing an extra $-\frac{\pi}{2}$ phase change. Collecting these factors and keeping in mind the fact that the wavefunction has to remain single valued after a cycle give us, for a value n related to the number of cycles,

$$\frac{\Delta S}{\hbar} - 2\frac{\pi}{2} = 2n\pi. \qquad (2.20)$$

he total phase change over the full cycle is

$$\Delta S = 2 \int_a^b p(x)\,dx, \qquad (2.21)$$

which taking (2.20) in consideration, can be written as

$$\oint p\,dx = \left(n + \frac{2}{4}\right) 2\pi\hbar. \qquad (2.22)$$

Generalizing this case to one without a specified number of turning points, replace the factor of two inside the brackets with an integer constant μ to give in general

$$\oint p\,dx = \left(n + \frac{\mu}{4}\right) 2\pi\hbar. \qquad (2.23)$$

For a given energy E the action S can be written as

$$S = \oint p\,dx = 2\pi\frac{E}{\omega} \qquad (2.24)$$

6

Equating (2.23) and (2.24) gives the energy quantization condition

$$E_n = \hbar\omega \left(n + \frac{\mu}{4}\right).$$ (2.25)

For the corresponding 3D problem this will have a slightly altered value because of the change in angular momentum conditions, this is gone into in greater detail in [19]. While we shall not be considering that case we shall progress to systems with more degrees of freedom.

2.1.2 Torus Quantization and the EBK Method

So far only the one-dimensional case has been considered, in reality systems with more degrees of freedom are investigated and the method is extended as follows. Instead of the trajectories existing in two dimensional phase space as in figure 2.1, when an integrable system with d degrees of freedom is investigated, its trajectories will exist on the surface of a d-dimensional torus that exists in $2d$-dimensional phase space. This is seen in the one dimensional case where the trajectories lie on a $d = 1$ dimensional path within a $2d = 2$ dimensional phase space and in the $d = 2$ case by the phase torus in figure 2.2. As in (2.23) for the one dimensional case, for d dimensions, every possible orbit will give a quantization condition

$$\oint p\, dx = \left(n_i + \frac{\mu_i}{4}\right) 2\pi\hbar, \qquad i = 1, \ldots, d.$$ (2.26)

It is now convenient to transform to the "action-angle" variables I and ϕ. This is done by defining, for a given E

$$\oint I\, d\phi = 2\pi I = \oint p\, dx$$ (2.27)

such that

$$I = \frac{1}{\pi} \int_{x_1}^{x_2} \sqrt{2m(E - V(x')))}\, dx'.$$ (2.28)

7
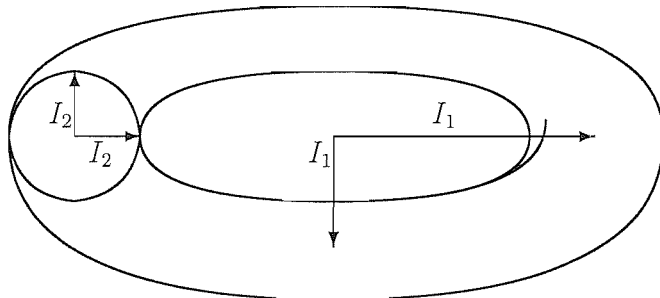
Figure 2.2: Torus quantization in terms of variables I_1 and I_2

Generalisation of this equation for M independent conditions can be seen in [20] and allows more complicated topologies to be studied. We are considering the one dimensional wavefunction (2.19) and transform to the action-angle variables, generalizing to N dimensions. This is done by considering

$$\psi(\mathbf{x}, \mathbf{I}) = \frac{1}{(2\pi\hbar)^{\frac{N}{2}}} \left| \frac{\partial^2 S(\mathbf{x}, \mathbf{I})}{\partial I_j \partial x_j} \right|^{\frac{1}{2}} \exp\left(\frac{i}{\hbar} S(\mathbf{x}, \mathbf{I}) \right). \tag{2.29}$$

In a similar fashion to the one-dimensional case, in order to preserve the single valued nature of the wavefunction at the turning points, there must exist N quantization conditions, these are given by

$$I_i = \frac{1}{2\pi} \oint \mathbf{p} \cdot d\mathbf{x} = \left(n_i + \frac{\mu_i}{4} \right) \hbar, \qquad i = 1, \dots, N. \tag{2.30}$$

By manipulating these conditions, we could then use them to determine the eigenvalues of the given system. These eigenvalues will be affected by changes in conditions at the boundary of the system, which shall be considered in a later section. The EBK quantization [21] was an important factor in the development of the trace formula of Berry and Tabor [22], showing that if the system could have its eigenvalues described by this quantization, then a

8

trace formula could be derived that depended on the classical period orbits. Will shall examine and use a similar approach in a later section.

While the systems looked at so far have all been completely integrable, it must be noted that these are by no means the only class of billiards. Systems such as the Sinai and stadium billiards do not have trajectories that can have their phase space constrained by invariant tori. As such, EBK quantization is not applicable to such systems and there are not enough constants of motion present in order to determine a quantization solution as in the case of integrable systems. We shall not be investigating these systems, but it should be noted that the processes studied that will be applied to integrable systems could in theory also be applied to chaotic systems given appropriate simplifications.

When the transition to chaotic systems is made we need take in account the exponential increase in the number of periodic orbits that need to be considered as the lengths taken increase. To analyse a quantum spectrum with respect to its period orbits was a relatively simple procedure, however the reverse is not the case. These extra orbits now affecting the chaotic system have meant additional techniques needed to be developed as the torus model will collapse. Using the Gutzwiller trace formula as a substitute for the EBK formula in calculating energy levels from periodic orbits is hence then only valid in integrable cases. From here we shall go on to look at the semiclassical trace formula and its uses in such cases and it is the additional solution methods available to integrable systems that we shall be using to verify the accuracy of the alternative approaches tackled.

2.2 Background to Quantum Mechanical Solution Approaches

In the process on looking at the behavior of the circular plate, there are a few main techniques that will be used in chapter 3 to investigate the spectra of the relevant systems. All three of these methods share a similar background in terms of the development of the underlying principles, though each has it's own emphasis on a particular section of this background. The trace formula has long been an important tool of semiclassical analysis, and while there are several alternatives, we shall be looking at and using the Gutzwiller trace formula; its applicability to simple systems makes it perfect for the modifications that we shall attempt to make. The development of this method is presented in section 2.2.1, an alternative route to a trace formula comes from the Poisson summation of the spectral density written in terms of the EBK quantization, a brief coverage of which is included in section 2.2.2.

2.2.1 Trace Formula

With non-integrable systems unable to be confined to multidimensional tori, semiclassical quantization is no longer possible and an alternative route to describing their behavior needed to be derived. In this section we shall present Gutzwiller's approach to a trace formula that is applicable to integrable and non-integrable systems.

Starting with the quantum mechanical propagator [23] we can now re-derive the relations which comprise the trace formula. In the situations we study we shall not be considering the effects of caustics, areas of singular behavior, in this thesis but their effects would need to be included in alternative

cases. The propagator K

$$K(\mathbf{r}, \mathbf{r}', t) \;=\; \left(\frac{1}{2\pi i\hbar}\right) \sqrt{\left| -\frac{\partial^2 R_0}{\partial \mathbf{r} \partial \mathbf{r}'} \right|} e^{\frac{i}{\hbar} R_0(\mathbf{r}, \mathbf{r}', t)} \qquad (2.31)$$

where $R_0(\mathbf{r}, \mathbf{r}', t)$ is Hamilton's principal function, is Fourier transformed to obtain a Green function representation.

$$G(\mathbf{r}, \mathbf{r}', E) \;=\; -\frac{i}{\hbar} \int_0^\infty dt K(\mathbf{r}, \mathbf{r}', t) e^{\left(\frac{i}{\hbar} Et\right)}. \qquad (2.32)$$

The next step was to use path integrals to calculate the propagator. In doing this, the right hand side of (2.32) will become dependent solely on classical terms, barring a factor of $\hbar$. The reasoning behind this is based on the fact that in the course of calculating the propagator, the stationary phase method is used, which only permits the survival of classically permitted paths. This fact is one of the most important tenets of semiclassical mechanics, that the quantum behavior can be related so closely to its classical counterpart. Armed with this knowledge we now have a semiclassical approximation for the Green function which can then also be evaluated using the stationary phase method to give

$$G(\mathbf{r}, \mathbf{r}', E) \;=\; -\frac{i}{\hbar} \left(\frac{1}{2\pi i\hbar}\right)^{\frac{d-1}{2}} \sum_r \sqrt{|\Delta_{BA,r}|} e^{\frac{i}{\hbar} S_r\left(\mathbf{r}, \mathbf{r}', E\right) - i\frac{v_r \pi}{2}}. \quad (2.33)$$

where $\Delta_{BA,r}$ is a matrix that depends on derivatives of the action S with respect to energy and path trajectories.

Recall that we are looking to find a representation of the single particle level density, which measures the number of eigenvalues per unit interval and hence contains information about the quantum irregularities of the system's quantum spectrum. This can be thought of as a smooth function which

11

represents the average behavior, and an additional function which oscillates about this average. This can be written as

$$\rho(E) = \tilde{\rho}(E) + \delta\rho(E). \tag{2.34}$$

The functions $\tilde{\rho}(E)$ and $\delta\rho(E)$ can then be determined separately. Often it is convenient to work in terms of the wavefunction instead of the energy, this is enabled by the relation

$$k = \frac{\sqrt{2mE}}{\hbar}. \tag{2.35}$$

The smooth function $\tilde{\rho}(E)$ is determined by the Thomas-Fermi level density. This is taken from the leading terms of a semiclassical expansion for the smooth part of the quantum density of states in powers of $\hbar$. As in the semiclassical limit $\hbar \to 0$, in simple cases only the first term need be considered. For more complicated cases or where more accuracy is required, this expansion can be taken to several terms to provide a more detailed estimate. For non-integrable cases however, quantization is not apparent and the technique cannot currently be applied. In these cases the smooth part of the level density can be derived from the Weyl Expansion. In billiards with smooth boundaries that are simply connected and smooth, such as those we shall consider, this is given by

$$\tilde{\rho} = \frac{k}{2\pi} \left(\frac{2m}{\hbar^2} \right) \mathcal{A} + \frac{1}{4\pi}\mathcal{L}, \tag{2.36}$$

where $\mathcal{A}$ is the area of the billiard and $\mathcal{L}$ the perimeter length.

Expressing the density of states in terms of the Green function as

$$\rho(E) = -\frac{1}{\pi}\text{Im}\left(Tr(G)\right) \tag{2.37}$$

requires that to calculate the oscillating part of the level density $\delta\rho(E)$ which is a sub-component of $\rho(E)$, we first need to calculate 2.37 by taking the trace

12

of the semiclassical approximation to the Green function

$$tr(G) \;=\; \int G(\mathbf{r}, \mathbf{r}', E)\, d\mathbf{r}. \qquad (2.38)$$

If we substitute the semiclassical form into the equation and manipulate the matrix $\Delta_{BA,r}$ by expanding its individual terms [24] we obtain for this trace,

$$tr(G) \;=\; -\frac{i}{\hbar} \sum_r \frac{(T_p)_r}{|M_r - I|}\, e^{\frac{i}{\hbar} S_r(E) - i\frac{\mu\pi}{2}}. \qquad (2.39)$$

In this equation, M_r is the *mondronomy matrix*, which relates the deviations between trajectory sets under a small change of initial conditions. The trace of this matrix will determine the stability of the system. In billiard systems the overall matrix is found by multiplying the matrices for each boundary interaction, this will mean that a typical billiard is well suited to this approach because of the fact that its trajectories are composed of straight lines and reflections.

To study the eigenvalues we then consider the density of states (2.37) expressed in terms of the semiclassical Green function. As the stationary phase method was used to derive the trace formula, this will be restricted to the classical paths as stated earlier. In billiard systems this will mean that the eigenvalue behavior can be extracted from the periodic orbits to give

$$\delta\rho(E) \;=\; \frac{1}{\hbar\pi} \sum_{po} \frac{T_{ppo}}{\sqrt{\left|\det\left(\tilde{M}_{po} - I\right)\right|}} \cos\left(\frac{1}{\hbar} S_{po} - \sigma_{po}\frac{\pi}{2}\right). \qquad (2.40)$$

which is Gutzwiller's trace formula for a billiard system of isolated orbits [25], [26]. This equation can then be altered to take into account the specific billiard that it is applied to by altering the conditions imposed by the various

terms of the equation. For the cases that involved billiards with additional symmetries this will then include an extra factor to account for this, but otherwise the solution will remain the same.

2.2.2 Poisson Summation

For integrable systems, there is another route to obtaining a trace formula. Berry and Tabor [22], [27] have shown that this will always be a valid approach due to the integrability. This approach begins with the EBK quantization condition, which in the case of the free plate is reached by starting from the exact equation to describe the behavior of the free plate, we substitute the asymptotic expansions for the Bessel functions and take the leading order contributions as $x \to \infty$ to give

$$-\sin\left(x - \frac{m\pi}{2} - \frac{\pi}{4}\right) - \cos\left(x - \frac{m\pi}{2} - \frac{\pi}{4}\right) = 0$$
$$\tan\left(x - \frac{m\pi}{2} - \frac{\pi}{4}\right) = -1 \qquad (2.41)$$

and hence

$$x = \left(n + \frac{m}{2}\right)\pi. \qquad (2.42)$$

Taking the eigenvalues of the circular disk from previous calculation as

$$k_{n_1,n_2} = \left(n_1 + \frac{n_2}{2}\right) \qquad (2.43)$$

We know that the spectral density can be written as a sum over delta functions where

$$\delta(k - k_{n_1,n_2}) = \lim_{t \to 0} \frac{1}{2\sqrt{\pi t}} e^{\left(k - \pi\left(k_{n_1,n_2}\right)\right)^2} \qquad (2.44)$$

and so we can write

$$\rho(k) = \sum_{n_1=0}^{\infty} \sum_{n_2=0} \lim_{t \to 0} \frac{1}{2\sqrt{\pi t}} e^{\left(k - \pi\left(n_1 + \frac{n_2}{2}\right)\right)^2}. \qquad (2.45)$$

14

From this we are looking to obtain the semiclassical form of the spectral density. In order to achieve this we must first of all apply Poisson summation in order to convert to a double integral. The rule of Poisson summation for a single sum is written as

$$\sum_{n=0}^{\infty} f(n) = \sum_{M=-\infty}^{\infty} \int_0^{\infty} f(n) e^{2\pi i M n}\, dn + \frac{1}{2} f(0). \qquad (2.46)$$

In the case we are considering we have to deal with a double sum and hence are required to apply this rule twice to give

$$\begin{aligned}
\rho(E) = & \sum_{M_1=-\infty}^{\infty} \sum_{M_2=-\infty}^{\infty} \int_0^{\infty} dn_1 \int_0^{\infty} dn_2 \delta\left(E - E(n_1, n_2)\right) e^{2\pi i (M_1 n_1 + M_2 n_2)} \\
& + \frac{1}{2} \sum_{M_1=-\infty}^{\infty} \int_0^{\infty} dn_1 \delta\left(E - E(n_1, 0)\right) e^{2\pi i (M_1 n_1)} \\
& + \frac{1}{2} \sum_{M_2=-\infty}^{\infty} \int_0^{\infty} dn_2 \delta\left(E - E(0, n_2)\right) e^{2\pi i (M_2 n_2)} \\
& + \frac{1}{4} \delta(E). \qquad (2.47)
\end{aligned}$$

It is this form of the density of states we we can then use in conjunction with the appropriate EBK quantization condition to derive a trace formula. This will vary depending on the condition used; the system we are going to investigate in a later chapter will pick up from where (2.47) stops. These approaches to solving billiard problems are what we shall be attempting to apply to plate problems by looking at elastic systems. Poisson summation is not restricted to just periodic orbit theory; it has also been used in the study of magnetic properties in metals [28] and this approach returns the same trace formula, highlighting the versatility of such an approach and supporting our attempt to apply this to elastic problems and as such will now outline the properties of the main problem we shall be considering.

2.3 Boundary Effects and the Elastic Plate

As we wrote in the introduction, it is our aim to examine the behavior of an elastic plate. By following a free energy minimisation method an equation of equilibrium for bending by external forces [29] can be derived

$$DV^4\xi - P = 0, \tag{2.48}$$

where D is the flexural rigidity of the plate, P is the external forcing term and ξ is a function of the displacement of the plate surface. To describe free oscillations in this plate the above equation can be manipulated to give a simplified version [30] and hence be used in modeling the transverse deflections arising in two dimensional plates under vibration. We are aware that in this situation that there is also the possibility of wave coupling at the free boundary that could have additional effects but shall not be investigating this. So consider a plate with the shear and rotation effects neglected. If a force is then applied to this plate [31], [32], the transverse displacement is given by

$$DV^4w = \rho\frac{\partial^2 w}{dt^2}, \tag{2.49}$$

with w a arbitrary wave solution of this equation and D denoting the flexural rigidity

$$D = \frac{Eh^3}{12(1 - \nu^2)}. \tag{2.50}$$

This is composed of several physical constants, E is Young's modulus, h is the thickness of the plate and ν is Poisson's ratio. On the assumption that we are only considering free vibrations of this plate, we can express the transverse motion as

$$w = \psi\cos(\omega t). \tag{2.51}$$

16

In this representation, ω is the frequency of vibration, and ψ a function that depends only on position within the plate. Now substitute (2.51) into (2.49) to yield a function in which the displacements can be modeled by the plate equation,

$$\nabla^4 \psi(\mathbf{r}) - k^4 \psi(\mathbf{r}) = 0. \tag{2.52}$$

This equation can be factorized into

$$(\nabla^2 + k^2)(\nabla^2 - k^2)\psi = 0 \tag{2.53}$$

Which can then be written in terms of two separate equations

$$\nabla^2 \psi(\mathbf{r}) + k^2 \psi(\mathbf{r}) = 0 \tag{2.54}$$
$$\nabla^2 \psi(\mathbf{r}) - k^2 \psi(\mathbf{r}) = 0, \tag{2.55}$$

producing waves that are both exponentially increasing and decreasing, and so any solution to (2.52) can then be written as a superposition of solutions to these two equations. This allows us to consider wavefunction solutions written as this superposition of terms and hence simplifying calculations.

2.3.1 Semiclassical Treatment of Boundary Conditions

A main issue in our investigation will be how we can include and verify the effects that interactions with the boundary of the elastic plate will have on the eigenvalues of the system and how we could incorporate this into any solution approaches that we use.

There are three sets of boundary conditions that will be considered for the problems investigated in this thesis. In order to define the solutions of the cases that will be studied, these conditions will be written [33] as follows. In each case, n denotes wave motion normal to the disk, and l motion along

the edge. For a clamped edge, all wave motion at the boundary is restricted to zero, giving the conditions

$$w_n = 0, \tag{2.56}$$

$$\frac{\partial w_n}{\partial r} = 0. \tag{2.57}$$

A supported edge has incident wave motion reduced to zero, with an extra condition placed on the on the surface waves that is dependent on the curvature of the plate and the Poisson ratio σ,

$$w_n = 0, \tag{2.58}$$

$$\frac{\partial^2 w_n}{\partial r^2} + \sigma \left(\frac{1}{a} \frac{\partial w_n}{\partial r} - \frac{n^2}{a^2} w_n \right) = 0. \tag{2.59}$$

In the free case, motion, both incident and along the boundary, is restricted by a pair of conditions dependent on all factors of the system

$$\frac{\partial}{\partial r} \left(\frac{\partial^2 w_n}{\partial r^2} + \frac{1}{r} \frac{\partial w_n}{\partial r} \right) - \frac{n^2}{a^2} \left((2-\sigma) \frac{\partial w_n}{\partial r} - \frac{3-\sigma}{a} w_n \right) = 0, \tag{2.60}$$

$$\frac{\partial^2 w_n}{\partial r^2} + \sigma \left(\frac{1}{a} \frac{\partial w_n}{\partial r} - \frac{n^2}{a^2} w_n \right) = 0. \tag{2.61}$$

These conditions can then be used in further calculations to determine solutions to the relevant problems. However, by considering ray dynamics of these systems, impacts with the boundary will have an effect upon the wave. This will add an additional phase to the wave which will vary depending on the condition at the boundary. In the high frequency limit, these boundary interactions can be thought of as behaving the same way as an interaction with a straight boundary. The only permitted solutions for this disk with a wave vector component along the boundary which will be written as p and a component q normal to the disk boundary are written as follows (taking the case when the wavenumber is greater than the modulus of the boundary wave as will be this case in systems studied in this chapter)

$$\psi(x, y) = e^{ipx} \left(e^{-iqy} + A e^{iqy} + B e^{-Qy} \right), \tag{2.62}$$

18
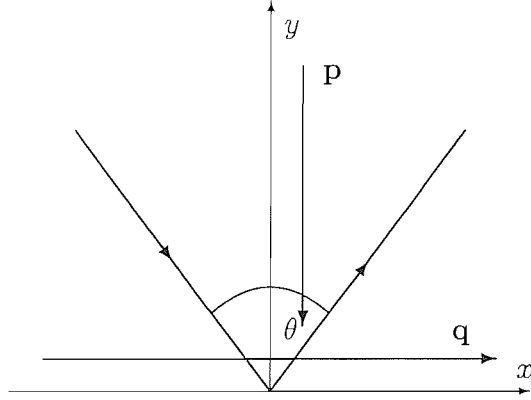
Figure 2.3: Boundary interactions with a curved edge approximated to a straight line.

using

$$p = k\cos\theta, \qquad (2.63)$$

$$q = k\sin\theta, \qquad (2.64)$$

$$Q = \sqrt{k^2 + p^2}. \qquad (2.65)$$

By solving this equation using the appropriate boundary conditions, the values of A and B can be found and the phase angle terms used previously can be calculated. In the clamped case use the boundary conditions (2.56) and (2.57) to obtain

$$\psi(0) = 1 + A - B = 0,$$
$$\frac{\partial\psi}{\partial y}(0) = -iq + Aiq - BQ = 0. \qquad (2.66)$$

Solving for A and B gives

$$A = \frac{iq - Q}{iq + Q}, \qquad (2.67)$$

$$B = -(A + 1). \qquad (2.68)$$

By letting $A = -e^{i\phi_c(\theta)}$, and substituting the values of q and Q it can then be seen that

$$\frac{1 + e^{i\phi_c}}{1 - e^{i\phi_c}} = \frac{\sqrt{1 + \cos^2\theta}}{i\sin\theta} \tag{2.69}$$

and so

$$-\tanh\left(\frac{i\phi_c}{2}\right) = \frac{i\sin\theta}{\sqrt{1 + \cos^2\theta}}, \tag{2.70}$$

with

$$\phi_c(\theta) = -2\arctan\left[\frac{\sin\theta}{\sqrt{1 + \cos^2\theta}}\right]. \tag{2.71}$$

$$\tag{2.72}$$

Solving in the same fashion for the simply supported and free boundary conditions give the relevant phases

$$\phi_{ss} = 0, \tag{2.73}$$

$$\phi_f = -2\arctan\left[\frac{\sin\theta}{\sqrt{1 + \cos^2\theta}}\left(\frac{1 + (1-\nu)\cos^2\theta}{1 - (1-\nu)\cos^2\theta}\right)\right]. \tag{2.74}$$

Boundary effects detailed in this section can also be thought of in terms of a boundary integral approach. By studying the effect on the plate equation on the boundary we can extract a transfer matrix from which a phase term that can be found. The method is demonstrated for the clamped edge boundary condition in the following section so that we can apply this to a more complex case in a later chapter.

These additional terms give us phase factors can be inserted into the semiclassical trace formula to model the extra effects contributed by the boundary, we shall be looking at these in a later chapter as a comparison to alternative results. The phases are an important factor in the difference between the quantum mechanical and elastic plate problems and so utilising

them is an essential step in our investigation into the link between these two areas. In order to be able to do this including additional terms we will look at deriving these terms from an alternative method.

2.3.2 Boundary Integrals

In this section we shall begin by establishing the coordinate system that the boundary conditions are defined in and verifying the accuracy of the free edge boundary condition as in Love [32] before moving on to calculations that involve it. After that we shall study the process that determines the clamped edge phase term by means of investigating the transfer matrix using the boundary integral equation method, hereafter referred to as BIEM.

We begin by presenting the method used in [30] to calculate the transfer matrix and subsequently extract a value for the phase angle on interaction with the boundary for these specific conditions. For a membrane system the Helmholtz equation can be solved using

$$u(x) = \int_S \frac{\partial}{\partial n_y} H_0(k|x - y|)\nu(y)\, d\sigma_y \qquad (2.75)$$

giving the quantization condition [34]

$$\det \left| \delta_{pp'} - 2 \left(\frac{\partial G^+}{\partial n_\beta} \right)_{pp'} \right| = 0. \qquad (2.76)$$

To determine the equivalent condition for the plate equation we consider this equation in the case of a clamped edge disk.

$$(\nabla^4 - k^4)\Psi = 0 \qquad (2.77)$$

with the boundary conditions on S

$$\Psi|_S, \qquad \left. \frac{\partial \Psi}{\partial n} \right|_S = 0. \qquad (2.78)$$
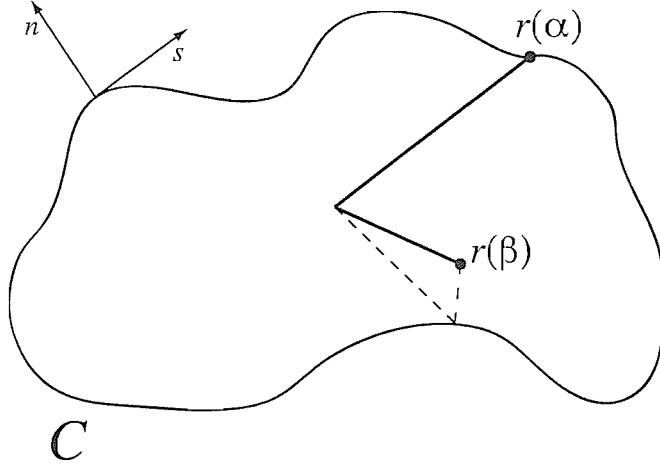
Figure 2.4: Arbitrary smooth boundary with α and β dependent points

Following the calculation in [30], any solution $W(\mathbf{r})$ of this equation can be decomposed into two elements $W^+(\mathbf{r})$ and $W^-(\mathbf{r})$ obtained from

$$W(\mathbf{r}) = W^+(\mathbf{r}) + W^-(\mathbf{r}) \tag{2.79}$$

Where these elements individually solve the equations

$$(\nabla^2 + k^2)W^+(\mathbf{r}) = 0 \tag{2.80}$$

$$(\nabla^2 - k^2)W^-(\mathbf{r}) = 0. \tag{2.81}$$

To construct the boundary integral equations for this problem, let us first consider the corresponding free problem

$$(\nabla \pm k^2)G^\pm(\mathbf{r}, \mathbf{r}'; k) = \delta(\mathbf{r} - \mathbf{r}') \tag{2.82}$$

Which has the solutions of $G^\pm$. On the boundary C we introduce the following notation The two variables α and β denote the distance along the boundary C from a fixed point to a function $\mathbf{r}(\alpha)$ or $\mathbf{r}(\beta)$, with the general

function **r** representing an arbitrary point within the boundary. We can then write the solutions to (2.80) and (2.81) as single layer potentials dependent on an arbitrary distribution function

$$W^+(\mathbf{r}) = \int_C G^+(\mathbf{r}, \mathbf{r}(\alpha))\mu(\alpha)\,d\alpha \qquad (2.83)$$

$$W^-(\mathbf{r}) = \int_C G^-(\mathbf{r}, \mathbf{r}(\alpha))\nu(\alpha)\,d\alpha. \qquad (2.84)$$

The Green functions can be expressed via the Bessel functions as

$$G^+(\mathbf{r}, \mathbf{r}'; k) = \frac{1}{4i}H_0^1(k|\mathbf{r} - \mathbf{r}'|) \qquad (2.85)$$

$$G^-(\mathbf{r}, \mathbf{r}'; k) = \frac{1}{2\pi}K_0(k|\mathbf{r} - \mathbf{r}'|) \qquad (2.86)$$

which have a logarithmic singularity as **r** approaches **r**'

$$G^\pm(\mathbf{r}, \mathbf{r}') \sim \frac{1}{2\pi}\ln|\mathbf{r} - \mathbf{r}'|. \qquad (2.87)$$

Due to this singularity, there is a discontinuity on the boundary for the limit of the normal derivative as the point $\mathbf{r}(\beta)$ approaches $\mathbf{r}(\alpha)$ from the interior of the domain. This can be dealt with by considering the effect at the singularity as the following. Using the Cartesian form of the normal derivative and of the Green function we have, on the boundary,

$$\frac{\partial G}{\partial n} = N_x\frac{\partial G}{\partial x} + N_y\frac{\partial G}{\partial y} \qquad (2.88)$$

$$G \sim \frac{1}{2\pi}\ln\sqrt{(x - x')^2 + (y - y')^2}. \qquad (2.89)$$

Applying this normal derivative to the approximate form of the Green function near the singularity gives

$$\frac{\partial G}{\partial n} = \frac{1}{2\pi}\left[\frac{N_x(x - x') + N_y(y - y')}{(x - x')^2 + (y - y')^2}\right]. \qquad (2.90)$$

However, we know from the properties of the coordinate system that

$$|N| = \sqrt{N_x^2 + N_y^2} = 1 \qquad (2.91)$$

$$\Rightarrow N_y = \sqrt{1 - N_x^2}. \qquad (2.92)$$

23

This allow as to write the normal derivative as

$$\frac{\partial G}{\partial n} \sim \frac{1}{2\pi} \frac{N_x(x - x') + \left(\sqrt{1 - N_x^2}\right)(y - y')}{(x - x')^2 + (y - y')^2}.$$ (2.93)

Considering the form of the delta function

$$\delta(X) = \frac{1}{\pi} \lim_{\epsilon \to 0} \frac{\epsilon}{X^2 + \epsilon^2}$$ (2.94)

It can be seen as $\beta \to \alpha$, since $x \to x'$ and $y \to y'$, the numerator of $\frac{\partial G}{\partial n}$ will tend to zero. This allows $\frac{\partial G}{\partial n}$ to be written in the form of the delta function where

$$\epsilon = N_x(x - x') + \left(\sqrt{1 - N_x^2}\right)(y - y')$$ (2.95)

$$X = \sqrt{(1 - N_x^2)(x - x')^2 - 2N_x\left(\sqrt{1 - N_x^2}\right)(x - x')(y - y') + N_x^2(y - y')}$$

(2.96)

By inspection it can be seen condition (2.96) is equivalent to the assumption that $x = x'$ and $y - y'$, hence

$$\delta(X) = \delta(\beta - \alpha).$$ (2.97)

This allows us to write

$$\int_{\beta \to \alpha} \frac{\partial G(\mathbf{r}, \mathbf{r}(\alpha))}{\partial n} f(\alpha)\, d\alpha \to \frac{1}{2}\int_C \delta(\beta - \alpha) f(\alpha)\, d\alpha + \int_C \frac{\partial G(\beta, \alpha)}{\partial n_\beta} f(\alpha)\, d\alpha$$

$$\to \frac{1}{2} f(\beta) + \int_C \frac{\partial G(\beta, \alpha)}{\partial n_\beta} f(\alpha)\, d\alpha$$ (2.98)

Now that we are able to include the behavior at the singularity, we can write the boundary conditions (2.78) in the boundary integral form

$$0 = \int_C G^+(\beta, \alpha)\, \mu(\alpha)\, d\alpha + \int_C G^-(\beta, \alpha)\, \nu(\alpha)\, d\alpha$$ (2.99)

$$0 = \frac{1}{2}\mu(\beta) + \frac{1}{2}\nu(\beta) + \int_C \frac{\partial G^+(\beta, \alpha))}{\partial n_\beta}\, \mu(\alpha)$$

$$+ \int_C \frac{\partial G^-(\beta, \alpha)}{\partial n_\beta} \nu(\alpha)\, d\alpha$$ (2.100)

We can consider the approximation that the boundary C can be separated into two parts, one a straight line at the point of interaction, and the other comprising the rest of the boundary

$$C \sim S_{line} + C_\Delta. \tag{2.101}$$

It should be noted that this calculation is performed under the assumption that any boundary considered is smooth and hence allows such a split. In this case, the normal derivatives over the straight line are equal to zero, and leave us with the following system of equations

$$0 = \int_{S_{line}} G^+(\beta, \alpha) \mu(\alpha) \, d\alpha + \int_{S_{line}} G^-(\beta, \alpha) \nu(\alpha) \, d\alpha$$
$$+ \int_{C_\Delta} G^+(\beta, \alpha) \mu(\alpha) \, d\alpha + \int_{C_\Delta} G^-(\beta, \alpha) \nu(\alpha) \, d\alpha \tag{2.102}$$

$$0 = \frac{1}{2}\mu(\beta) + \frac{1}{2}\nu(\beta) + \int_{C_\Delta} \frac{\partial G^+(\beta, \alpha))}{\partial n_\beta} \mu(\alpha)$$
$$+ \int_{C_\Delta} \frac{\partial G^-(\beta, \alpha)}{\partial n_\beta} \nu(\alpha) \, d\alpha. \tag{2.103}$$

As we are only considering cases in which the boundary is smooth and periodic, the solutions will themselves be periodic and the components of (2.83) and (2.84) can be described by the following Fourier representations

$$\mu(\alpha) = \int_{-\infty}^{\infty} e^{ip\alpha} \mu_p \, dp, \tag{2.104}$$

$$\nu(\alpha) = \int_{-\infty}^{\infty} e^{ip\alpha} \nu_p \, dp, \tag{2.105}$$

$$G^\pm = \int \int G^\pm_{p,p'} e^{ip\beta - ip'\alpha} \, dp \, dp' \tag{2.106}$$

and the following leading order semiclassical approximations

$$\frac{\partial G^+(\beta, \alpha)}{\partial n_\beta} = -i \int \int q G^+_{p,p'} e^{ip\beta - ip'\alpha} \, dp \, dp' \tag{2.107}$$

$$\frac{\partial G^-(\beta, \alpha)}{\partial n_\beta} = \int \int Q G^-_{p,p'} e^{ip\beta - ip'\alpha} \, dp \, dp'. \tag{2.108}$$

$$\tag{2.109}$$

25

With the values p, q and Q defined in (2.63-2.65), the Fourier components μ_p and ν_p have to satisfy the system of equations (2.102)-(2.106) that can be defined by

$$(M_0 \delta_{p,p'} + M_{p,p'}) \begin{pmatrix} \mu_{p'} \\ \nu_{p'} \end{pmatrix} = 0. \tag{2.110}$$

where the integration over the straight line and the remainder of the curve are determined by M_0 and $M_{p,p'}$ respectively. These matrices can be written as

$$
\begin{aligned}
M_0 &= \begin{pmatrix} -\frac{i}{2q} & -\frac{1}{2Q} \\ \frac{1}{2} & \frac{1}{2} \end{pmatrix} \\
&= \frac{1}{2} \begin{pmatrix} -\frac{i}{q} & -\frac{1}{Q} \\ 1 & 1 \end{pmatrix}
\end{aligned}
\tag{2.111}
$$

$$
\begin{aligned}
M_{pp'} &= \begin{pmatrix} G^+_{pp'} & G^-_{pp'} \\ \left(\frac{\partial G^+}{\partial n_\beta}\right)_{pp'} & \left(\frac{\partial G^-}{\partial n_\beta}\right)_{pp'} \end{pmatrix} \\
&= \begin{pmatrix} G^+_{pp'} & G^-_{pp'} \\ -iq G^+_{pp'} & Q G^-_{pp'} \end{pmatrix}
\end{aligned}
\tag{2.112}
$$

By then writing $T_{pp'} = -M_0^{-1} M_{pp'}$ this can now be written as

$$(\delta_{p,p'} - T_{pp'}) \begin{pmatrix} \mu_{p'} \\ \nu_{p'} \end{pmatrix} = \begin{pmatrix} 0 \\ 0 \end{pmatrix} \tag{2.113}$$

where

$$T_{pp'} = \begin{pmatrix} -2\frac{Q-iq}{Q+iq}\left(\frac{\partial G^+}{\partial n_\beta}\right)_{pp'} & \frac{4iq}{Q+iq}\left(\frac{\partial G^-}{\partial n_\beta}\right)_{pp'} \\ -\frac{4Q}{Q+iq}\left(\frac{\partial G^+}{\partial n_\beta}\right)_{pp'} & -2\frac{Q-iq}{Q+iq}\left(\frac{\partial G^+}{\partial n_\beta}\right)_{pp'} \end{pmatrix} \tag{2.114}$$

It can be seen that $G^- \propto K_0$ is exponentially small as $k \to \infty$, and so the assumption made is that its derivative is also exponentially small

$$\left(\frac{\partial G^-}{\partial n_\beta}\right) \to 0, \tag{2.115}$$

26

Meaning that $T_{pp'}$ can now, in this limit, be written as

$$T_{pp'} = \begin{pmatrix} -2\frac{Q-iq}{Q+iq}\left(\frac{\partial G^+}{\partial n_\beta}\right)_{pp'} & 0 \\ -\frac{4Q}{Q+iq}\left(\frac{\partial G^+}{\partial n_\beta}\right)_{pp'} & 0 \end{pmatrix}. \tag{2.116}$$

Now the quantization condition

$$\det\left|\delta_{p,p'} - T_{pp'}\right| = 0 \tag{2.117}$$

reduces to

$$1 - 2\frac{Q-iq}{Q+iq}\left(\frac{\partial G^+}{\partial n_\beta}\right)_{p,p'} = 0. \tag{2.118}$$

Referring back to the quantization condition for the membrane case (2.76), the two equations can be seen to only differ by the factor

$$\frac{Q-iq}{Q+iq} = e^{i\Phi_c} \tag{2.119}$$

that multiples the normal derivative of the Green function. This can then be equated to the exponential of $i\Phi_c$, where Φ_c is the phase angle for reflection at the boundary. This interaction then determines the introduction of a phase term for the clamped boundary condition. The phase term produced is the same as found by studying the problem using the approach as seen in 2.3.1, although it is not known if for other boundary conditions this is still the case as no calculations for these cases are presented, this shall be looked at in a later chapter.

We have seen in this chapter the background and development of solution approaches that link the billiard and plate problems. Having presented this we can now approach the elastic problem and hope to show which of these approaches provide accurate results and where those that do not could be improved.

Chapter 3

Semiclassical Analysis of Elastic Plates

The quantum billiard has long been used, in a wide variety of shapes and with many boundary conditions, as a model to look into the behavior of chaotic systems. While this work often introduces and develops new theories, because of the relative youth of the topic of quantum chaos, many of the more complicated cases of the simplest models have been left to one side. The disk billiard, modeling a circular elastic plate is one such model. However, if we consider the case of the plate described by the plate equation with a free boundary condition, while this has been approached many times before, the accuracy of the results at a low wave-number still leaves a lot to be desired.

It is the aim of this chapter to look at the use of quantum techniques to study the numerical errors that are associated with semiclassical approximations for plates in order to see where such results could be improved. By doing this for both circular and rectangular plates it is hoped that obvious factors will emerge to facilitate further investigation.
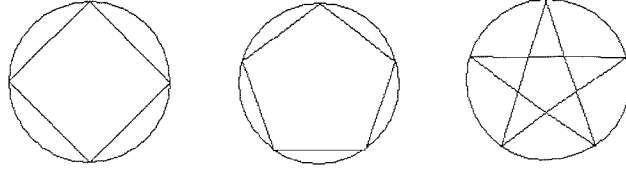
Figure 3.1: Periodic orbits with a) $v = 4, w = 0$, b) $v = 5, w = 0$ and c) $v = 5, w = 1$

3.1 Trace Formula Eigenvalues

We shall look at alternative methods for determining the eigenvalues of this plate system, starting with some results from established methods to provide a comparison to the alternatives presented later in the thesis. Here we alter the trace formula solution in its application to elastic plates by means of the inclusion of a boundary phase term so that we can observe the effectiveness of this approach.

3.1.1 Circular Plate

The periodic orbits for the disk can be labeled by the use of two variables v and w, where these are constants which define the orbit, v giving the number of boundary interactions and w the 'crossovers' of the orbit as shown in figure 3.1.1.

Using these variables, two values, the length of the periodic orbit and the angle of incidence with the boundary can be written

$$L_{vw} = 2vR \sin \psi_{vw}, \qquad (3.1)$$

$$\psi_{vw} = \frac{\pi w}{v}. \qquad (3.2)$$

29

The Jacobian J_{vw} for this system becomes

$$J_{vw} = \frac{2v(r^2 - R^2 \cos^2 \psi_{vw})}{pR \sin \psi_{vw}}. \tag{3.3}$$

Substituting (3.3) in (2.33) gives the trace formula representation of $\delta\rho(E)$ for the simply supported disk plate

$$\delta_{scl}(E) = \frac{1}{E_0}\sqrt{\frac{\hbar}{\pi p R}}\sum_{w=1}^{\infty}\sum_{v=2w}^{\infty} f_{vw}\frac{\sin^{\frac{3}{2}}(\psi_{vw})}{\sqrt{v}}\sin(\Phi_{vw}), \tag{3.4}$$

where f_{vw}, ψ_{vw} and Φ_{vw} all depend on the orbit parameters v and w. The phase change due to a boundary impact on a simply supported boundary is zero, as stated in section 2.3.1, however with alternative boundary conditions, the non-zero phases will alter the behavior of the relevant trace function. The phase accumulated by the periodic orbit must then be summed and added to the argument of the sine function in (3.4)

$$\psi \rightarrow \psi + \psi_{bc}, \tag{3.5}$$

where ψ_{bc} corresponds to either the phase value for the simply supported, clamped or free case.

The major benefit of investigating simple models is that there exists fairly reliable data with which to compare any new results. Once the new approach has been verified to be accurate for this simple case, it could then be extended to more complicated cases safe in the knowledge that the underlying reasoning behind the process is sound. We shall here compare the results from the trace formula approach as detailed in section 2.2.1 with the exact solutions taken from [35], this will allow us to notice which areas merit further investigation should their results be less accurate than others. Here we look at the results from the disk plate under the clamped, simply supported and free boundary conditions. In all cases following, the trace formula eigenvalues
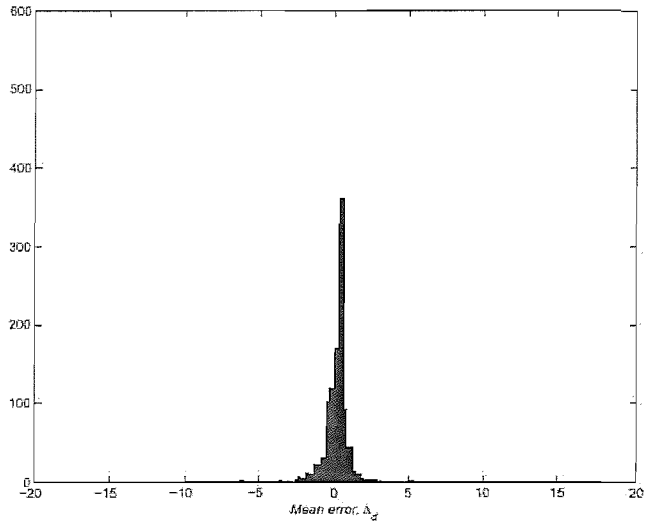
Figure 3.2: Clamped disk error distribution up to $k = 500$
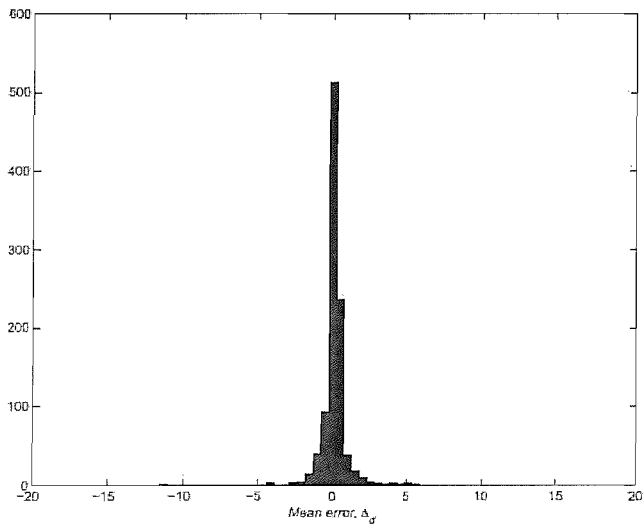
Figure 3.3: Simply supported disk error distribution up to $k = 500$
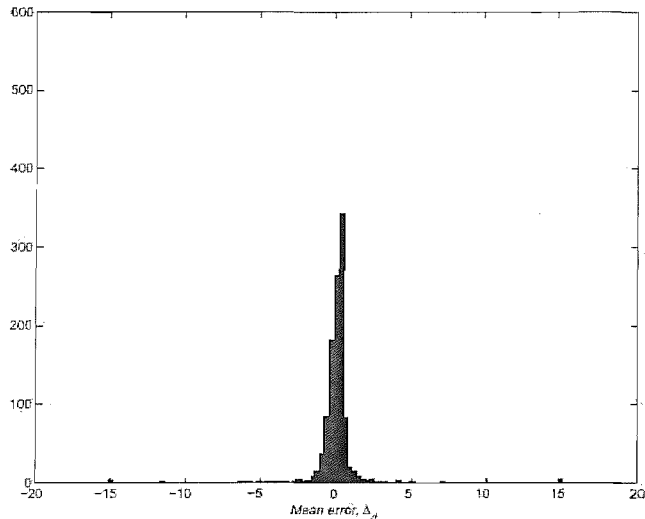
Figure 3.4: Free disk error distribution up to $k = 500$

were computed using a numerical program written especially to extract this data from the given formulae. We can see that when compared to the exact results up to $k = 500$ (figures 3.1.1, 3.1.1 and 3.1.1), all three boundary conditions produce accurate error distributions, showing that the standard approach is accurate as $k \to \infty$, this was to be expected. As stated, we are interested in the behavior at low k, and the first thirty eigenvalues for the clamped, simply supported and free boundary conditions are presented in figure A.1 in appendix A, the error due to the first eigenvalue in the free case omitted from the histogram for the purposes of clarity. Both the clamped and simply supported results are accurate in this region, while the free results are not as much so. We will now, as a confirmation of this fact, look at the effect of adding the phase term to the trace formula in the case of another model, the rectangular plate. According to [30], an extra condition due to the existence of boundary nodes should be included when studying the free plate. It is this extra factor, not included in these calculation for simplicity,
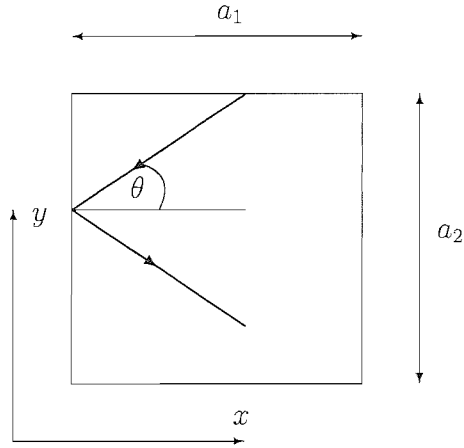
Figure 3.5: Boundary interaction angle of arbitrary periodic orbit for rectangular plate with length a_1 and height a_2.

which could be needed to be added in order to give more accurate results when using this method for the free edge plate.

3.1.2 Rectangular Plate

While for the smooth circular plate the results corresponded to what we expected, this is a special case in its simplicity. We shall now look at another system, the two dimensional rectangular plate as this will allow us to study the effects of adding non smooth boundaries with varying conditions. The period orbits for this system exist within a rectangular plate of size a_1a_2. Studying this problem will allow us to directly observe any of the more subtle effects produced by changing the boundary condition. These orbits can be classified in terms of the values M_1 and M_2. M_1 denotes the number of passes along the x-axis and similarly M_2 the number of passes along the y-axis. This system is time reversible, and will introduce degeneracies that will be dealt

33
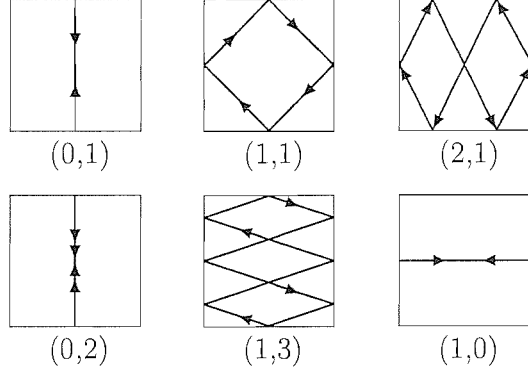
Figure 3.6: Sample periodic orbits for rectangular plate

with by including a factor of two. For an orbit (M_1, M_2)

$$\theta = \tan^{-1}\left(\frac{a_2 m_2}{a_1 m_1}\right), \tag{3.6}$$

$$L_{m_1 m_2} = 2\sqrt{a_1^2 m_1^2 + a_2^2 m_2^2}. \tag{3.7}$$

The Jacobian for this case can then be written as

$$J_{m_1 m_2} = \frac{L_{m_1 m_2}^3}{p(2m_1 a_1)^2}. \tag{3.8}$$

Due to the symmetries of this plate, its trace formula is taken from

$$\delta\rho_{scl}(E) = \frac{1}{\hbar\pi}\frac{1}{(2\pi\hbar)^{\frac{f}{2}}}\sum_{po}\frac{T_{po}V_{po}}{|J_{m_1 m_2}|^{\frac{1}{2}}\left|\det\left(\tilde{M}_{po} - I\right)\right|^{\frac{1}{2}}}\cos\Phi. \tag{3.9}$$

where

$$\Phi = \left(\frac{S_{po}}{\hbar} - \sigma_{po}\frac{\pi}{2} - \frac{f\pi}{4}\right), \tag{3.10}$$

the value V_{po} is the unit cell volume of the relevant phase subspace, $S_{po} = pL_{po}$ being the classical action and $T_{po} = \frac{S_{po}}{2E}$ the period for one orbit. In the case of the rectangular plate, the determinant of $\left(\tilde{M}_{po} - I\right)$ is equal to unity giving the oscillating level density for this system as

$$\delta\rho_{scl}(E) = \frac{ma_1 a_2}{\hbar^2 \pi^{\frac{3}{2}}}\sqrt{2}\sum_{po}\sum_{n=1}^{\infty}\sqrt{\frac{\hbar}{nS_{po}}}\cos\left(\frac{n}{\hbar}S_{po} - \frac{\pi}{4}\right). \tag{3.11}$$

34
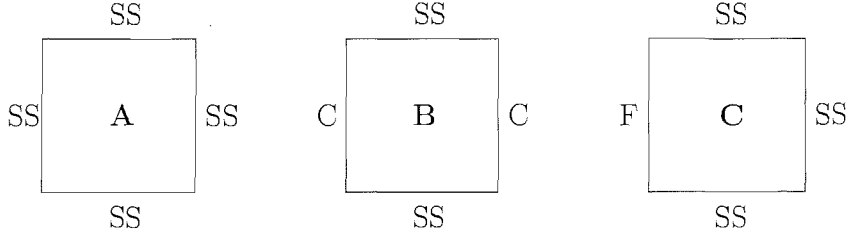
Figure 3.7: Boundary conditions for the examples studied - All simply supported in case A , two sides simply supported two sides clamped for case B and three sides simply supported with one free in case C

When considering the rectangular plate, a slightly altered trace formula is used,

$$\delta\rho(E) = \frac{ma_1a_2}{\hbar^2\pi^{\frac{3}{2}}}\sqrt{2}\sum_{\Gamma}\sum_{n=1}^{\infty}\sqrt{\frac{\hbar}{nS_\Gamma}}\cos\left(\frac{n}{\hbar}S_\Gamma - \frac{\pi}{4}\right) \qquad (3.12)$$

The phase alterations are then added in the cosine term to compensate for the interactions at each boundary segment. For the all-boundary simply supported case (plate A) the results calculated using the trace formula match the exact results almost exactly as shown in figure A.2 (Appendix A). This is to be expected if we remember that for the circular plate the two sets of results were identical due to using the same method of solution. The similarities in the method used for the rectangular plate are similar, although not identical. Given the fact that both methods are derived from the same principles as the disk case, we can then consider the errors produced here to be those generated by rounding errors in the numerical calculations. The results for case B where two edges are simply supported and the other two are clamped are also shown in figure A.2 (Appendix A). These results, although less accurate than for case A, are still well within expected limits for this case.

35

It is when we begin to consider edges that are governed by the free boundary condition (also see figure A.2 in Appendix A)that errors in the $k \to 0$ region begin to creep in. Simply making one edge freely supported introduces larger errors, and while the results are still reasonably accurate, there is a definite trend toward this accuracy dissolving should we alter other edges to the free condition. Although further results are not shown for brevity's sake, this trend continues as we increase the number of sides with the free edge boundary condition. Why would this be?

Looking at these results it is clear to see that there is clearly something amiss with the free edge boundary condition. The results obtained from its use are much less accurate than for the other boundary conditions when we are considering small k, this leads us to believe that there may well be terms in this boundary condition that could be improved upon with additional focus on lower order terms. When the phase term (3.10) is calculated, the clamped and simply supported cases involve at most a single derivative in the boundary conditions, meaning that no terms have to be neglected in the calculated. However, the free case involves up to third order derivatives, and lower order terms are neglected. While this assumption allows for a simpler calculation that is valid as $k \to \infty$, in the region where $k \to 0$ these neglected terms could possibly effect the term. This addition term will be investigated at a later point in this thesis. We shall firstly look at a different approach to a trace formula via Poisson summation.

3.2 Poisson Summation Approach

In section 2.2.2 we detailed the Poisson summation process as used to formulate a trace formula for a general system. In [36], this process is applied

to the basic rectangular membrane in order to determine the effectiveness of the approach. It is our aim here to extended this approach to the free edge case so that we can determine if the suggestion of the previous section that the free edge boundary condition provides less accurate results would also be true for alternative cases. If this is indeed the case then such a conclusion would provide us with an avenue for further study.

Assuming a rectangular domain with M_1 and M_2 denoting horizontal and vertical reflections respectively, the trace formula can then be calculated from the eigenvalue equation

$$k_{n_1,n_2} = \pi\sqrt{\frac{M_1^2}{a_1^2} + \frac{M_2^2}{a_2^2}}. \tag{3.13}$$

After some manipulation this provides a semiclassical approximation for the density of states

$$\rho(k) = \frac{a_1 a_2}{\pi}\sqrt{\frac{k}{2\pi}} \sum_{M_1=-\infty}^{\infty} \sum_{M_2=-\infty}^{\infty} L_{M_1,M_2}^{-\frac{1}{2}} \cos\left(kL_{M_1,M_2} - \frac{\pi}{4}\right)$$
$$+ \sum_{i=1,2}\frac{a_i}{2\pi}\sum \cos\left(2kMa_i\right) + \frac{\delta(k)}{4}. \tag{3.14}$$

If the cumulative density function is then plotted against the mode count from (3.13), the trace formula found is a good approximation even when computed using small numbers of reflections. Extending this problem to thin plates leads us to the plate equation detailed in section 2.3, where plates that have simply supported and clamped edges give a trace formula that behaves as expected, the mode-counts for such a comparison provide another good approximation. Experimental verification of results such as this along with additional developments can be seen in [[15], [37]-[41]]. We will now use the same approach to study the behavior of the free edge circular plate and then compare the eigenvalues with results obtained from alternative approaches.

3.2.1 Initial Structure

Taking the formula for the density of states from (2.47) and the EBK form of the eigenvalue equation in section 2.1.2 and inserting the known forms of the delta function and the spectral density, the density of states can now be written as

$$\rho(k) = F_1 + F_2 + F_3 \tag{3.15}$$

where

$$F_1 = \sum_{M_1=-\infty}^{\infty} \sum_{M_2=-\infty}^{\infty} \int_0^\infty dn_1 \int_0^\infty dn_2 \lim_{t\to 0} \frac{1}{2\sqrt{\pi t}} e^{\left(k-\pi\left(n_1+\frac{n_2}{2}\right)\right)^2} e^{2\pi i (M_1 n_1 + M_2 n_2)},$$
$$\tag{3.16}$$

$$F_2 = \frac{1}{2} \sum_{M_1=-\infty}^{\infty} \int_0^\infty dn_1 \lim_{t\to 0} \frac{1}{2\sqrt{\pi t}} e^{(k-n_1)^2} e^{2\pi i (M_1 n_1)}, \tag{3.17}$$

$$F_3 = +\frac{1}{2} \sum_{M_2=-\infty}^{\infty} \int_0^\infty dn_2 \lim_{t\to 0} \frac{1}{2\sqrt{\pi t}} e^{\left(k-\pi\frac{n_2}{2}\right)^2} e^{2\pi i (M_2 n_2)}. \tag{3.18}$$

At this stage the final delta function term from (2.47) is neglected due to its minimal contribution, but can be reinserted at a later point if so required. In order to convert ρ into its semiclassical form we can now solve each integral independently.

If we have an integral of the form

$$I = \int_0^\infty e^{-(ax^2+bx+c)}\, dx \tag{3.19}$$

then its solution is given by

$$I = \frac{1}{2}\sqrt{\frac{\pi}{a}} e^{\frac{b^2-4ac}{4a}} erfc\left(\frac{b}{2\sqrt{a}}\right). \tag{3.20}$$

Where $erfc$ is the complementary error function defined by

$$erfc(x) = \frac{2}{\sqrt{\pi}} \int_x^\infty e^{-u^2}\, du. \tag{3.21}$$

In the case we are considering this gives us

$$F_2 = -\frac{1}{2\pi} \sum_{M_1=-\infty}^{\infty} e^{2ikM_1} \tag{3.22}$$

$$F_3 = -\frac{1}{\pi} \sum_{M2=-\infty}^{\infty} e^{4ikM_2} \tag{3.23}$$

which with a little manipulation can be written as

$$F_2 = -\frac{1}{2\pi} - \frac{1}{\pi} \sum_{M_1}^{\infty} \cos(2kM_1) \tag{3.24}$$

$$F_3 = -\frac{1}{\pi} - \frac{2}{\pi} \sum_{M_2}^{\infty} \cos(4kM_1). \tag{3.25}$$

However, when considering F_1 it must be noted that due to the double integral things become a little more complicated and a slightly different approach must be followed in order to retrieve an accurate solution.

3.2.2   Calculation of F_1 component

When considering F_1 it is useful to affect a change of variables. First of all, in order to remove the k factor inside the first exponential we write $n_1 = kP_1$ and $n_2 = kP_2$, this then allows us to use the change of variables to a radial coordinate system

$$P_1 = \frac{R}{\pi} \cos^2 \theta \tag{3.26}$$

$$P_2 = \frac{2R}{\pi} \sin^2 \theta. \tag{3.27}$$

The integral F_1 can now be written as

$$F_1 = \sum_{M_1,M_2=-\infty}^{\infty} \int_0^{\infty} dR \int_0^{\pi/2} d\theta\, J(R,\theta) \lim_{t \to 0} \frac{1}{2\sqrt{\pi t}} e^{-\frac{k^2}{4t}(1-R)^2} e^{A(M_1,M_2,\theta)} \tag{3.28}$$

39

Where $A(M_1, M_2, \theta) = 2ikR(M_1 \cos^2 \theta + 2M_2 \sin^2 \theta)$ and the Jacobian $J(R, \theta)$ can be found to be

$$J(R, \theta) \quad = \quad \frac{4R}{\pi^2} \sin \theta \cos \theta. \qquad (3.29)$$

Now we rearrange F_1 in order to separate as far as possible the variables R and θ

$$F_1 \quad = \quad \frac{2}{\pi^2} \sum_{M_1, M_2 = -\infty}^{\infty} \lim_{t \to 0} \frac{1}{\sqrt{\pi t}} \int_0^\infty dR\, F(R) \int_0^{\pi/2} d\theta\, G(\theta, R). \quad (3.30)$$

Where the integrands are given by

$$F(R) \quad = \quad R e^{-\frac{k^2}{4t}(1-R)^2} e^{ikR(M_1 + 2M_2)}, \qquad (3.31)$$

$$G(\theta, R) \quad = \quad \sin \theta \cos \theta e^{ikR(M_1 - 2M_2) \cos 2\theta}. \qquad (3.32)$$

Solve the integral involving $G(\theta, R)$ to give

$$I_G \quad = \quad -\frac{\sin(k(M_1 - 2M_2)R)}{2k(M_1 - 2M_2)R}, \qquad (3.33)$$

then write the remaining integral as

$$I_F \quad = \quad -\frac{1}{2k(M_1 - 2M_2)} \int_0^\infty dR\, e^{-\frac{k^2}{4t}(1-R)^2} e^{ikR(M_1 + 2M_2)} \sin(k(M_1 - 2M_2)R).$$

$$(3.34)$$

We can then place these back into the full equation for F_1 and separate the equation into parts depending on positive and negative values of the summation variables. Using the following substitutions

$$f(M_1, M_2) \quad = \quad e^{ikR(M_1 + M_2)} \qquad (3.35)$$

$$g(M_1, M_2) \quad = \quad e^{-\frac{k^2}{4t}(1-R)^2} \frac{\sin(k(M_1 - 2M_2)R)}{2k(M_1 - 2M_2)} \qquad (3.36)$$

we can then write F_1 in the form

$$F_1 \quad = \quad -\frac{2}{\pi^2} \sum_{M_1 > 0} \sum_{M_2 > 0} \lim_{t \to 0} \frac{1}{\sqrt{\pi t}} \int_0^\infty dR\, [(f(M_1, M_2) + f^*(M_1, M_2)) g(M_1, M_2)].$$

$$(3.37)$$

40

Due to the properties of $f(M_1, M_2)$ and $f^*(M_1, M_2)$ this can then be written as

$$F_1 \; = \; -\frac{4}{\pi^2}\mathbb{R}\left[\sum_{M_1, M_2 > 0}\lim_{t \to 0}\frac{1}{\sqrt{\pi t}}\int_0^\infty dR e^{ikR(M_1 + 2M_2)}g(M_1, M_2)\right].$$

(3.38)

If we then return the function $g(M_1, M_2)$, we can perform the integration within F_1. Taking the real part of this result leave us with

$$F_1 \; = \; \frac{2}{\pi^2}\sum_{M_1 > 0, M_2 > 0}\frac{1}{k^2(M_1 - M_2)}\left(\sin(2iM_1 k) + \sin(4iM_2 k)\right)$$

(3.39)

and so we can write the calculated value for $\rho(k)$

$$\rho(k) \; = \; \frac{2}{\pi^2}\sum_{M_1 > 0, M_2 > 0}\frac{1}{k^2(M_1 - M_2)}\left(\sin(2iM_1 k) + \sin(4iM_2 k)\right)$$
$$-\frac{3}{2\pi} - \frac{1}{\pi}\sum_{M_1}^\infty \cos(2kM_1) - \frac{2}{\pi}\sum_{M_2}^\infty \cos(4kM_1),$$

(3.40)

giving us a trace formula that will allow us to calculate the eigenvalues of a circular plate with the edge behavior governed by the free edge boundary condition.

3.2.3 Results and Comparisons

So does the trace formula retrieved through the Poisson summation methods improve at all upon that previously used? Overall the spread of mean errors when compared to results calculated from the exact solution gives us the error distribution shown in figure 3.8 which is very similar to that seen for the comparison made with the original approach. We now know that both approaches give accurate results once applied to the region where $k \to \infty$,

41
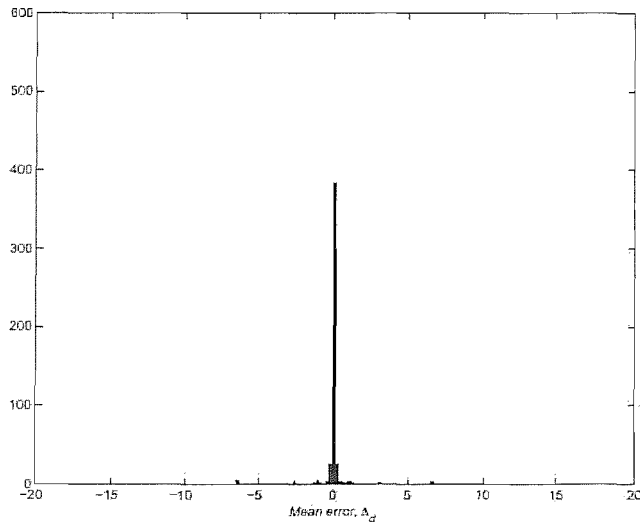
Figure 3.8: Error distribution for Poisson summation approach trace formula up to $k = 500$

however, this was to be expected, and we are also interested in the accuracy specifically in the region of low k, where we know that the free boundary condition produces less accurate results than hoped. The histograms for the error distribution at low k are shown in figure 3.9 for the original trace formula and in figure 3.10 for the new trace formula. Both distributions have a central peak showing that the results are basically accurate, with there being less spread in the new trace formula and hence more accurate for the eigenvalues it calculates. Compared the results from the EBK eigenvalue equation the new trace formula will be much more accurate as the eigenvalue equation itself is used in the calculation this is to be expected. However, this approach is limited by the fact that its dependence on the EBK eigenvalue equation will mean that it will be unable to calculate eigenvalues at low k which depend on the lower order contributions neglected to reach this equation.
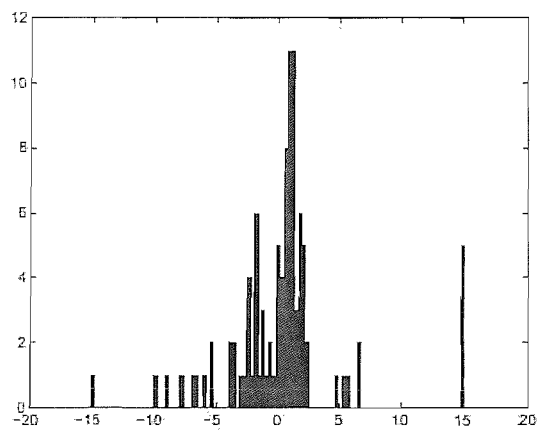
Figure 3.9: Original free approach error distribution under $k = 50$
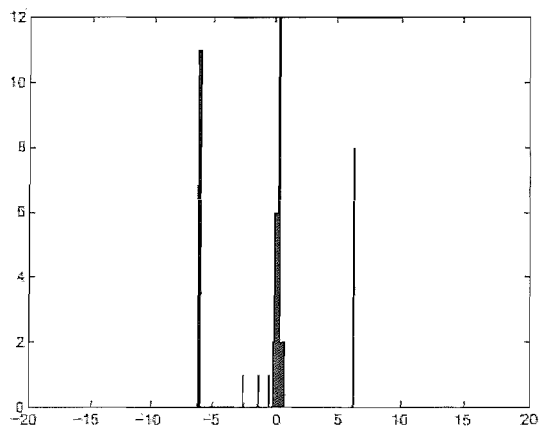
Figure 3.10: Poisson summation approach error distribution under $k = 50$

43

From this we see that calculating the eigenvalues with the Poisson summed method for the free edge boundary condition provides some improved accuracy over the original trace formula with phase modification term, although for the low k terms there is still much room for improvement due to the lower order contributions that have been neglected. All this leads us to the conclusion that the phase corrections of Bogomolny are not accurate for small k when considering the free edge and that considering any neglected terms in this region may provide an improvement to the numerical results.

While the use of the trace formula in this chapter is accurate for appropriate systems, it relies upon the use of classical paths as the periodic orbits to derive its form. Introducing diffractive elements into a system that previously only contained orbits that could be defined by classical paths alone means that the semiclassical propagator will no longer be able to sum over *all* paths; it will neglect the quantum mechanical effects that are due to the non specular nature of the diffractive point.

So why do the results for the rectangle work at all if they included such diffractive effects? In the simple case studied in this chapter the symmetry of the plate cancels out additional effects, but this will break down once the angle moves away from $\pi/2$ at the corners. This can start to be seem when we have different boundaries on the edges either side of the corner, this initial break in symmetry produces a reduction in apparent accuracy.

We have seen that the for the circle, in both the billiard and plate, results are accurate. However when we move to the rectangular plate this correspondence is not present and the effects of diffraction produced by the corners is thought to be an important factor in this breakdown and so this leads us to study the effects of diffraction in a later chapter. To examine this properly we need to look at the analytic behavior of this system and see if the phase

terms normally utilised are completely accurate for such cases. By rederiving these terms taking lower order terms and curvature into effects we can examine the results and see if improvement is possible.

Chapter 4

Lower Order Phase Corrections

In the previous chapter we looked at the effects of calculating the eigenvalues of a disk under various boundary conditions. The main approach was to consider the Gutzwiller trace formula with an additional phase term added in order to compensate for the change from simply supported to clamped and free. It was seen that while for the clamped and simply supported conditions this provided satisfactory results at both high and low frequencies, the addition of the free edge phase term was not quite as effective. At higher frequencies the results were accurate, but at a lower frequency the eigenvalues were not as accurate as for the alternative conditions and appeared to be more erratic. While the trace formula obtained through the Poisson summation method was an improvement, in this section we shall look at an alternative approach. In Bogomolny and Hughes [30] the boundary integral equation method is used to calculate a phase term for the clamped edge boundary condition. This term, when compared to the result found via the half plane solutions of the wave equation can be seen to match the expected result. However, the same calculation is not performed for the free edge condition and such a conclusion cannot immediately be drawn for this phase term.

The main aim of this chapter is to perform this calculation to verify whether or not the resulting phase term agrees with that which has been previously used. It is hoped that by performing this calculation an alternative phase term may be found that could then be used to produce a more accurate set of eigenvalues at a lower frequency in the free case.

Once this has been covered we shall move onto the free edge calculation, in the process of which we shall have to consider additional analysis not covered by the original clamped calculation. Once the results from the leading order approximations have been determined, we shall compare this to the result [30] and go on to investigate the effect of lower order terms on the result.

4.1   Coordinate Systems

The following section will establish the alternative coordinate system used, which allows a general boundary to be studied. We shall consider the curve γ, defined as a function of the arc-length s, with the tangent vector defined by $\mathbf{T}(s) = \dot{\mathbf{r}}(s)$.

$$\mathbf{r}(s) \quad = \quad x(s)\mathbf{i} + y(s)\mathbf{j}. \tag{4.1}$$

As $\mathbf{T}(s)$ is the tangent vector we can assume the following properties

$$|\mathbf{T}(s)| = 1, \qquad \mathbf{T}(s).\mathbf{T}(s) = 1 \tag{4.2}$$

$$\frac{\partial}{\partial s}(\mathbf{T}(s).\mathbf{T}(s)) \quad = \quad 2\dot{\mathbf{T}}(s).\mathbf{T}(s) = 0. \tag{4.3}$$

Hence $\dot{\mathbf{T}}(s)$ is perpendicular to $\mathbf{T}(s)$ and can be seen to be proportional to the normal vector $\mathbf{N}(s)$,

$$\dot{\mathbf{T}}(s) \quad = \quad \kappa(s)\mathbf{N}(s) \tag{4.4}$$

$$|\mathbf{N}(s)| \quad = \quad 1. \tag{4.5}$$
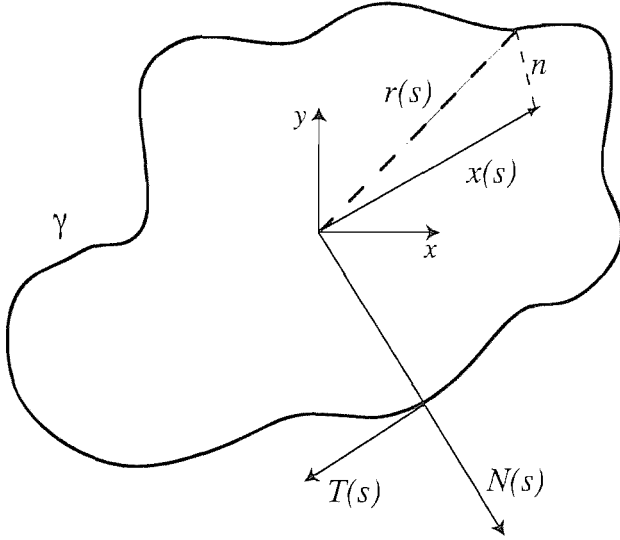
Figure 4.1: Arbitrary smooth boundary with coordinate elements

The constant κ is introduced to maintain proportionality between the tangent and normal vectors, and is determined by the local curvature of γ. We can now introduce coordinates in the neighborhood of γ

$$x^a(s,n) \;=\; r^a(s) + nN^a(S), \qquad a = 1, 2. \tag{4.6}$$

Here n denotes the distance from the boundary of the point $r^a(s)$, by taking the derivative of this function where $\dot{N} = -\kappa T$ we receive

$$
\begin{aligned}
dx^a &= \dot{r}^a(s)\, ds + n\dot{N}^a(s)\, ds + N^a(s)\, dn \\
&= T^a(s)\, ds + n\left(\ddot{T}^a(s)\right) ds + N^a(s)\, dn \\
&= (1 - n\kappa)T^a(s)\, ds + N^a(s)\, ds \qquad a = 1, 2. \tag{4.7}
\end{aligned}
$$

From this we can extract the following derivatives

$$\frac{\partial x^a}{\partial s} = (1 - n\kappa)T^a(s), \qquad T^a = (N_y, -N_x) \tag{4.8}$$

$$\frac{\partial x^a}{\partial n} = N^a(s), \qquad N^a = (N_x, N_y). \tag{4.9}$$

48

This then gives us

$$\frac{\partial x}{\partial s} = (1 - n\kappa)N_y \tag{4.10}$$

$$\frac{\partial x}{\partial n} = N_x \tag{4.11}$$

$$\frac{\partial y}{\partial s} = -(1 - n\kappa)N_x \tag{4.12}$$

$$\frac{\partial y}{\partial s} = N_y. \tag{4.13}$$

Using these relations and the fact that

$$\frac{\partial \psi}{\partial s} = \frac{\partial \psi}{\partial x}\frac{\partial x}{\partial s} + \frac{\partial \psi}{\partial y}\frac{\partial y}{\partial s} \tag{4.14}$$

$$\frac{\partial \psi}{\partial n} = \frac{\partial \psi}{\partial x}\frac{\partial x}{\partial n} + \frac{\partial \psi}{\partial y}\frac{\partial y}{\partial n} \tag{4.15}$$

we can now write the general tangential and normal derivatives of a function ψ in terms of Cartesian coordinates.

$$\frac{\partial \psi}{\partial s} = (1 - n\kappa)\left(N_y\frac{\partial \psi}{\partial x} - N_x\frac{\partial \psi}{\partial y}\right) \tag{4.16}$$

$$\frac{\partial \psi}{\partial n} = N_x\frac{\partial \psi}{\partial x} + N_y\frac{\partial \psi}{\partial y}. \tag{4.17}$$

To consider these derivatives on the boundary it is a case of simply taking $n = 0$.

We shall now briefly examine the free edge boundary conditions, re-deriving them from physical equilibrium principles. This is in order to verify the accuracy of the condition used and the ensure that any additional terms, either of lower order or dependent on the curvature of the boundary, are not neglected at too early a stage. By transforming (4.16) and (4.17) we receive

$$\frac{\partial w}{\partial x} = \frac{N_y}{(1 - n\kappa)}\frac{\partial w}{\partial s} + N_x\frac{\partial w}{\partial n} \tag{4.18}$$

$$\frac{\partial w}{\partial y} = \frac{-N_x}{(1 - n\kappa)}\frac{\partial w}{\partial s} + N_y\frac{\partial w}{\partial n}., \tag{4.19}$$

49

with the additional conditions

$$\frac{\partial N_x}{\partial s} = \kappa N_y, \qquad \frac{\partial N_y}{\partial s} = -\kappa N_x \tag{4.20}$$

$$\frac{\partial N_x}{\partial n} = \frac{\partial N_y}{\partial n} = 0. \tag{4.21}$$

For a free plate, the components G and H of the stress couple [32] are given by

$$-\frac{G}{D} = \cos^2\theta\left(\frac{\partial^2 w}{\partial x^2} + \sigma\frac{\partial^2 w}{\partial y^2}\right) + \sin^2\theta\left(\frac{\partial^2 w}{\partial y^2} + \sigma\frac{\partial^2 w}{\partial x^2}\right)$$
$$+(1-\sigma)\sin 2\theta\frac{\partial^2 w}{\partial x\partial y} \tag{4.22}$$

$$\frac{H}{D(1-\sigma)} = \sin\theta\cos\theta\left(\frac{\partial^2 w}{\partial y^2} - \frac{\partial^2 w}{\partial x^2}\right) + (\cos^2\theta - \sin^2\theta)\frac{\partial^2 w}{\partial x\partial y}. \tag{4.23}$$

Where G is a representation of the flexural couple, H a representation of the torsional couple and D is a constant based on the elastic properties of the plate, called the flexural rigidity. Using the change of boundary variables presented in (4.18) and (4.19) and appropriate N_x and N_y substitutions, these equations can be converted to

$$G = -D\left[\frac{\partial^2 w}{\partial n^2} + \sigma\frac{\partial^2 w}{\partial s^2} - \sigma\kappa\frac{\partial w}{\partial n}\right] \tag{4.24}$$

$$H = -D(1-\sigma)\left[\frac{\partial w^2}{\partial s\partial n} + \kappa\frac{\partial w}{\partial s}\right]. \tag{4.25}$$

Both of these are calculated for the case where $n = 0$, i.e. the behavior on the boundary. While G corresponds to the result in the original text, the result for H is slightly different and in the text [32] is given by

$$H = D(1-\sigma)\frac{\partial}{\partial n}\left(\frac{\partial w}{\partial s}\right). \tag{4.26}$$

50

By inspection it is seen that in this case the additional factor that is dependent on the curvature κ has been either missed or neglected. Stating that this result is valid for all boundaries is hence incorrect, only being valid for boundaries with zero curvature, i.e. straight edges. Either way, for the equations to be valid for any boundary whether straight or curved, this term cannot immediately be discarded and shall be included in future calculations. For a free plate, the conditions under which the physical forces are in equilibrium are fulfilled when

$$G \;=\; 0 \tag{4.27}$$

$$N - \frac{\partial H}{\partial s} \;=\; 0. \tag{4.28}$$

In this case, N is representing the shearing force normal to the plane of the plate and is given by

$$N \;=\; -D\frac{\partial}{\partial n}\nabla^2 w \tag{4.29}$$

$$\;=\; -D\left[\frac{\partial^3 w}{\partial s^2 \partial n} + \frac{\partial^3 w}{\partial n^3} - \kappa\frac{\partial^2 w}{\partial n^2}\right]. \tag{4.30}$$

By calculating the full results from (4.27) and (4.28), taking care not to specify the boundary case $n = 0$ until the end, we find that

$$\frac{\partial^2 w}{\partial n^2} + \sigma\frac{\partial^2 w}{\partial s^2} - \sigma\kappa\frac{\partial w}{\partial n} \;=\; 0 \tag{4.31}$$

$$\frac{\partial^3 w}{\partial n^3} + (2 - \sigma)\left(\frac{\partial^3 w}{\partial s^2 \partial n} + \frac{\partial \kappa}{\partial s}\frac{\partial w}{\partial s}\right) + 3\kappa\frac{\partial^2 w}{\partial s^2} - (1 + \sigma)\kappa^2\frac{\partial w}{\partial n} \;=\; 0,$$
$$\tag{4.32}$$

noticing that these correspond exactly to the conditions (2.60). With the method presented in section 2.3.2, we will now proceed to apply the same process using the free edge boundary conditions instead. To begin with we will have to deal with some of the higher order terms presented by these conditions.

51

4.2 Higher order integrals

Having seen that the transfer matrix for the clamped edge condition presents us with a phase angle that agrees with results calculated in an alternative manner. It is the intention of this section to calculate the transfer matrix for the free edge boundary condition. From this point, the resultant phase angle, if available, will then be compared with the phase angle derived from an alternative approach.

$$\frac{\partial \Phi}{\partial n} = N_x \frac{\partial \Phi}{\partial x} + N_y \frac{\partial \Phi}{\partial y}. \tag{4.33}$$

It has also been stated (4.21) that the derivatives of N_x and N_y with respect to n are equal to zero, hence the derivative of (4.33) with respect to n becomes

$$\begin{aligned} \frac{\partial^2 \Phi}{\partial n^2} &= N_x \frac{\partial}{\partial n} \left(\frac{\partial \Phi}{\partial x} \right) + N_y \frac{\partial}{\partial n} \left(\frac{\partial \Phi}{\partial y} \right) \\ &= N_x^2 \frac{\partial^2 \Phi}{\partial x^2} + 2 N_x N_y \frac{\partial^2 \Phi}{\partial x \partial y} + N_y^2 \frac{\partial^2 \Phi}{\partial y^2}. \end{aligned} \tag{4.34}$$

Similarly the third derivative is

$$\frac{\partial^3 \Phi}{\partial n^3} = N_x^3 \frac{\partial^3 \Phi}{\partial x^3} + 3 N_x N_y \left(N_x \frac{\partial^3 \Phi}{\partial x^2 \partial y} + N_y \frac{\partial^3 \Phi}{\partial x \partial^2 y} \right) + N_y^3 \frac{\partial^3 \Phi}{\partial y^3}. \tag{4.35}$$

To evaluate the behavior of these functions on the boundary, we look at the effect of a singularity at the point where $\mathbf{r}(\alpha) = \mathbf{r}(\beta)$. This is accomplished by considering the boundary in the region of this point as a semicircle with radius tending to zero (figure 4.2), as this limit is reached the behavior will be the same without having to directly evaluate the result at the singularity. Using the notation defined earlier, we write

$$\tilde{\mathbf{n}} = (N_x, N_y) \tag{4.36}$$

$$\tilde{\mathbf{s}} = (N_y, -N_x) \tag{4.37}$$
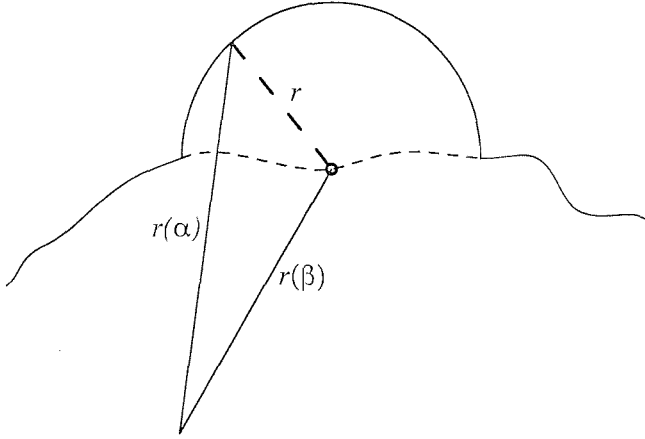
Figure 4.2: Boundary deformation at singularity point

and define the position of the point $\mathbf{r}(\alpha)$ on the boundary around the semi-circle as

$$
\begin{aligned}
\mathbf{R}(\alpha) &= (x - x', y - y') \\
&= (R\cos\theta, R\sin\theta).
\end{aligned}
\tag{4.38}
$$

We can then write (4.33) for the case of the Green function around the semi-circle as

$$
\begin{aligned}
\frac{\partial G}{\partial n} &= \frac{1}{2\pi} \frac{N_x(x - x') + N_y(y - y')}{(x - x')^2 + (y - y')^2} \\
&= \frac{1}{2\pi} \frac{\mathbf{n} \cdot \mathbf{R}}{R^2} \\
&= \frac{1}{2\pi R}.
\end{aligned}
\tag{4.39}
$$

As we are looking at the case of the semi-circle we use

$$
\mathbf{R} = ((x - x'), (y - y'))
\tag{4.40}
$$

$$
N_x = \cos\theta
\tag{4.41}
$$

$$N_y = \sin\theta \tag{4.42}$$

but this calculation would be valid for alternative deformations as long as the correct forms for N_x and N_y are used. We can now calculate the effect on the boundary integral equation around this singularity by performing the integral at the limit of $\mathbf{r}(\beta) \to \mathbf{r}(\alpha)$,

$$
\begin{aligned}
\int_{\beta \to \alpha} \frac{\partial G}{\partial n} f(s)\,ds &= \lim_{R \to 0}\left(\int_0^\pi \frac{1}{2\pi R} f(0) R\,d\theta + \int_0^\pi \frac{R}{2\pi R}\frac{\partial f}{\partial s}(0)R\,d\theta + O(R^2) \right) \\
&= \int_0^\pi \frac{1}{2\pi} f(0)\,d\theta \\
&= \frac{f(0)}{2}.
\end{aligned}
\tag{4.43}
$$

This allows the boundary integral equations in this case to be written

$$
\int_C \frac{\partial G(\mathbf{r}, \mathbf{r}(\alpha))}{\partial n} f(\alpha)\,d\alpha \;\to\; \frac{1}{2}f(\beta) + \int_C \frac{\partial G(\beta, \alpha)}{\partial n_\beta} f(\alpha)\,d\alpha, \tag{4.44}
$$

as shown earlier. We can also write the higher order derivatives as

$$
\begin{aligned}
\frac{\partial^2 G}{\partial n^2} &= \tilde{\mathbf{n}} \cdot \nabla\left(\tilde{\mathbf{n}} \cdot \nabla G\right) \\
&= \tilde{\mathbf{n}} \cdot \nabla\left(\frac{\partial G}{\partial n}\right) \\
&= -\frac{1}{2\pi R^2}
\end{aligned}
\tag{4.45}
$$

and

$$
\begin{aligned}
\frac{\partial^3 G}{\partial n^3} &= \tilde{\mathbf{n}} \cdot \nabla\left(\frac{\partial^2 G}{\partial n^2}\right) \\
&= \frac{1}{2\pi R^3}
\end{aligned}
\tag{4.46}
$$

Proceeding with the calculation in the same manner will mean the appearance of a singularity that cannot be dealt with using this process, and so the problem needs to be approached in an alternative manner. Recall the fact that

$$
\left. \frac{\partial G}{\partial n} \right|_{\beta \to \alpha} = \delta\left(r_\beta - r_\alpha\right), \tag{4.47}
$$

54

so we can write

$$\frac{\partial^2 G}{\partial n^2}\bigg|_{\beta \to \alpha} = \int \mathbf{n} \cdot \nabla_\beta \left(\delta \left(r_\beta - r_\alpha\right)\right) f(\alpha)\, ds$$

$$= \int f(\alpha) \nabla_\beta \left(\delta \left(r_\beta - r_\alpha\right)\right) \cdot \mathbf{n}\, ds$$

$$= \int f(\alpha) \nabla_\beta \left(\delta \left(r_\beta - r_\alpha\right)\right) \cdot d\mathbf{s}_n. \qquad (4.48)$$

If we then consider the identity

$$A\nabla B = -B\nabla A + \nabla (AB)$$

$$\Rightarrow \int \left(\nabla_\beta B\right) A \cdot d\mathbf{s}_n = \int \left(\nabla_\beta (AB) - B\nabla_\beta A\right) \cdot d\mathbf{s}_n$$

$$= -\int B\nabla_\beta A \cdot \cdot d\mathbf{s}_n + \int \nabla_\beta (AB) \cdot d\mathbf{s}_n \quad (4.49)$$

taking

$$A = f(\alpha) \qquad\qquad B = \delta \left(r_\beta - r_\alpha\right), \qquad\qquad (4.50)$$

(4.48) then becomes

$$\int f(\alpha) \nabla_\beta \left(\delta \left(r_\beta - r_\alpha\right)\right) \cdot d\mathbf{s}_n = -\int \delta \left(r_\beta - r_\alpha\right) \nabla_\beta (f(\alpha)) \cdot d\mathbf{s}_n$$

$$+ \int \nabla_\beta \left(f(\alpha)\delta \left(r_\beta - r_\alpha\right)\right) \cdot d\mathbf{s}_n.$$

$$(4.51)$$

Over the loop we can take

$$\int \nabla_\beta \left(f(\alpha)\delta \left(r_\beta - r_\alpha\right)\right) \cdot d\mathbf{s}_n = 0, \qquad\qquad (4.52)$$

leaving us with

$$\frac{\partial^2 G}{\partial n^2}\bigg|_{\beta \to \alpha} = -\int \delta \left(r_\beta - r_\alpha\right) \nabla_\beta (f(\alpha)) \cdot d\mathbf{s}_n$$

$$= -\frac{1}{2} \frac{\partial f}{\partial n}\bigg|_\beta. \qquad\qquad (4.53)$$

The boundary integral representation incorporating the singularity as $\beta \to \alpha$ can now be written in the form

$$\int_C \frac{\partial^2 G(\mathbf{r}, \mathbf{r}(\alpha))}{\partial n^2} f(\alpha) \, d\alpha \quad \to \quad -\frac{1}{2} \frac{\partial f(\beta)}{\partial n} + \int_C \frac{\partial^2 G(\beta, \alpha)}{\partial n_\beta^2} f(\alpha) \, d\alpha.$$

$$(4.54)$$

For the higher order normal derivative we write

$$\frac{\partial^3 G}{\partial n^3} \bigg|_{\beta \to \alpha} = \int \mathbf{n} \cdot \left(\frac{\partial^2 G}{\partial n^2} \right) f(\alpha) \, ds$$

$$= \int f(\alpha) \nabla_\beta \left(\frac{\partial^2 G}{\partial n^2} \right) \cdot d\mathbf{s}_n.$$

$$(4.55)$$

Using (4.49) and taking

$$A = f(\alpha) \qquad B = \frac{\partial^2 G}{\partial n^2}$$

$$(4.56)$$

allows us to write

$$\frac{\partial^3 G}{\partial n^3} \bigg|_{\beta \to \alpha} = -\int \frac{\partial^2 G}{\partial n^2} \nabla_\beta(f(\alpha)) \cdot d\mathbf{s}_n$$

$$+ \int \nabla_\beta \left(\frac{\partial^2 G}{\partial n^2} f(\alpha) \right) \cdot d\mathbf{s}_n$$

$$= \int \frac{\partial G}{\partial n} \nabla_\beta \left(\nabla_\beta(f(\alpha)) \right) \cdot d\mathbf{s}_n$$

$$= \int \delta \left(r_\beta - r_\alpha \right) \nabla_\beta^2 f(\alpha) \cdot d\mathbf{s}_n$$

$$= \frac{1}{2} \frac{\partial^2 f}{\partial n^2} \bigg|_\beta.$$

$$(4.57)$$

The boundary integral form of the third order normal derivative of the Green function becomes

$$\int_C \frac{\partial^3 G(\mathbf{r}, \mathbf{r}(\alpha))}{\partial n^3} f(\alpha) \, d\alpha \quad \to \quad \frac{1}{2} \frac{\partial^2 f(\beta)}{\partial n^2} + \int_C \frac{\partial^3 G(\beta, \alpha)}{\partial n_\beta^3} f(\alpha) \, d\alpha.$$

$$(4.58)$$

56

It is also necessary to determine the behavior of the derivatives with respect to s.

$$\begin{aligned}
\frac{\partial G}{\partial s} &= \frac{(1-n\kappa)}{2\pi}\frac{N_y(x-x')-N_x(y-y')}{(x-x')^2+(y-y')^2} \\
&= \frac{(1-n\kappa)}{2\pi}\frac{\tilde{\mathbf{s}}\cdot\mathbf{R}}{R^2} \\
&= 0
\end{aligned} \tag{4.59}$$

This could be calculated by replacing the specific values of N_x and N_y for the semicircular deformation, but it can instead be seen from figure 4.1 that the arc terms is perpendicular to the radial distance $\mathbf{R}$ and so $\mathbf{s}.\mathbf{R}$ is obviously equal to zero. For the second order derivative

$$\begin{aligned}
\frac{\partial^2 G}{\partial s^2} &= (1-n\kappa)\left(N_y^2\frac{\partial^2 G}{\partial x^2}-2N_xN_y\frac{\partial^2 G}{\partial x\partial y}+N_x^2\frac{\partial^2 G}{\partial y^2}\right) \\
&\quad -\kappa(1-n\kappa)\left(N_x\frac{\partial G}{\partial x}+N_y\frac{\partial G}{\partial y}\right)-n\frac{\partial\kappa}{\partial s}\left(N_y\frac{\partial G}{\partial x}-N_x\frac{\partial G}{\partial y}\right)
\end{aligned} \tag{4.60}$$

As we are considering a point on the boundary, we can now set $n=0$ to give

$$\begin{aligned}
\frac{\partial^2 G}{\partial s^2} &= \left(N_y^2\frac{\partial^2 G}{\partial x^2}-2N_xN_y\frac{\partial^2 G}{\partial x\partial y}+N_x^2\frac{\partial^2 G}{\partial y^2}\right) \\
&\quad -\kappa\left(N_x\frac{\partial G}{\partial x}+N_y\frac{\partial G}{\partial y}\right).
\end{aligned} \tag{4.61}$$

Taking the derivatives of the Green function and inserting the values of N_x and N_y gives

$$\left.\frac{\partial^2 G}{\partial s^2}\right|_{\beta\to\alpha} = \frac{1}{2\pi R^2}-\frac{\kappa}{2\pi R}. \tag{4.62}$$

If we consider the fact that we have taken κ from (4.4) to be defined as $\kappa=\frac{1}{R}$ then this derivative disappears at the point where $\beta\to\alpha$, and so we can write

$$\int_C\frac{\partial^2 G^{\pm}(\mathbf{r},\mathbf{r}(\alpha))}{\partial s^2}f(\alpha)\,d\alpha \;\to\; \int_C\frac{\partial^2 G^{\pm}(\beta,\alpha)}{\partial s^2}f(\alpha)\,d\alpha. \tag{4.63}$$

57

The remaining mixed derivative can be found in the following fashion. Starting from (4.47) and following the same procedure as (4.47-4.54) we write

$$
\begin{aligned}
\left.\frac{\partial^2 G}{\partial n \partial s}\right|_{\beta \to \alpha} &= \mathbf{s} \cdot \nabla_\beta \left(\delta\left(r_\beta - r_\alpha\right)\right) f(\alpha)\, ds \\
&= \int f(\alpha) \nabla_\beta \left(\delta\left(r_\beta - r_\alpha\right)\right) \cdot d\mathbf{s}_s \\
&= -\int \delta\left(r_\beta - r_\alpha\right) \nabla_\beta f(\alpha) \cdot d\mathbf{s}_s \\
&\quad + \int \nabla_\beta \left(f(\alpha)\delta\left(r_\beta - r_\alpha\right)\right) \cdot d\mathbf{s}_s \\
&\quad - \frac{1}{2}\frac{\partial f}{\partial s}.
\end{aligned}
\tag{4.64}
$$

This allows us to then calculate

$$
\begin{aligned}
\left.\frac{\partial^3 G}{\partial n \partial s^2}\right|_{\beta \to \alpha} &= \mathbf{s} \cdot \left(\frac{\partial^2 G}{\partial n \partial s}\right) f(\alpha)\, ds \\
&= f(\alpha) \nabla_\beta \left(\frac{\partial^2 G}{\partial n \partial s}\right) \cdot d\mathbf{s}_s \tag{4.65} \\
&= -\int \frac{\partial^2 G}{\partial n \partial s} \nabla_\beta (f(\alpha)) \cdot d\mathbf{s}_s \\
&\quad + \int \nabla_\beta \left(f(\alpha)\frac{\partial^2 G}{\partial n \partial s}\right) \cdot d\mathbf{s}_s \\
&= -\int \frac{\partial^2 G}{\partial n \partial s} \nabla_\beta (f(\alpha)) \cdot d\mathbf{s}_s \\
&= \int \delta\left(r_\beta - r_\alpha\right) \nabla_\beta^2 f(\alpha) \cdot d\mathbf{s}_s \\
&= \left.\frac{1}{2}\frac{\partial^2 f}{\partial s^2}\right|_\beta,
\end{aligned}
\tag{4.66}
$$

with the remaining boundary integral form for this derivative given by

$$
\int_C \frac{\partial^3 G^\pm\left(\mathbf{r}, \mathbf{r}(\alpha)\right)}{\partial n \partial s^2} f(\alpha)\, d\alpha \;\to\; \frac{1}{2}\frac{\partial^2 f(\beta)}{\partial s^2} + \int_C \frac{\partial^3 G^\pm\left(\beta, \alpha\right)}{\partial n \partial s^2} f(\alpha)\, d\alpha.
\tag{4.67}
$$

Considering this information it is now our aim to we can then find the

matrices to satisfy

$$(M_0 \delta_{p,p'} + M_{p,p'}) \begin{pmatrix} \mu_{p'} \\ \nu_{p'} \end{pmatrix} = 0. \tag{4.68}$$

as in the clamped case. Additional calculations to this effect to determine the straight line integrals and leading order derivatives are presented in Appendix B.

4.3   Calculation of Transfer Matrix

We can now establish from (4.31,4.32) the following equations

$$
\begin{aligned}
N &= -\frac{1}{2}\frac{\partial}{\partial n}(\mu(\beta) + \nu(\beta)) - \frac{\sigma\kappa}{2}(\mu(\beta) + \nu(\beta)) + \frac{\sigma}{2}p^2 \left(\frac{1}{Q} - \frac{1}{iq} \right) \\
&\quad -(Q - iq) + \int_{C_\Delta} \left(\frac{\partial^2 G^+(\beta,\alpha)}{\partial n^2} + \sigma\frac{\partial^2 G^+(\beta,\alpha)}{\partial s^2} - \sigma\kappa\frac{\partial G^+(\beta,\alpha)}{\partial n} \right) \mu(\alpha)\, d\alpha \\
&\quad + \int_{C_\Delta} \left(\frac{\partial^2 G^-(\beta,\alpha)}{\partial n^2} + \sigma\frac{\partial^2 G^-(\beta,\alpha)}{\partial s^2} - \sigma\kappa\frac{\partial G^-(\beta,\alpha)}{\partial n} \right) \nu(\alpha)\, d\alpha
\end{aligned}
$$

$$\tag{4.69}$$

where we can take only the terms that will give the highest order contributions to leave

$$
\begin{aligned}
N &= -\frac{1}{2}\frac{\partial}{\partial n}(\mu(\beta) + \nu(\beta)) + \frac{\sigma}{2}p^2 \left(\frac{1}{Q} - \frac{1}{iq} \right) - (Q - iq) \\
&\quad + \int_{C_\Delta} \left(\frac{\partial^2 G^+(\beta,\alpha)}{\partial n^2} + \sigma\frac{\partial^2 G^+(\beta,\alpha)}{\partial s^2} \right) \mu(\alpha)\, d\alpha \\
&\quad + \int_{C_\Delta} \left(\frac{\partial^2 G^-(\beta,\alpha)}{\partial n^2} + \sigma\frac{\partial^2 G^-(\beta,\alpha)}{\partial s^2} \right) \nu(\alpha)\, d\alpha. \tag{4.70}
\end{aligned}
$$

Similarly for the second condition, neglecting all but the terms that will provide the highest order contributions gives

$$
M = \frac{1}{2}\frac{\partial^2}{\partial n^2}(\mu(\beta) + \nu(\beta))
$$

$$+(2-\sigma)\int_{C_\Delta}\left(\frac{\partial^3 G^+(\beta,\alpha)}{\partial n \partial s^2}\mu(\alpha)+\frac{\partial^3 G^-(\beta,\alpha)}{\partial n \partial s^2}\nu(\alpha)\right)d\alpha$$

$$+\int_{C_\Delta}\left(\frac{\partial^3 G^+(\beta,\alpha)}{\partial n^3}\mu(\alpha)+\frac{\partial^3 G^-(\beta,\alpha)}{\partial n^3}\nu(\alpha)\right)d\alpha. \qquad (4.71)$$

Substituting the previous calculations into these equation gives us

$$
\begin{aligned}
N &= \frac{1}{2}\left(iq+\frac{i\sigma p^2}{q}\right)\mu(\beta)-\left(Q-\frac{\sigma p^2}{Q}\right)\nu(\beta) \\
&\quad -\int_{C_\Delta}\left(q^2+\sigma p^2\right)G^+(\beta,\alpha)\mu(\alpha)\,d\alpha \\
&\quad +\int_{C_\Delta}\left(Q^2-\sigma p^2\right)G^-(\beta,\alpha)\nu(\alpha)\,d\alpha \qquad (4.72)
\end{aligned}
$$

and

$$
\begin{aligned}
M &= -\frac{1}{2}\left(q^2+(2-\sigma)p^2\right)\mu(\beta)+\frac{1}{2}\left(Q^2-(2-\sigma)p^2\right)\nu(\beta) \\
&\quad \int_{C_\Delta}\left(iq^3+(2-\sigma)ip^2 q\right)G^+(\beta,\alpha)\mu(\alpha)\,d\alpha \\
&\quad -\int_{C_\Delta}\left(Q^3+(2-\sigma)p^2 Q\right)G^-(\beta,\alpha)\nu(\alpha)\,d\alpha. \qquad (4.73)
\end{aligned}
$$

We know that both (4.70) and (4.71) are equal to zero and so we can then write the matrices M_0 and $M_{pp,}$ from (4.68) as

$$M_0 = \frac{1}{2}\begin{pmatrix} M_0^{(1,1)} & M_0^{(1,2)} \\ M_0^{(2,1)} & M_0^{(2,2)} \end{pmatrix} \qquad (4.74)$$

$$M_{p,p'} = \begin{pmatrix} M_{p,p'}^{(1,1)}G_{p,p'}^+ & M_{p,p'}^{(1,2)}G_{p,p'}^- \\ M_{p,p'}^{(2,1)}G_{p,p'}^+ & M_{p,p'}^{(2,2)}G_{p,p'}^- \end{pmatrix} \qquad (4.75)$$

Where

$$M_0^{(1,1)} = -\frac{1}{iq}\left(q^2+p^2\right) \qquad (4.76)$$

$$M_0^{(1,2)} = -\frac{1}{Q}\left(Q^2-p^2\right) \qquad (4.77)$$

$$M_0^{(2,1)} = -q^2-(2-\sigma)p^2 \qquad (4.78)$$

$$M_0^{(2,2)} = Q^2-(2-\sigma)p^2 \qquad (4.79)$$

and

$$M_{p,p'}^{(1,1)} = -q^2 - \sigma p^2 \tag{4.80}$$

$$M_{p,p'}^{(1,2)} = Q^2 - \sigma p^2 \tag{4.81}$$

$$M_{p,p'}^{(2,1)} = -(iq)\left(q^2 + (2-\sigma)p^2\right) \tag{4.82}$$

$$M_{p,p'}^{(2,2)} = -Q\left(Q^2 + (2-\sigma)p^2)\right). \tag{4.83}$$

As in the clamped calculation, we can now find

$$T_{p,p'} = -M_0^{-1}M_{p,p'} \tag{4.84}$$

which can be written as

$$T_{p,p'} = -\begin{pmatrix} T_{p,p'}^{(1,1)}\left(\frac{\partial G^+}{\partial n_\beta}\right)_{p,p'} & T_{p,p'}^{(1,2)}\left(\frac{\partial G^-}{\partial n_\beta}\right)_{p,p'} \\ T_{p,p'}^{(2,1)}\left(\frac{\partial G^+}{\partial n_\beta}\right)_{p,p'} & T_{p,p'}^{(2,2)}\left(\frac{\partial G^-}{\partial n_\beta}\right)_{p,p'} \end{pmatrix}. \tag{4.85}$$

It can be seen that

$$
\begin{aligned}
T_{p,p'}^{(1,1)} &= \frac{1}{iq}\frac{1}{\det(M_0)}\left(M_0^{(2,2)}M_{(p,p')}^{(1,1)} - M_0^{(1,2)}M_{(p,p')}^{(2,1)}\right) \\
&= \frac{2iQ}{2qQ}\frac{T_{1,1}}{\det(M_0)},
\end{aligned}
\tag{4.86}
$$

we take the elements of this equation as

$$
\begin{aligned}
2QT^{(1,1)} &= Q\left(Q - (2-\sigma)p^2\right)\left(q^2 + \sigma p^2\right) \\
&\quad + iq\left(Q^2 - \sigma p^2\right)\left(q^2 + (2-\sigma)p^2\right)
\end{aligned}
\tag{4.87}
$$

$$
\begin{aligned}
2iqQ\det(M_0) &= Q(q^2 + \sigma p^2)(Q^2 - (2-\sigma)p^2) \\
&\quad - iq(Q^2 - \sigma p^2)(q^2 + (2-\sigma)p^2).
\end{aligned}
\tag{4.88}
$$

These values can then be reorganized to a form

$$T_{p,p'}^{(1,1)} = \frac{1 + iA}{1 - iA} \tag{4.89}$$

61

with

$$A = \frac{q}{Q} \left[\frac{(Q^2 - \sigma p^2)(q^2 + (2 - \sigma)p^2)}{(q^2 + \sigma p^2)(Q^2 - (2 - \sigma)p^2)} \right]. \tag{4.90}$$

The other elements of $T_{p,p'}$ can also been calculated for the sake of completeness, although as in the clamped case, if we consider that $G^- \to 0$ as $k \to \infty$ then these additional coefficients can be neglected in the final analysis.

Recalling that

$$\det \left| 1 - 2e^{i\Phi_f} \left(\frac{\partial G^+}{\partial n_\beta} \right) \right| = 0 \tag{4.91}$$

and using

$$\log \left(\frac{1 + iA}{1 - iA} \right) = \arctan A \tag{4.92}$$

we can extract the desired phase angle for the free edge boundary condition solution of the plate equation, found using the boundary integral method,

$$\Phi_f = -2 \arctan \frac{q}{Q} \left[\frac{(Q^2 - \sigma p^2)(q^2 + (2 - \sigma)p^2)}{(q^2 + \sigma p^2)(Q^2 - (2 - \sigma)p^2)} \right]. \tag{4.93}$$

This can then be converted into a form dependent on the angle of interaction with the boundary

$$\Phi_f = -2 \arctan \left[\frac{\sin \theta}{\sqrt{1 + \cos^2 \theta}} \left(\frac{1 + (1 - \sigma) \cos^2 \theta}{1 - (1 - \sigma) \cos^2 \theta} \right)^2 \right]. \tag{4.94}$$

Here we have seen that this alternative approach has not resulted in a new phase term for the free edge boundary condition, but instead the outcome agrees with [30]

4.4 Lower Order Contributions

In the previous section we assumed that $G^- \to 0$ in order to retrieve the phase term. While this may be the case in the first approximation, we will

now consider the effects of the lower order terms on the result in order to verify that this assumption is valid. First we look at the possibility of a correction term in the determinant of $T_{p,p'}$, putting aside the behavior of the Green functions at high frequency.

$$\det |\delta_{p,p'} - T_{pp'}| = 0 \tag{4.95}$$

can also be written

$$1 - T^{(1,1)} \left(\frac{\partial G^+}{\partial n_\beta} \right)_{p,p'} + \left(T^{(1,2)} T^{(2,1)} - T^{(1,1)} T^{(2,2)} \right) \left(\frac{\partial G^+}{\partial n_\beta} \right)_{p,p'} \left(\frac{\partial G^-}{\partial n_\beta} \right)_{p,p'}$$
$$- T^{(2,2)} \left(\frac{\partial G^-}{\partial n_\beta} \right)_{p,p'} = 0. \tag{4.96}$$

This is valid for both the clamped and the free boundary conditions; if we take the matrix entries from the clamped case, we find that

$$T^{(1,2)} T^{(2,1)} - T^{(1,1)} T^{(2,2)} = -16 \frac{iqQ}{(Q+iq)^2} - 4 \left(\frac{Q-iq}{Q+iq} \right)^2 \tag{4.97}$$

By rearranging (4.97) it becomes clear that the denominator and numerator cancel, leaving only a factor of order one. In fact, by recalling (2.63-2.65) it is obvious that all of the wave-number terms will cancel, leaving

$$T^{(1,2)} T^{(2,1)} - T^{(1,1)} T^{(2,2)} \simeq O(1). \tag{4.98}$$

Similarly for the second term

$$T^{(2,2)} = -2 \frac{Q-iq}{Q+iq}$$
$$\simeq O(1). \tag{4.99}$$

We know from previous investigations that these terms have little to no effect on the low frequency eigenvalues in the clamped case, and when you

63

do consider the Green function's behavior this is of little surprise. Is this also the case for the free boundary conditions? Are there factors of k not present in the clamped case that could make one of the additional terms contribute to the final behavior? The elements of the the transfer matrix for the free case have been calculated to be

$$T^{(1,1)} = \frac{Q(q^2 + \sigma p^2)(Q^2 - (2-\sigma)p^2) + iq(Q^2 - \sigma p^2)(q^2 + (2-\sigma)p^2)}{|M_0|}$$

(4.100)

$$T^{(1,2)} = \frac{2iQp^2(2-\sigma)(q^2 + \sigma p^2)}{|M_0|}$$

(4.101)

$$T^{(2,1)} = \frac{2qp^2(2-\sigma)(Q^2 - \sigma p^2)}{|M_0|}$$

(4.102)

$$T^{(2,2)} = \frac{-q(Q^2 - \sigma p^2)(q^2 + (2-\sigma)p^2) + iQ(q^2 + \sigma p^2)(Q^2 + (2-\sigma)p^2)}{|M_0|}$$

(4.103)

with

$$|M_0| = Q(q^2 + \sigma p^2)(Q^2 - (2-\sigma)p^2) - iq(Q^2 - \sigma p^2)(q^2 + (2-\sigma)p^2) \quad (4.104)$$

Purely by inspection it can be seen that since in all cases any k terms will cancel, all of these values will be of order one, meaning that the correction terms will also be of order one. As in the clamped case, the behavior of the Green functions will mean that the phase term obtained via this method is as valid as that for the clamped case. Of course, this has all neglected the lower order terms that were neglected during the calculation, could these have any effect? The clamped case has no such terms, but the free case will not be so clearly defined. While there are not orders of k present that could influence the 'correction terms', there may be an effect in the initial value of $T^{(1,1)}$. To investigate this, we shall recalculate the transfer matrix to include the possibility of $O(\frac{1}{k})$ terms, lower order terms than this will be neglected.

64

The elements of M_0 and $M_{p,p'}$ will now be taken as

$$M_0^{(1,1)} = -\frac{1}{iq}\left(q^2 + \sigma p^2 - i\sigma\kappa q\right) \tag{4.105}$$

$$M_0^{(1,2)} = -\frac{1}{Q}\left(Q^2 - \sigma p^2 + \sigma\kappa Q\right) \tag{4.106}$$

$$M_0^{(2,1)} = -q^2 - (2-\sigma)p^2 + 3i\kappa^2\frac{p^2}{q} \tag{4.107}$$

$$M_0^{(2,2)} = Q^2 - (2-\sigma)p^2 + 3i\kappa^2\frac{p^2}{Q} \tag{4.108}$$

and

$$M_{p,p'}^{(1,1)} = -q^2 - \sigma p^2 - i\sigma\kappa q \tag{4.109}$$

$$M_{p,p'}^{(1,2)} = Q^2 - \sigma p^2 + \sigma\kappa Q \tag{4.110}$$

$$M_{p,p'}^{(2,1)} = -(iq)\left(q^2 + (2-\sigma)p^2\right) - 3\kappa p^2 \tag{4.111}$$

$$M_{p,p'}^{(2,2)} = -Q\left(Q^2 + (2-\sigma)p^2\right) - 3\kappa p^2. \tag{4.112}$$

As used in previous calculations, (4.86) is still valid, with the elements now defined as

$$2QT^{(1,1)} = A + iB \tag{4.113}$$

$$2iqQ\det(M_0) = A - iB, \tag{4.114}$$

using

$$A = Q\left[(Q^2 - (2-\sigma)p^2)(q^2 + \sigma p^2) - 3\kappa\frac{p^2}{Q}(Q^2 - \sigma p^2)\right] \tag{4.115}$$

$$B = q\left[(Q^2 - \sigma p^2)(q^2 + (2-\sigma)p^2) + 2\kappa\frac{p^2}{q}(q^2 + \sigma p^2) + \sigma\kappa Q(Q^2 + q^2)\right]. \tag{4.116}$$

Following the same steps as before gives us a phase term of

$$\phi_f = -2\arctan\left(\frac{B}{A}\right) \tag{4.117}$$

which can also be written in terms of the angle of interaction with the boundary as

$$\phi_f = -2\arctan\left(\frac{\sin\theta}{\sqrt{1+\cos^2\theta}}\frac{C}{D}\right), \tag{4.118}$$

where

$$\begin{aligned}
C = {} & (1+(1-\sigma)\cos^2\theta)^2 k^4 \\
& +\kappa\left[\frac{3\cos^2\theta}{\sin^2\theta}(1-(1-\sigma)\cos^2\theta)+\sigma\sqrt{1+\cos^2\theta}(1+2\cos^2\theta)\right]k^3
\end{aligned} \tag{4.119}$$

$$D = (1-(1-\sigma)\cos^2\theta)^2 k^4 - \kappa\left[\frac{2\cos^2\theta}{\sqrt{1+\cos^2\theta}}(1+(1-\sigma)\cos^2\theta)\right]k^3. \tag{4.120}$$

For these terms are there regions of θ in which a high curvature will dominate the small wavenumber and produce additional effects that were neglected in the original approach? For an arbitrary value of σ if there is any point where $C < D$ then all specular reflection in that region would be suspect. In the case of circle where $\kappa = 1$ this produces the graph in figure 4.3. Here we see that $C > 0, D < 0$ for the entire range of reflections and so this situation produces valid results, however this may not be the case for all values of σ, κ and k so caution is still needed. What we can see is that at certain angles this ratio will have more of an effect than others and so investigating the effects of curvature while including lower order terms is a significant area for further study.

This corresponds to our earlier stated aims in that we have determined the existence of factors that are important to consider in the process of applying quantum mechanical methods to elastic systems. Including additional orders into account for this calculation would then include in the correction term a factor dependent upon the derivative of the curvature. In the model we are
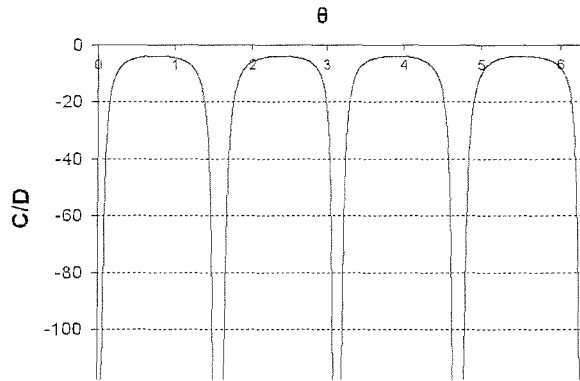
Figure 4.3: Ratio of phase calculation terms (4.119, 4.120) plotted against diffraction angle θ from 0 to 2π.

studying, this term is equal to zero and hence has no effect, however for a more complicated boundary this may have an effect and if needed can then be calculated for further accuracy.

In our verification of the derivation of the free edge boundary condition we found that the results produced in ([32]), while correct for the specific examples quoted, are not correct in the general case as stated. Instead, the conditions for the circular disk as stated in ([65]) have been shown to be correct and were used in all subsequent calculations. It was the aim to do that rederivation so that we could study the effects of curvature with accurate boundary conditions dependent on the curvature and effects of lower order k. We found here that by including terms of order $1/k$ there are more parts of the boundary condition that need to be included in the phase term calculation if we are to extract more than just the first order results, but how much of an impact do these extra parts have? As $k \to \infty$ we wouldn't expect there to be much effect at all, this term will only affect the system at low values of k and so for large numbers of eigenvalues the error distribution histograms

67
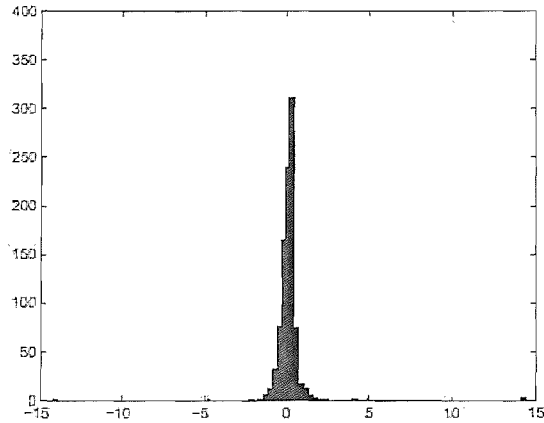
Figure 4.4: Original phase term error distribution up to $k = 500$

should be similar. Looking at figures 4.4 and 4.5 shows the distributions for the original term and the corrected term respectively for eigenvalues up to $k = 500$. The corrected term can be seen to be slightly more accurate, but not by a huge margin, as would be expected for a large number of eigenvalues. However, we already knew that the original was acceptable for $k \rightarrow \infty$, what about at low values of k?

The eigenvalues generated by the two phase terms are compared against exact solutions in figure A (Appendix A), with the errors for eigenvalues where $k \leq 50$ plotted in the histograms shown in figure 4.6 for the original term and figure 4.7 for the corrected term. Both graphs have had the initial outlier removed for clarity of presentation, but it can be seen that at the lower values of k the corrected term produces slightly more accurate. The peak in figure 4.6 appears to be more well defined than in figure 4.7, suggesting that even as $k \rightarrow 50$ the effect of the term is becoming negligible. While it is an improvement, it has to be said that there is still a fair amount of error remaining and this new term does not give us the improvement we hoped for
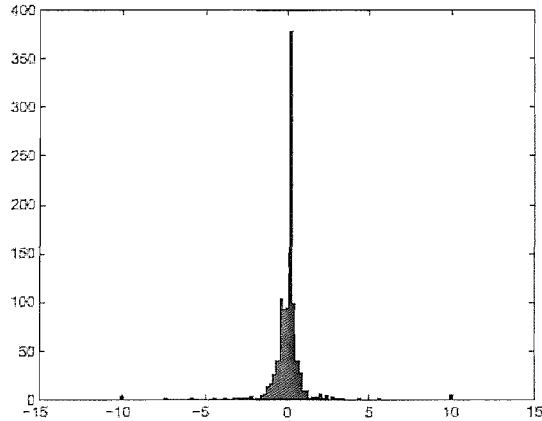
Figure 4.5: Corrected phase term error distribution up $k = 500$

in terms of determining the placement of eigenvalues.

We here find that by comparing the two graphs produced by the trace formula for the elastic system, it can be seen that in the cumulative distribution function (figure 4.9) generated by including the improved phase terms the steps are noticeably flattened. This shows us that the extra terms included in the phase factor using lower order corrections provide a significant improvement on previous results. This has little effect on the accuracy of the eigenvalues themselves, but it does show that the new term is an improvement over the original in terms of overall accuracy. While we have shown this only in the case of the simple circular disk, it is realistic to think that applying this to further cases would provide similar results.

Our initial goal was to apply quantum mechanical techniques to elastic plates and here we have shown that not only can this be done, but that current methods can be improved upon for cases such as the free edge boundary condition where lower order terms become important. The difference in the graphs (fig 4.8, 4.9) show that neglecting the lower order terms means losing
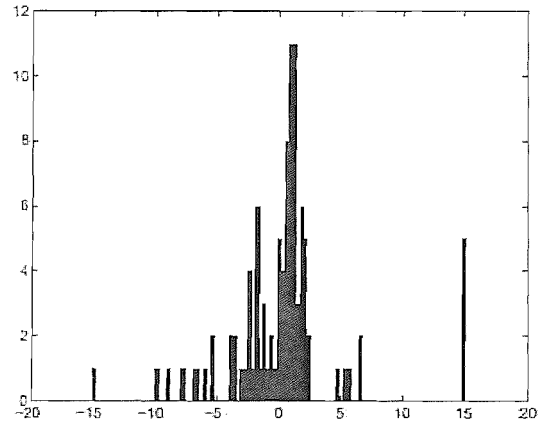
Figure 4.6: Original phase term under $k = 50$ error distribution
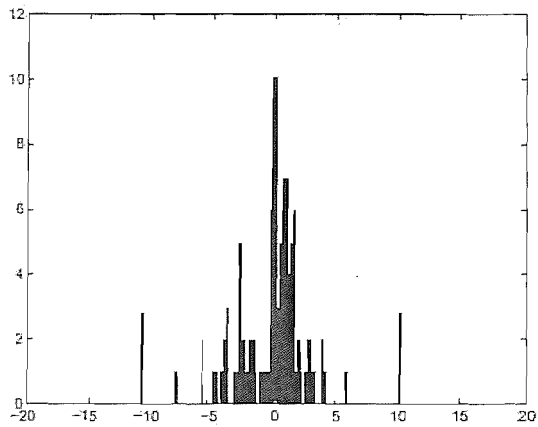
Figure 4.7: Corrected phase term under $k = 50$ error distribution
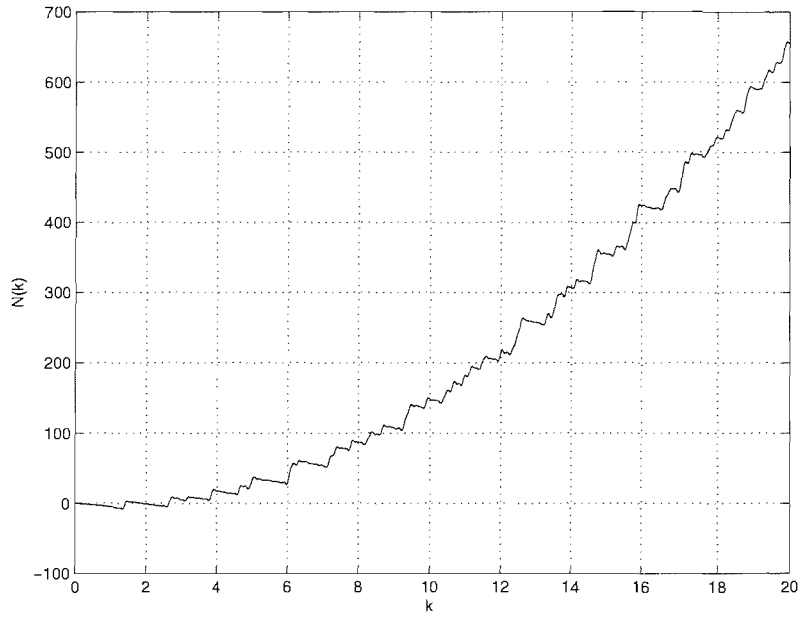
Figure 4.8: Original phase term cumulative frequency up to $k = 20$
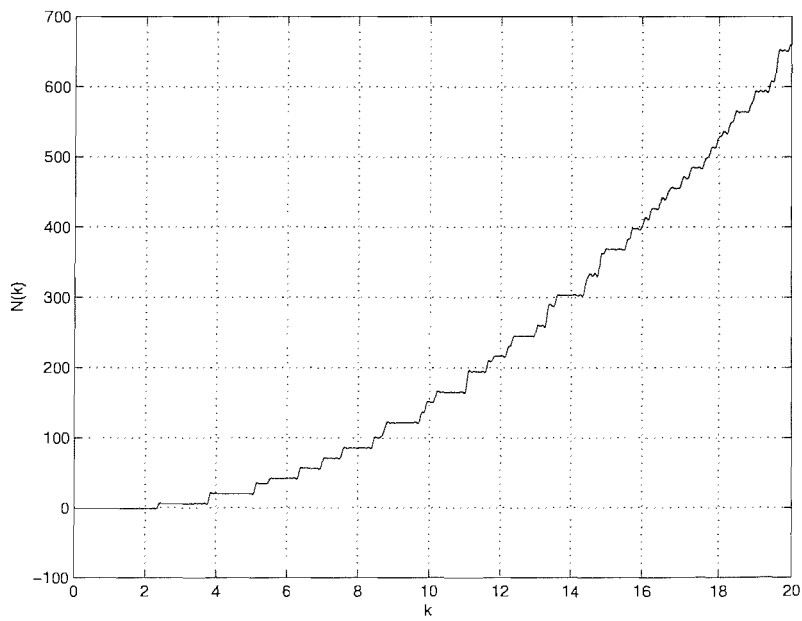
Figure 4.9: Corrected phase term cumulative frequency up to $k = 20$

vital information and hence they should be included even in simple cases such as this. This will be even more appropriate given study of cases where the curvature of the boundary is more complicated.

Chapter 5

Diffractive Effects in the

Circular Plate

We saw in the previous chapter that in certain cases, such as those of extreme curvature, the phase terms calculated by Bogomolny were not correct. It is the aim of this chapter to consider such cases, and examine the feasibility of modeling semiclassical effects on plates where diffractive effects are present, this will be looked at for both the pinched and the annulus scattering cases. We begin by presenting the quantum mechanical approach to solving a simple billiard diffraction problem, which will be considered later in the chapter for the plate case.

5.1   Quantum Mechanical Diffraction

In the case of a disk C in two dimensions under Dirichlet boundary conditions, the system can considered as a quantum billiard with an associated Green function that is a solution of

$$(\nabla^2 + k^2)G(\mathbf{r}, \mathbf{r}'; k) \;=\; \delta(\mathbf{r} - \mathbf{r}'), \qquad \mathbf{r}, \mathbf{r}' \in C \tag{5.1}$$

$$(\nabla^2 + k^2)G(\mathbf{r}, \mathbf{r}'; k) = 0, \qquad \mathbf{r}, \mathbf{r}' \in \partial C. \tag{5.2}$$

In the region away from the discontinuity and boundary, the $G(\mathbf{r}, \mathbf{r}'; k)$ will behave as the free Green function $G_f(\mathbf{r}, \mathbf{r}'; k)$, where

$$G_f(\mathbf{r}, \mathbf{r}'; k) = -\frac{i}{4} H_0^{(+)}(k|\mathbf{r} - \mathbf{r}'|). \tag{5.3}$$

If wave decompositions of both the free Green function and the delta function are performed and then substituted back into (5.1), after performing an integration to remove the delta function we can then rewrite the free Green function in the form

$$G_f(\mathbf{r}, \mathbf{r}'; k) = \sum_{m=-\infty}^{\infty} [A(kr') J_m(kr) + B(kr') N_m(kr)] \, e^{im(\theta - \theta')}. \tag{5.4}$$

Where A and B are constants and θ and θ' define the angle of interaction with the diffracting point. To model diffractive effects we now consider a disk of radius a as the scattering center, writing the solution of (5.1) as the sum of the free Green Function and a diffractive correction.

$$G(\mathbf{r}, \mathbf{r}'; k) = G_f(\mathbf{r}, \mathbf{r}'; k) + G_d(\mathbf{r}, \mathbf{r}'; k), \qquad r' \geq r \tag{5.5}$$

where

$$G_d(\mathbf{r}, \mathbf{r}'; k) = \frac{i}{4} \sum_{m=-\infty}^{\infty} e^{im(\theta - \theta')} H_m^{(+)}(kr') \left(H_m^{(-)}(kr) - \frac{H_m^{(+)}(ka)}{H_m^{(+)}(ka)} H_m^{(+)}(kr) \right) \tag{5.6}$$

This is taken for the disk case from the more general formula

$$G_d(\mathbf{r}, \mathbf{r}'; k) = \frac{i}{4} \sum_{m=-\infty}^{\infty} (S_m(k) - 1) H_m^+(kr') H_m^+(kr) e^{im(\theta - \theta')} \tag{5.7}$$

that includes the term $S_m(k)$, the matrix ([42], [43]) that determines the scattering behavior of the wave m. Investigation of this scattering matrix
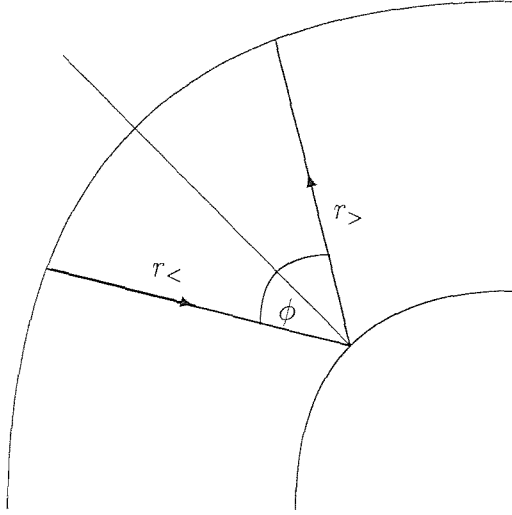
Figure 5.1: Scattering at angle θ from an annulus

would allow a wide variety of physical properties to be modeled, however in the case studied here we restrict the effects to simple behavior as we are looking at the general applicability and not specific cases. Now (5.5) can be rearranged and written [44] in a form

$$G(\mathbf{r}, \mathbf{r}'; k) = G_f(\mathbf{r}, \mathbf{r}'; k) + G_f(\mathbf{r}, \zeta; k) d(\phi) G_f(\zeta, \mathbf{r}'; k). \qquad (5.8)$$

The diffraction coefficient $d(\phi)$ is dependent on the angle ϕ that separates two points $\mathbf{r}$ and $\mathbf{r}'$ from the scattering center ζ as seen in figure 5.1.

In this assumption the system has been simplified to considering the problem as a the case of two semi-infinite line meeting at the scattering point, hence effects from the external boundary are assumed to not have an influence in the locality of the discontinuity introduced. This gives us in the case of the disk billiard

$$d(\phi) = -4i \sum_{m=-\infty}^{\infty} e^{im(\phi-\pi)} \frac{J_m(ka)}{H_m^{(+)}} \qquad (5.9)$$

75

suggesting that the the Green function structure composed of the free Green function plus a correction term is valid for a disk as well as for a wedge. Problems such as these can be extended [45] to include potentials $V(x)$ acting as scatterers, in the case studied here it assumed that any potential is essentially constant in the region of influence and as such does not alter the wavelength. It is our aim to apply this method to the elastic disk and determine validity of such an application, which means that we must first describe the system to which it shall be applied.

5.2 Pinched Circular Plate

With the later use of the diffraction coefficient method in mind, we shall first examine simple systems that such a process could be applied to. This will enable us to look at diffractive effects in plate scenarios and determine if there is a link between the quantum methods and the elastic plate solutions.

5.2.1 Pinched Model

For the *pinched* disk, a solution can be found by adding the extra condition that the Green function and its derivative are also equal to zero at the center point, treated as an inner boundary with radius that tends to zero. A physical example of this is a cymbal with the edge held in place as is the center clamped support. In the case of the pinched disk, the solution to the plate equation is given by:

$$
\begin{aligned}
G(\mathbf{r}, \mathbf{r}') \;=\; \sum_m \Big\{ &\frac{i}{8k^2} H_m(kr) J_m(kr') - \frac{1}{4\pi k^2} K_m(kr) I_m(kr') \\
&+ x_m J_m(kr) + y_m Y_m(kr) + u_m I_m(kr) + v_m K_m(kr) \Big\}\, e^{[im(\theta - \theta')]}
\end{aligned}
$$

(5.10)

76

with x_m, y_m, u_m and v_m being defined as ratios of determinants of matrices that are composed of various combinations of Bessel functions. For the unit disk

$$\Delta\rho(k) = \int_0^{2\pi} \int_0^1 dr\, d\theta \lim_{r\to r_0} \Delta G(r, r; k), \tag{5.11}$$

the numerical computations for the eigenvalue solutions of this system can be then be investigated by applying this variation of the oscillating semiclassical level density. This will be expanded upon in a later section, first we need to establish in which cases the periodic orbits alter the level eigenvalues.

5.2.2 Non-Pinched Correspondence

We will now examine the Green function solution to the plate equation, and in comparison to the solution to the membrane case, determine which orbits will have an effect on the eigenvalues and need to be taken into account for the modifications. The Green function solutions for the plate equation can be written as

$$\begin{aligned}
G(r, r') &= G_0(r, r') + G_1(r, r'), &\tag{5.12} \\
G_0(r, r') &= \frac{i}{8k^2} H_m^+(kr) J_m(kr') - \frac{1}{4\pi k^2} K_m(kr) I_m(kr'), &\tag{5.13} \\
G_1(r, r') &= x_m J_m(kr) + y_m Y_m(kr) + u_m I_m(kr) + v_m K_m(kr). &\tag{5.14}
\end{aligned}$$

For the clamped case, the boundary conditions are as follows. These describe the system clamped at the exterior ($r = R$) and pinched at the center ($r = a$)

$$G\big|_{r=R} = 0, \qquad \frac{\partial G}{\partial n}\bigg|_{r=R} = 0, \tag{5.15}$$

$$G\big|_{r=a} = 0, \qquad \frac{\partial G}{\partial n}\bigg|_{r=a} = 0. \tag{5.16}$$

77

By imposing clamped boundary conditions on the above Green function, the following coefficients can be determined;

$$x_m = \frac{D_m^{(1)}}{D_m}, \qquad y_m = \frac{D_m^{(2)}}{D_m}, \qquad u_m = \frac{D_m^{(3)}}{D_m}, \qquad v_m = \frac{D_m^{(4)}}{D_m}, \qquad (5.17)$$

where

$$D_m^{(1)} = \begin{vmatrix} A_m^{(1)} & Y_m(kR) & I_m(kR) & K_m(kR) \\ A_m^{(2)} & Y_m'(kR) & I_m'(kR) & K_m'(kR) \\ A_m^{(3)} & Y_m(ka) & I_m(ka) & K_m(ka) \\ A_m^{(4)} & Y_m'(ka) & I_m'(ka) & K_m'(ka) \end{vmatrix}, \qquad (5.18)$$

$$D_m^{(2)} = \begin{vmatrix} J_m(kR) & A_m^{(1)} & I_m(kR) & K_m(kR) \\ J_m'(kR) & A_m^{(2)} & I_m'(kR) & K_m'(kR) \\ J_m(ka) & A_m^{(3)} & I_m(ka) & K_m(ka) \\ J_m'(ka) & A_m^{(4)} & I_m'(ka) & K_m'(ka) \end{vmatrix}, \qquad (5.19)$$

$$D_m^{(3)} = \begin{vmatrix} J_m(kR) & Y_m(kR) & A_m^{(1)} & K_m(kR) \\ J_m'(kR) & Y_m'(kR) & A_m^{(2)} & K_m'(kR) \\ J_m(ka) & Y_m(ka) & A_m^{(3)} & K_m(ka) \\ J_m'(ka) & Y_m'(ka) & A_m^{(4)} & K_m'(ka) \end{vmatrix}, \qquad (5.20)$$

$$D_m^{(4)} = \begin{vmatrix} J_m(kR) & Y_m(kR) & I_m(kR) & A_m^{(1)} \\ J_m'(kR) & Y_m'(kR) & I_m'(kR) & A_m^{(2)} \\ J_m(ka) & Y_m(ka) & I_m(ka) & A_m^{(3)} \\ J_m'(ka) & Y_m'(ka) & I_m'(ka) & A_m^{(4)} \end{vmatrix}, \qquad (5.21)$$

$$D_m = \begin{vmatrix} J_m(kR) & Y_m(kR) & I_m(kR) & K_m(kR) \\ J_m'(kR) & Y_m'(kR) & I_m'(kR) & K_m'(kR) \\ J_m(ka) & Y_m(ka) & I_m(ka) & K_m(ka) \\ J_m'(ka) & Y_m'(ka) & I_m'(ka) & K_m'(ka) \end{vmatrix}, \qquad (5.22)$$

with

$$A_m^{(1)} = \frac{1}{4\pi k^2} K_m(kR) I_m(kr') - \frac{i}{8k^2} H_m(kR) J_m(kr'), \qquad (5.23)$$

78

$$A_m^{(2)} = \frac{1}{4\pi k^2} K_m'(kR) I_m(kr') - \frac{i}{8k^2} H_m'(kR) J_m(kr'), \qquad (5.24)$$

$$A_m^{(3)} = \frac{1}{4\pi k^2} K_m(kr') I_m(ka) - \frac{i}{8k^2} H_m(kr') J_m(ka), \qquad (5.25)$$

$$A_m^{(4)} = \frac{1}{4\pi k^2} K_m(kr') I_m'(ka) - \frac{i}{8k^2} H_m(kr') J_m'(ka). \qquad (5.26)$$

As the case where a tends to zero is being studied, the asymptotics for small arguments can be substituted for the Bessel functions with a terms in the argument [46],

$$J_m(ka) \sim \frac{1}{m!}\left(\frac{ka}{2}\right)^m, \qquad J_m'(ka) \sim \frac{1}{2(m-1)!}\left(\frac{ka}{2}\right)^{m-1}, \quad (5.27)$$

$$Y_m(ka) \sim -\frac{(m-1)!}{\pi \left(\frac{ka}{2}\right)^m}, \qquad Y_m'(ka) \sim \frac{m!}{2\pi \left(\frac{ka}{2}\right)^{m+1}}, \qquad (5.28)$$

$$I_m(ka) \sim \frac{1}{m!}\left(\frac{ka}{2}\right)^m, \qquad I_m'(ka) \sim \frac{1}{2(m-1)!}\left(\frac{ka}{2}\right)^{m-1}, \quad (5.29)$$

$$K_m(ka) \sim \frac{(m-1)!}{2\left(\frac{ka}{2}\right)^m}, \qquad K_m'(ka) \sim -\frac{m!}{4\left(\frac{ka}{2}\right)^{m+1}}. \qquad (5.30)$$

In the case where $a \to 0$ and $m \neq 0$, it can be seen that $J_m(ka) \to 0$, $I_m(ka) \to 0$ and also the derivatives tend to zero With these values tending to zero it becomes obvious that $A_m^3 \to 0$ and $A^4 \to 0$ also. Without evaluating the other matrix entries, this gives us

$$D_m^{(1)} = \begin{vmatrix} A_m^{(1)} & Y_m(kR) & I_m(kR) & K_m(kR) \\ A_m^{(2)} & Y_m'(kR) & I_m'(kR) & K_m'(kR) \\ 0 & Y_m(ka) & 0 & K_m(ka) \\ 0 & Y_m'(ka) & 0 & K_m'(ka) \end{vmatrix}, \qquad (5.31)$$

$$D_m^{(2)} = \begin{vmatrix} J_m(kR) & A_m^{(1)} & I_m(kR) & K_m(kR) \\ J_m'(kR) & A_m^{(2)} & I_m'(kR) & K_m'(kR) \\ 0 & 0 & 0 & K_m(ka) \\ 0 & 0 & 0 & K_m'(ka) \end{vmatrix}, \qquad (5.32)$$

79

$$
D_m^{(3)} = \begin{vmatrix} J_m(kR) & Y_m(kR) & A_m^{(1)} & K_m(kR) \\ J'_m(kR) & Y'_m(kR) & A_m^{(2)} & K'_m(kR) \\ 0 & Y_m(ka) & 0 & K_m(ka) \\ 0 & Y'_m(ka) & 0 & K'_m(ka) \end{vmatrix}, \tag{5.33}
$$

$$
D_m^{(4)} = \begin{vmatrix} J_m(kR) & Y_m(kR) & I_m(kR) & A_m^{(1)} \\ J'_m(kR) & Y'_m(kR) & I'_m(kR) & A_m^{(2)} \\ 0 & Y_m(ka) & 0 & 0 \\ 0 & Y'_m(ka) & 0 & 0 \end{vmatrix}. \tag{5.34}
$$

Here it can be seen that $D_m^{(2)}$ and $D_m^{(4)}$ are equal to zero meaning that only x_m and u_m have non-zero values. This corresponds to the unpinched case, where only the equivalent coefficients are non-zero. When $m = 0$ however, this behavior alters, and the coefficients are different from those of the unpinched case. These calculations can be performed in a more rigorous fashion by expanding about $a = 0$ and then letting $a \to 0$ whilst removing the tail of the expansion, in which case we find that the coefficients correspond exactly to the unpinched case except when $m = 0$. This is as we would expect for the case where diffractive orbits contribute in the $m = 0$ case due to the point scattering about the pinched center of the disk. We shall use this fact to alter the trace formula solution investigated in 3) and include diffractive effects in its results.

5.3 Trace Formula Modifications

Having established the fact that only the orbits that pass through the center of a pinched plate, i.e. the $m = 0$ terms will effect solutions in the pinched case, we can now construct a modification term to apply to the trace formula in order to now produce eigenvalues for the pinched case so that we can verify
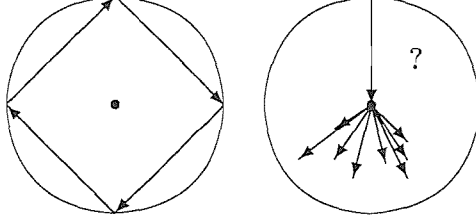
Figure 5.2: In periodic orbits which do not come in contact with the center point there is no diffraction and hence will produce the same results for both pinched and unpinched cases. When an axisymmetric orbit is considered, there will an interaction that will distinguish the two cases.

the applicability of this method to a an elastic case involving diffractive terms.

5.3.1 Diffractive Correction Term

We have already stated that for the unit disk

$$\Delta\rho(k) = \int_0^{2\pi} \int_0^1 dr\, d\theta \lim_{r \to r_0} \Delta G(r, r; k). \tag{5.35}$$

By only considering the periodic orbits that would interact with the center diffractive point, we are able to isolate the contributions of the axisymmetric case

$$\delta\rho_{pin}(k) = \lim_{\epsilon \to 0} \Im \left(\frac{J_0'(k + i\epsilon)}{k J_0(k + i\epsilon)} \right) \tag{5.36}$$

Now substitute the Bessel functions with their associated asymptotic expansions and convert to hyperbolic form to obtain

$$\delta\rho_{pin}(k) = \lim_{\epsilon \to 0} \Im \left(\frac{e^{ik-\epsilon} - e^{-ik+\epsilon}}{i \left[e^{i(k+i\epsilon)} + e^{-i(k+i\epsilon)} \right]} \right) \tag{5.37}$$

$$= \lim_{\epsilon \to 0} \Im \left(-\frac{1}{i} \frac{(1 - e^{2ik-2\epsilon})}{(1 + e^{2ik-2\epsilon})} \right) \tag{5.38}$$

$$= \lim_{\epsilon \to 0} \Im \left(i(1 - e^{2ik-2\epsilon}) \sum_{r=0}^{\infty} (-e^{2ik-2\epsilon})^r \right) \tag{5.39}$$

81

$$= \lim_{\epsilon \to 0} \left(1 + 2 \sum_{r=1}^{\infty} (-1)^r \cos(2kr - 2\epsilon r) \right) \quad (5.40)$$

$$= 1 + 2 \sum_{r=1}^{\infty} (-1)^r \cos(2kr). \quad (5.41)$$

This gives the $n = 0$ correction term for the pinched disk

$$\delta \rho_{pin}(k) = 1 + 2 \sum_{r=1}^{\infty} (-1)^r \cos(2kr) = 1 + 2 \sum_{r=1}^{\infty} \cos(\pi r) \cos(2kr),$$

$$(5.42)$$

compare this to the $n = 0$ term for the unpinched disk

$$\delta \rho_{unp}(k) = 1 + 2 \sum_{r=1}^{\infty} \cos(2kr). \quad (5.43)$$

The original trace formula solution can now be modified to take these corrections into account,

$$\delta \rho_{cor}(k) = \delta \rho(k) + \delta \rho_{pin}(k) - \delta \rho_{unp}(k)$$

$$= \delta \rho(k) + 2 \sum_{r=1}^{\infty} \cos(2kr) \left[\cos(\pi r) - 1 \right]. \quad (5.44)$$

This equation can now be looked at to determine if it produces useful results for modeling diffractive effects in a pinched plate. We shall do this by comparing numerical results computed from this formula with other results available from alternative methods.

5.3.2   Results and Comparisons

In figures 5.3 and 5.4, the peaks above the $g = 0$ axis represent the eigenvalues found by using the trace formula method and its associated correction terms. The peaks below the axis, if present, are the solutions found by the EBK method, along with solutions for $n \geq 1$. By comparing the simply
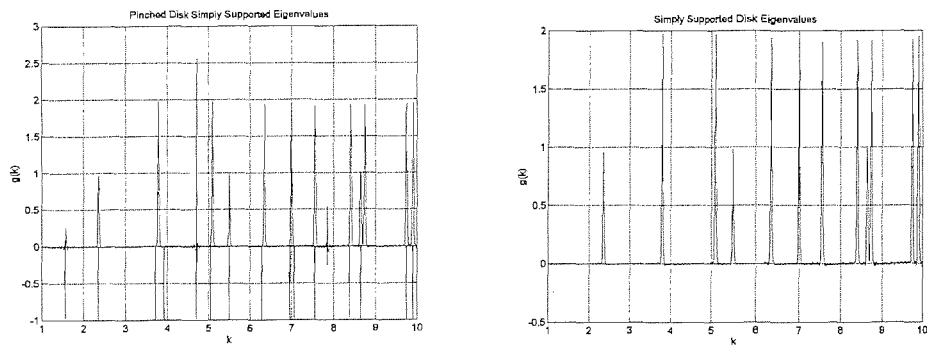
Figure 5.3: Simply supported disk eigenvalues, on the left with and on the right without center condition
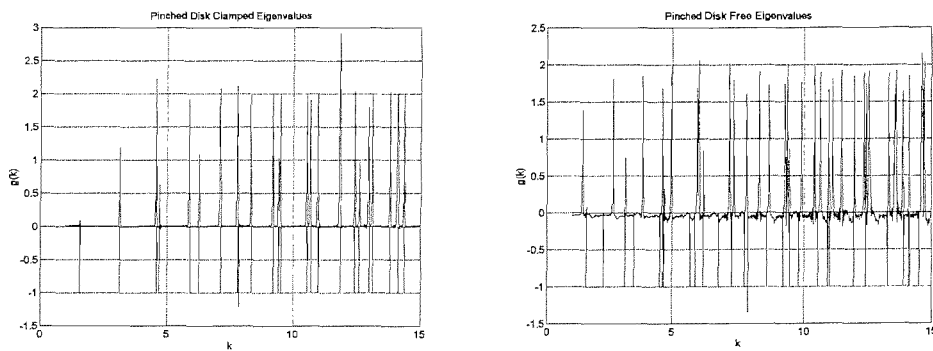
Figure 5.4: Clamped (left) and free (right) disk eigenvalues

83

supported case with and without the additional center condition, the extra eigenvalues produced by the pinch can be identified. For the clamped and simply supported cases, it can be seen that the two methods agree particularly well, the free case is a little less accurate, however the $m = 0$ peaks are presents, thus verifying the earlier calculations that showed the $m = 0$ case will be altered in the pinched case.

In these cases the boundary is still smooth, but internally the orbits are bouncing off of an internal scatterer, so what have we learnt from studying the pinched disk? There is a clash of limits affecting the results, but we have seen that further investigation is warranted into the effects of a scatterer on the eigenvalues of a plate as the study of the trace formula method has shown that it can be be used to identity eigenvalues of certain billiards and plates, indicating that including semiclassical diffractive effects is possible for plates.

5.4 Scattering From An Annulus Plate

While the pinched disk model provides us with a glimpse into the application of diffractive effects in semiclassical systems, it is only a simple case in that it avoids certain important limit considerations by having a well determined zero radius center scatterer. In real systems this will not be the case and so we look to extended this to the annulus disk scatterer.

Depending on the value of ka these systems will behave differently, as would be expected. If $ka \gg 1$ then the orbits tend toward acting as in a general geometrically scattered structure, whereas in the case of $ka \to 0$ the effect of the scatterer will become increasingly small, but still producing a noticeable effect. This can be seen by looking at the *s-wave limit*. In this limit, only the orbits that would otherwise pass directly through the

scatterer have any effect upon the system. For the problem looked at in the beginning of this chapter, the use of the quantum mechanical approach returns a diffraction coefficient [44] of

$$d \approx \frac{2\pi}{log\left(\frac{2}{ka}\right) - \gamma_e + \frac{i\pi}{2}},\tag{5.45}$$

where $\gamma_e \sim 0.577$ is Euler's constant. This form of d is valid for small ka and can be seen to be independent of the scattering angle ϕ. We shall examine a similar case for the plate later in this chapter with the goal of finding a similar diffraction condition.

5.4.1 EBK Comparison

How do diffractive effects change the semiclassical behavior when modeled on the plate? We shall now investigate this plate problem by looking at the comparison to the EBK results in order to question the assumption that it is only the $m = 0$ orbits that interact directly with a pinched center. The system being studied is a circular disk of radius a with a clamped point at $r = 0$. In order to transfer this to a more general case this point is assumed to be an annulus of radius b, where $b \to 0$. Due to the discontinuity at the clamp, the general solution can be written as a sum of Bessel functions

$$w_m = AJ_m(kr) + BY_m(kr) + CI_m(kr) + DK_m(kr),\tag{5.46}$$

the conditions on the outer edge at $r = a$ are determined by (2.56-2.61). At first the $n = 0$ cases will be calculated to determine if these results match with those obtained from the EBK calculations. As an extra check, the general n case will then be studied to ensure the validity of the $n = 0$ calculations and that the method is not limited to one case. As the center clamp will be in place for all variations of this system, its effects can be considered here.
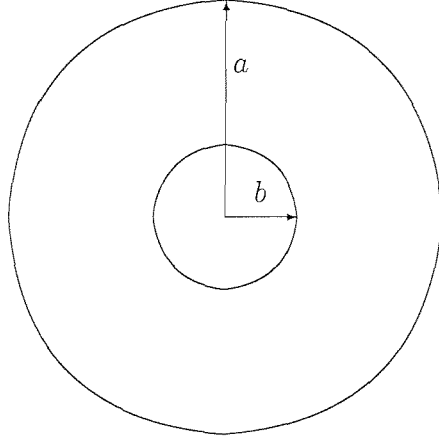
Figure 5.5: Annulus plate with outer radius a and inner radius b.

The condition for the clamp is the same as a standard clamped boundary condition

$$w_m\big|_b = 0, \tag{5.47}$$

$$\frac{\partial w_m}{\partial r}\bigg|_b = 0. \tag{5.48}$$

For the $n = 0$ case this gives

$$AJ_0(kb) + BY_0(kb) + CI_0(kb) + DK_0(kb) = 0, \tag{5.49}$$

$$AJ_1(kb) + BY_1(kb) - CI_1(kb) + DK_1(kb) = 0. \tag{5.50}$$

By examining the behavior of these equations under L'Hopital's rule

$$Y_m(x) = \frac{2}{\pi}\left(\ln\left(\frac{x}{2}\right) + \gamma\right)J_m(x) - F_1(x, m) \tag{5.51}$$

$$K_m(x) = (-1)^{m+1}\left(\ln\left(\frac{x}{2}\right) + \gamma\right)I_m(x) + F_2(x, m) \tag{5.52}$$

where $\gamma = 0.5772...$ is Euler's constant and $F_1(x, m)$ and $F_2(x, m)$ are correction sums, it can be seen that

$$A + C - D(\gamma - \ln 2) + \frac{2B}{\pi}(\gamma - \ln 2) = 0. \tag{5.53}$$

Hence

$$C = -A \tag{5.54}$$

$$D = \frac{2B}{\pi} \tag{5.55}$$

Similar constants are assumed for the general n case. Inserting these constants into the boundary conditions will now be looked at to see what effect if any varying these may have.

5.4.2   Axisymmetric Solution

Clamped

The external boundary conditions for this case give:

$$AJ_0(ka) + BY_0(ka) + CI_0(ka) + DK_0(ka) = 0 \tag{5.56}$$

$$AJ_1(ka) + BY_1(ka) - CI_1(ka) + DK_1(ka) = 0. \tag{5.57}$$

Substitute (5.54),(5.55) and rearrange to obtain

$$A(J_0(ka) - I_0(ka)) = -B\left(Y_0(ka) + \frac{2}{\pi}K_0(ka)\right) \tag{5.58}$$

$$A(J_1(ka) + I_1(ka)) = -B\left(Y_1(ka) + \frac{2}{\pi}K_1(ka)\right). \tag{5.59}$$

Divide (5.58) by (5.59) to give

$$\frac{J_0(ka) - I_0(ka)}{J_1(ka) - I_1(ka)} = \frac{Y_0(ka) + \frac{2}{\pi}K_0(ka)}{Y_1(ka) + \frac{2}{\pi}K_1(ka)}. \tag{5.60}$$

By only taking the highest order terms and replacing the Bessel functions with their associated asymptotic expansions for large k

$$J_m(x) \sim \sqrt{\frac{2}{\pi x}}\cos\left(x - \frac{\pi}{4} - \frac{m\pi}{2}\right), \tag{5.61}$$

$$Y_m(x) \sim \sqrt{\frac{2}{\pi x}}\sin\left(x - \frac{\pi}{4} - \frac{m\pi}{2}\right), \tag{5.62}$$

$$I_m(x) \sim \frac{e^x}{\sqrt{2\pi x}}, \tag{5.63}$$

$$K_m(x) \sim \frac{e^{-x}}{\sqrt{2\pi x}}, \tag{5.64}$$

in each part of the equation, (5.60) can be reduced to

$$-\frac{I_0(ka)}{I_1(ka)} = \frac{Y_0(ka)}{Y_1(ka)}$$

$$-1 = \tan\left(ka - \frac{\pi}{4}\right). \tag{5.65}$$

With this case taken using $a = 1$

$$k = m\pi + \frac{\pi}{2}. \tag{5.66}$$

Free

For the $n = 0$ case, the boundary conditions (2.60) and (2.61) reduce to

$$\frac{\partial}{\partial r}\left(\frac{1}{r}\frac{\partial}{\partial r}\left(r\frac{\partial w_0}{\partial r}\right)\right) = 0, \tag{5.67}$$

$$\frac{\partial}{\partial r}\left(\frac{\partial w_0}{\partial r} + \frac{\sigma}{a}w_0\right) = 0. \tag{5.68}$$

Things are simplified if derivatives of order 2 or higher are written in terms of lower orders. The formulae for this are given by

$$\frac{\partial^3 J_n}{\partial r^3} = -\frac{1}{r}\frac{\partial^2 J_n}{\partial r^2} + \left(\frac{1}{kr^2} - k^3\right)\frac{\partial J_n}{\partial r}, \tag{5.69}$$

$$\frac{\partial^3 I_n}{\partial r^3} = -\frac{1}{r}\frac{\partial^2 I_n}{\partial r^2} + \left(\frac{1}{kr^2} + k^3\right)\frac{\partial I_n}{\partial r}, \tag{5.70}$$

$$\frac{\partial^2 J_n}{\partial r^2} = -\frac{1}{r}\frac{\partial J_n}{\partial r} - \left(k^2 - \frac{n^2}{r^2}\right)J_n, \tag{5.71}$$

$$\frac{\partial^2 I_n}{\partial r^2} = -\frac{1}{r}\frac{\partial I_n}{\partial r} + \left(k^2 + \frac{n^2}{r^2}\right)I_n. \tag{5.72}$$

The functions Y_n and K_n behave similarly to J_n and I_n respectively. Using (5.69)-(5.72), (5.67) and (5.68) can be rewritten as

$$A[J_1(ka) - I_1(ka)] = -B\left[Y_1(ka) + \frac{2}{\pi}K_1(ka)\right] \tag{5.73}$$

88

and

$$A \left[J_0(ka) + I_0(ka) - \frac{1-\sigma}{ka} \left(J_1(ka) + I_1(ka) \right) \right]$$
$$= -B \left[Y_0(ka) - \frac{2}{\pi} K_0(ka) - \frac{1-\sigma}{ka} \left(Y_1(ka) + \frac{2}{\pi} K_1(ka) \right) \right]. \qquad (5.74)$$

Rearranging to remove A and B gives us

$$\frac{Y_0(ka)}{Y_1(ka)} = 2 \left(\frac{1-\sigma}{ka} \right) - \frac{I_0(ka)}{I_1(ka)}. \qquad (5.75)$$

As we are considering the case where $k \to \infty$, the $\frac{1-\sigma}{ka}$ term is negligible and we are left, by following a similar method as for the clamped case, with

$$k = m\pi + \frac{\pi}{2}. \qquad (5.76)$$

Simply Supported

As we are considering the $n = 0$ case, the boundary conditions now reduce to

$$\frac{\partial^2 w_0}{\partial r^2} + \frac{\sigma}{a} \frac{\partial w_0}{\partial r} = 0, \qquad (5.77)$$

$$w_0 = 0. \qquad (5.78)$$

Substituting (5.46) gives

$$A \left[-\frac{k^2}{2} (I_0 + I_2) - \frac{k\sigma}{a} I_1 - \frac{k^2}{2} (J_0 - J_2) - \frac{k\sigma}{a} J_1 \right]$$
$$= B \left[-\frac{k^2}{\pi} (K_0 + K_2) + \frac{2k\sigma}{a\pi} K_1 + \frac{k^2}{2} (Y_0 - Y_2) + \frac{k\sigma}{a} Y_1 \right] \qquad (5.79)$$

and

$$A (J_0(ka) - I_0(ka)) = -B \left(Y_0(ka) + \frac{2}{\pi} K_0(ka) \right). \qquad (5.80)$$

From here (5.79) can be written as

$$A \left[-kI_0 - \frac{\sigma}{a} I_1 - kJ_0 - \frac{\sigma}{a} J_1 \right] = B \left[-\frac{2k}{\pi} K_0 + \frac{2\sigma}{a\pi} K_1 + kY_0 + \frac{\sigma}{a} Y_1 \right]. (5.81)$$

Using (5.80) and (5.81) and the same method as the previous cases gives

$$\cos(ka) = \sin(ka) \qquad (5.82)$$

and hence

$$k = m\pi + \frac{\pi}{4}. \qquad (5.83)$$

These problems can also be considered in a more general case by solving with additional terms, the solutions being consistent with the simple cases. What we see is that the addition of the clamped conditions at the center of the disk will only affect the $m = 0$ solutions in the case of the pinched disk, as these are the only orbits that will interact with this diffractive point. However, although the clamped and free cases both give the same result for $m = 0$ as expected, the simply supported case is different. It was originally thought that due to the local nature of the problem involving the addition of a point at the center of the disk, the axisymmetric orbits would interact with this point only and that external boundary conditions would not be relevant. It has been seen from this work that either the method used is incomplete, or that the boundary conditions do indeed have an effect on the $m = 0$ eigenvalues. The $m = 0$ solutions for all these cases match with published results [31], leading to the conclusion that the addition of the center clamp is not necessarily as local a problem as originally thought and that by extending it to include scattering by an annulus we can now investigate the use of the quantum mechanical techniques presented at the beginning of the chapter on this system.

5.4.3 Elastic Plate Scattering Model

In the light of earlier work suggesting that effects due to diffraction may not be as local a problem as originally conceived, another approach is attempted

here in order to try and find a reason for this. For this case we need to solve

$$(\nabla^4 + k^4)U = \delta(\underline{r} - \underline{r}').\tag{5.84}$$

It is known that $U = G(\underline{r}, \underline{r}'; k)$ is a solution for this system, in order to find the find the construction of G we need to consider that it will be the sum of two elements, G_f and G_S

$$G(\mathbf{r}, \mathbf{r}'; k) = G_f(\mathbf{r}, \mathbf{r}'; k) + G_S(\mathbf{r}, \mathbf{r}'; k)\tag{5.85}$$

As developed by Keller [4], G_S is said to have the structure

$$G_S(\mathbf{r}, \mathbf{r}'; k) = \frac{\hbar^2}{2m} G_f(\mathbf{r}, \mathbf{r}'; k) d(\theta) G_f(\mathbf{r}, \mathbf{r}'; k)\tag{5.86}$$

with θ being the scattering angle at the point of interaction with the scatterer. The free Green function for this system, G_f is

$$G_f = AH_0^+(kr) + BK_0(kr).\tag{5.87}$$

The scattering Green function G_S is what needs to be determined for this problem in order to complete the structure of G. We first expand the components in (5.84) to give

$$G(\underline{r}, \underline{r}'; k) = \sum_{m=-\infty}^{+\infty} g_m(r, r') e^{im(\theta - \theta')},\tag{5.88}$$

$$\delta(\underline{r} - \underline{r}') = \frac{1}{2\pi r} \delta(r - r') \sum_{m=-\infty}^{+\infty} e^{im(\theta - \theta')}.\tag{5.89}$$

We can then use the radial form of ∇^4 in order to rewrite (5.84)

$$\nabla^4 = \partial_r^4 + \frac{2}{r}\partial_r^3 - \frac{1}{r^2}\partial_r^2 + \frac{1}{r}\partial_r + \frac{2}{r^2}\partial_r^2\partial_\theta^2 + \frac{4}{r^4}\partial_\theta^2 + \frac{1}{r^4}\partial_\theta^4\tag{5.90}$$

$\Rightarrow$

$$\sum_{m=-\infty}^{+\infty} \left\{ g^{(4)} + \frac{2}{r} g^{(3)} - f_1(r) g^{(2)} + f_2(r) g^{(1)} + f_3(r) g \right\} e^{im(\theta - \theta')}$$

$$= \frac{1}{2\pi r} \delta(r - r') \sum_{m=-\infty}^{+\infty} e^{im(\theta - \theta')},\tag{5.91}$$

91

where $g^{(n)} = \partial_r^n g$, and f_1, f_2 and f_3 are functions of r giving the relevant coefficients. In order to contain all possible elements of the waves, we can write

$$g_{m1}(r, r') = AH_m^+(kr) + BH_m^-(kr) + CI_m(kr) + DK_m(kr) \quad (5.92)$$
$$\text{for } a < r < r'$$

$$g_{m2}(r, r') = EH_m^+(kr) + FK_m(kr) \quad (5.93)$$
$$\text{for } r' < r < \infty$$

There are several conditions for this system that need to be defined if we are to investigate further.

1. The inner radius is clamped, giving

$$g_m(r, r')|_{r=a} = 0$$
$$\text{and } \partial_r g_m(r, r')|_{r=a} = 0.$$

2. The two expansions for g_m need to be continuous as $r = r'$, hence

$$g_{m1}(r, r') = g_{m2}(r, r') \qquad \text{at } r = r'.$$

3. In order to maintain continuity,

$$g^{(2)} = g^{(1)} = g = 0.$$

4. The remaining $g^{(3)}$ and $g^{(4)}$ terms must fulfill equation (5.91).

Condition (4) can be written as follows

$$g^{(4)} + \frac{2}{r} g^{(3)} = \frac{1}{2\pi r} \delta(r - r')$$
$$\Rightarrow \quad \partial_r \left(r g^{(3)} + g^{(2)} \right) = \frac{1}{2\pi} \partial(r - r')$$
$$\Rightarrow \quad r g^{(3)} + g^{(2)} \Big|_{r'_-}^{r'_+} = \frac{1}{2\pi}, \quad (5.94)$$

92

but from condition (3), $g^{(2)} = 0$, so

$$rg^{(3)}\Big|_{r'_-}^{r'_+} = \frac{1}{2\pi}. \tag{5.95}$$

Now the six conditions imposed upon the system can be written as follows

$$AH_m^+(ka) + BH_m^-(ka) + CI_m(ka) + DK_m(ka) = 0 \tag{5.96}$$

$$AH_m^{+\prime}(ka) + BH_m^{-\prime}(ka) + CI_m'(ka) + DK_m'(ka) = 0 \tag{5.97}$$

$$(A - E)H_m^+(kr') + BH_m^-(kr') + CI_m(kr') + (D - F)K_m(kr') = 0 \tag{5.98}$$

$$(A - E)H_m^{+\prime}(kr') + BH_m^{-\prime}(kr') + CI_m'(kr') + (D - F)K_m'(kr') = 0 \tag{5.99}$$

$$(A - E)H_m^{+\prime\prime}(kr') + BH_m^{-\prime\prime}(kr') + CI_m''(kr') + (D - F)K_m''(kr') = 0 \tag{5.100}$$

$$(A - E)H_m^{+\prime\prime\prime}(kr') + BH_m^{-\prime\prime\prime}(kr') + CI_m'''(kr') + (D - F)K_m'''(kr') = -\frac{1}{2\pi k^3 r} \tag{5.101}$$

By considering the conditions only at $r = r'$ we can extract the values for $A - E$, B, C, and $D - F$. For convenience, the m subscripts and (kr') are omitted from the presentation of the Bessel and Hankel functions and are to be assumed. From equation (5.98)

$$(A - E)H^+(kr') + BH^-(kr') + CI(kr') + (D - F)K(kr') = 0. \tag{5.102}$$

The values of the constants in this equation are calculated in appendix C, we then use these values to construct the Green Function that we will use to look at the diffractive problem in the next section.

5.4.4 Formulation of the Green Function

The coefficients determined in appendix C can now be placed in (5.92) and (5.93). For $a < r < r'$ this gives

$$
\begin{aligned}
g_{m1}(r, r') &= \frac{1}{16i} \frac{W_a(K, H^-)}{W_a(K, H^+)} H^+(kr') H^+(kr) + \frac{1}{4\pi} \frac{W_a(K, I)}{W_a(K, H^+)} K(kr') H^+(kr) \\
&\quad -\frac{1}{4\pi} K(kr') I(kr) + \frac{1}{16i} \frac{W_a(H^-, H^+)}{W_a(K, H^+)} H^+(kr') K(kr) \\
&\quad +\frac{1}{4\pi} \frac{W_a(I, H^+)}{W_a(K, H^+)} K(kr') K(kr) - \frac{1}{16i} H^+(kr') H^-(kr), \quad (5.103)
\end{aligned}
$$

whereas for $r' < r < \infty$ this gives

$$
\begin{aligned}
g_{m2}(r, r') &= \frac{1}{16i} \frac{W_a(K, H^-)}{W_a(K, H^+)} H^+(kr') H^+(kr) + \frac{1}{4\pi} \frac{W_a(K, I)}{W_a(K, H^+)} K(kr') H^+(kr) \\
&\quad -\frac{1}{4\pi} K(kr) I(kr') + \frac{1}{16i} \frac{W_a(H^-, H^+)}{W_a(K, H^+)} H^+(kr') K(kr) \\
&\quad +\frac{1}{4\pi} \frac{W_a(I, H^+)}{W_a(K, H^+)} K(kr') K(kr) - \frac{1}{16} H^-(kr') H^+(kr). \quad (5.104)
\end{aligned}
$$

By inspection this is very similar in structure to (5.103), so by representing r and r' as either incoming or outgoing depending on the domain, both (5.104) and (5.103) can be written as

$$
\begin{aligned}
g_m(r, r') &= \frac{1}{8i} \frac{W_a(K, J)}{W_a(K, H^+)} H^+(kr_<) H^+(kr_>) \\
&\quad + \frac{1}{4\pi ka} \frac{1}{W_a(K, H^+)} \left[K(kr_<) H^+(kr_>) + H^+(kr_<) K(kr_<) \right] \\
&\quad + \frac{1}{4\pi} \frac{W_a(I, H^+)}{W_a(K, H^+)} K(kr_<) K(kr_>) \\
&\quad - \left[\frac{1}{8i} J(kr_<) H^+(kr_>) + \frac{1}{4\pi} I(kr_<) K(kr_>) \right]. \quad (5.105)
\end{aligned}
$$

By using [46]

$$
H_m^+(z) \approx e^{-\frac{im\pi}{2}} H_0^+(z) \tag{5.106}
$$

$$
H_m^-(z) \approx e^{\frac{im\pi}{2}} H_0^-(z) \tag{5.107}
$$

94

$$K_m(z) \approx K_0(z) \tag{5.108}$$

$$I_m(z) \approx I_0(z), \tag{5.109}$$

the equation (5.105) can be written as

$$
\begin{aligned}
g_m(r, r') &= \frac{1}{8i} \frac{W_a(K, J)}{W_a(K, H^+)} e^{im\pi} H_0^+(kr_<) H_0^+(kr_>) \\
&\quad + \frac{1}{4\pi ka} \frac{e^{\frac{im\pi}{2}}}{W_a(K, H^+)} \left[K_0(kr_<) H_0^+(kr_>) + H_0^+(kr_<) K_0(kr_<) \right] \\
&\quad + \frac{1}{4\pi} \frac{W_a(I, H^+)}{W_a(K, H^+)} K_0(kr_<) K_0(kr_>) \\
&\quad - \left(\frac{1}{8i} J(kr_<) H^+(kr_>) + \frac{1}{4\pi} I(kr_<) K(kr_>) \right)
\end{aligned}
\tag{5.110}
$$

Looking at this, it can be seem that $\frac{1}{8i} J(kr_<) H^+(kr_>) + \frac{1}{4\pi} I(kr_<) K(kr_>)$ is the free Green function for this system. By subtracting this from (5.110) we are hence left with terms which appear to correspond to $G_f d G_f$ in the hypothesis that for a scattering system, $G = G_f + G_f d(r_<, r_>) G_f$. Looking back at the start of this chapter, this is what what we were hoping to extract in order to investigate the applicability of this method to elastic problems. The terms we receive are

$$
\begin{aligned}
G_S &= \frac{1}{8i} \frac{W_a(K, J)}{W_a(K, H^+)} e^{im\pi} H_0^+(kr_<) H_0^+(kr_>) \\
&\quad + \frac{1}{4\pi ka} \frac{e^{\frac{im\pi}{2}}}{W_a(K, H^+)} \left[K_0(kr_<) H_0^+(kr_>) + H_0^+(kr_<) K_0(kr_<) \right] \\
&\quad + \frac{1}{4\pi} \frac{W_a(I, H^+)}{W_a(K, H^+)} K_0(kr_<) K_0(kr_>).
\end{aligned}
\tag{5.111}
$$

A vital point that we need to verify in the process of determining the usefulness of this approach for this system is to ensure that the solutions match established frameworks for limiting behavior. So if (5.111) is to match with the structure of $G_f d(r_<, r_>) G_f$ it needs to be of the form

$$
G_S = \frac{d(r_<, r_>)}{(8i)^2} H_0^+(kr_<) H_0^+(kr_>)
$$

$$+\frac{d(r_<, r_>)}{4\pi}\frac{1}{8i}\left[K_0(kr_<)H_0^+(kr_>) + H_0^+(kr_<)K_0(kr_<)\right]$$

$$+\frac{d(r_<, r_>)}{(4\pi)^2}K_0(kr_<)K_0(kr_>). \tag{5.112}$$

Although this is very similar on first inspection to (5.111), for it to be correct it would require

$$
\begin{aligned}
d(r_<, r_>) &= 8i\frac{W_a(K, J)}{W_a(K, H^+)}e^{im\pi} \\
&= \frac{8i}{ka}\frac{e^{\frac{im\pi}{2}}}{W_a(K, H^+)} \\
&= 4\pi\frac{W_a(I, H^+)}{W_a(K, H^+)} \tag{5.113}
\end{aligned}
$$

Due to the differing exponential factors in these terms, there is no diffraction coefficient that will balance for first order limits and if we hope to obtain them an additional step must be considered. We shall now look at what changes to this approach may be necessary to receive a workable diffraction coefficient that matches that of the quantum mechanical method we are following.

5.4.5   Calculation of Diffraction Coefficient

We have assumed that $a < r_{<,>}$. When we compare the coefficients in the asymptotic limit

$$\frac{1}{4\pi}\frac{W_a(I, H^+)}{W_a(K, H^+)}K_0(kr_<)K_0(kr_>) \sim \frac{1}{4\pi}e^{2ka-kr_<-kr_>} \tag{5.114}$$

this assumption will mean that this term is exponentially small. Similarly for

$$\frac{1}{4\pi ka}\frac{1}{W_a(K, H^+)}\left[K_0(kr_<)H_0^+(kr_>) + H_0^+(kr_<)K_0(kr_<)\right] \sim e^{ka}\left[e^{-kr_<-kr_>}\right].$$
$$\tag{5.115}$$

With these two terms contributing only exponentially small terms to the system, they can be neglected in this assumption leaving only the terms

including $H^+(kr_<)H^+(k_>)$ to give a non-exponentially small contribution. Having made these assumptions we have

$$g_m - g_{free} \sim \frac{1}{8i} \frac{W_a(K,J)}{W_a(K,H^+)} H_m^+(kr_<) H_m^+(kr_>)$$

$$\sim \frac{e^{im\pi}}{8i} \frac{W_a(K,J)}{W_a(K,H^+)} H_0^+(kr_<) H_0^+(kr_>). \qquad (5.116)$$

This will not be the exact G_S for the plate, but it will be for the corresponding membrane and it is assumed that the cases are similar enough to use the same value. With the inclusion of the sum over m terms from the original G we can write

$$d = -8i \sum_{m=-\infty}^{+\infty} e^{im(\phi-\pi)} \frac{W_a(K,J)}{W_a(K,H^+)}. \qquad (5.117)$$

By expanding this as a power series about $ka = 0$ and neglecting the terms of $O(ka^2)$ we find that for all values of $m \neq 0, \pm 1$ the diffraction coefficient is equal to zero. This leaves

$$
\begin{aligned}
d &= -8i \sum_{m=-1}^{+1} e^{im(\phi-\pi)} \frac{W_a(K,J)}{W_a(K,H^+)} \\
&= -8i \left\{ 1 + \frac{\pi}{4i\gamma + \pi + 4i\ln\left(\frac{ka}{2}\right)} \left(e^{i(\phi-\pi)} + e^{-i(\phi-\pi)} \right) \right\} \\
&= -8i \left\{ 1 - \frac{\pi \cos\phi}{2i\left[\ln\left(\frac{ka}{2}\right) + \gamma - \frac{i\pi}{4}\right]} \right\}. \qquad (5.118)
\end{aligned}
$$

From what we have seen here, the original thought that the quantum mechanical diffraction coefficient approach could be applied to plates has been shown to not be as immediately successful as would have been hoped. We could only retrieve a valid form of diffraction coefficient in this later case by discarding a large number of terms in order to have matching limiting behavior. What of the diffraction coefficient we do receive? Well this one includes dependency on the angle of impact, something that is not present

in the simplified version of the billiard case. The variable dependency on the two limits $a \rightarrow 0$ and $k \rightarrow \infty$ also causes concern when trying to determine the accuracy of this result as taking the limits in different orders could well produce inconsistent results.

The discarding of lower order terms is something that should also be of concern. While not an exact parallel, in chapter 4 we saw that the additional of lower terms had a visible effect on the results and so immediately discarding them just to match limits suggests that there are issues with this approach which would still need to resolved, it would be the aim to include the same order terms across all calculations for consistency purposes and this is not the case here. One of the aims of this chapter was to see if using the quantum scattering approach would produce a simple extension of diffraction to elastic plates, and from the problems that we have encountered here this does not seem to be the case. We did produce a correction term for the semi-classical trace formula in the case of the pinched plate, which was another of our aims. This suggests that there is some validity in the approach.

It could well be the case that this approach would be valid in the full three dimensional elastic problem, taking coupling of longitudinal and transverse waves into account. However this is beyond the scope of this thesis, and so instead we look for another approach to the diffractive problem by considering star graphs.

Chapter 6

Statistical Properties of the Plate Equation Governed Star Graph

Having seen in the previous chapters a variety of models for the quantum billiard based on diffraction with questionable results we hope that by looking at an alternative approach we can verify the use of an alternative methods. In this chapter we continue the investigation into various semiclassical methods by looking at studying similar problems by using *star graphs*. Star graphs provide an interesting avenue into the problem of diffraction, not only allowing us to model systems such as the elastic plate we are studying, but frames and structures also. While we shall not be looking at those problems it is worth noting that through investigation of this method the application of quantum processes to fields such as structural engineering could provide unique insight into vibrational effects.

6.1 Seba Billiards

A graph is defined as a collection of vertices numbering $v + 1$, where the length of an edge on the graph is given by

$$L(v_i, v_j) \in [0, L],\qquad(6.1)$$

with L chosen to determine maximum edge length. In order to make this a star graph as opposed to a graph in general , we impose the condition that the vertex denoted by v_0 has a valency $V = 0$ and all other vertices v_j have valency $V = 1$. This gives us a graph of j edges connected by vertex v_0, an example of which is shown in figure 6.1. We shall be using this in order to model the behavior of a plate with added center condition as in the previous chapters. Diffractive models such as this are interesting to study due to the radical changes introduced by the introduction of a scatterer on an integrable system [8] and the destruction of the phase tori constructed to model these systems by this chaotic behavior. This will leave us with a system that is neither integrable and follows Poissonian statistics [47] or totally chaotic and follow Random Matrix Theory (RMT) predictions [48], [49]; this is also considered in [50] where the two point correlation form factor K is calculated for the rectangular billiard. In this chapter we shall be considering similar effects on the disk billiard, studied here using the approach developed for star graphs in [51].

In most cases diffractive systems such as those studied in this chapter, all classically non-chaotic, include measure zero objects that influence the behavior at the quantum level. For example, we took the annulus billiard, and shrunk the internal radius until the inner ring could be considered as a point scatterer. This scatterer is of measure zero, and as such is irrelevant in the classical calculations as it has no effect of the behavior. This scatterer

does effect the quantum system however, causing a wave chaos to develop, contributing significantly to any effects on the energy level distribution. This kind of behavior, as in the example above, where a system displays quantum chaotic behavior despite being classically dynamic, is referred to as a *Seba Billiard*. This idea introduced by Seba [8] was developed by articles applying the concept to further scattering systems, [52], [53] and corresponds directly to star graphs, which we shall now consider with the aim of investigating their statistical properties when applied to the elastic plate problem

6.2 Quantum Graphs

Quantum graphs are models created in order to investigate the connections between the statistical properties of a system and its periodic orbits [54], [55], [52]. These graphs are networks of wires restricted to one dimension, connected at nodes and modeled with various boundary conditions. The graphs are generally applicable to physical systems, being used in many areas such as condensed matter physics and chemical modeling [56], [57]. The development of quantum graphs is based on modeling the problems as systems of thin wires, where the thickness is much smaller than any other length scale in the problem and hence the wires can be treated as one dimensional, reducing the problem to include only transverse waves and simplifying the corresponding operator considered on the wire. A quantum graph is purely a model for a more mathematically complicated system, in our case used to explore the connection between the behavior of a systems quantum energy level statistics in relation to its classical periodic orbits. The connection to the periodic orbits is useful in this case due to the fact that for graphs, the trace formula can be solved exactly, and as such the result can be easily

classified rather than using a semiclassical approximation. This links to the classical dynamics of the system in a similar way to how the Gutzwiller trace formula links to Hamiltonian behavior. The fact that the trace formula is exact makes quantum graphs very useful tools in the study of many aspects of quantum chaos. However at this time there are few conclusive results in the investigation of the subject, as although some graphs can be shown to display RMT behavior, in order to extract useful information from them, larger and larger graphs need to be studied, needing combinatorial techniques in order to recover useful results. It is our aim to study a system that will fall into an *intermediate* ensemble due to the introduction of a chaotic scatterer to an integrable system [8], and hope to show that its statistical properties agree with previously studied cases [58], [55].

6.3   The Hydra

6.3.1   Quantum Model

Each graph is composed of a series of bonds, the structure of the graph being determined by the connectivity matrix C_{ij}, this is a square matrix with the elements defined by

$$C_{ij} = C_{ji} = \begin{cases} 1 & \text{if } i \text{ and } j \text{ are connected} \\ 0 & \text{otherwise} \end{cases} \qquad i, j = 1, ..., V. \qquad (6.2)$$

For each bond a coordinate x_{ij} is assigned, this is zero at the vertex i and L_{ij} $(= L_{ji})$ at j. Along each bond we define the wavefunction $\Psi_{ij}(x_{ij})$ as the component of Ψ along the bond $b = (i, j)$. This wavefunction must satisfy any boundary conditions applied at the vertices to ensure continuity and 'current' conservation. By continuity, at each vertex i, Ψ must approach a

value Φ_i regardless of which vertex i is approached from. The conservation condition places a restraint on the derivatives of Ψ. This particular graph is named the *hydra*.

- Continuity

$$\Psi_{ij}(x)\big|_{x=0} = \Phi_i, \qquad \Psi_{ij}(x)\big|_{x=L_{ij}} = \Phi_j, \qquad \forall i < j, C_{ij} \neq 0 \quad (6.3)$$

- Conservation

$$\sum_{j<i} C_{ij} \left(iA_{ji} - \frac{d}{dx} \right) \Psi_{ji}(x)\big|_{x=L_{ij}}$$

$$+ \sum_{j>i} C_{ij} \left(-iA_{ij} + \frac{d}{dx} \right) \Psi_{ji}(x)\big|_{x=0} = \lambda_i \Phi_i. \qquad (6.4)$$

In the case of modeling the general quantum graph,that represents the basic diffractive billiard system Ψ is given by

$$\left(\frac{d}{dx} - A_b \right)^2 \Psi_b(x) = k^2 \Psi_b(x), \qquad b = (i,j) \qquad (6.5)$$

with A_b representing the effect of forces such as a magnetic vector potential. When $\lambda \to \infty$, the bonds do not interact and act as a model for the particles bouncing independently within their bonds, leading to a similar torus phase space as in the EBK method. Quantum star graphs that can be used to model Seba billiards are composed of bonds of various lengths, connected by a central vertex as in figure 6.1. The external force term is dropped, giving the Schrödinger equation for Ψ

$$-\frac{d^2}{dx^2} \Psi_{ij}(x) = k^2 \Psi_{ij}(x), \qquad x \in [0, L_{ij}]. \qquad (6.6)$$

The continuity and conservations are given as in (6.3) and (6.4). Assuming the eigenvalues can then be found, the spectral density is defined by

$$\rho(k) = \sum_{i=1}^{\infty} \delta(k - k_i) \qquad (6.7)$$

103
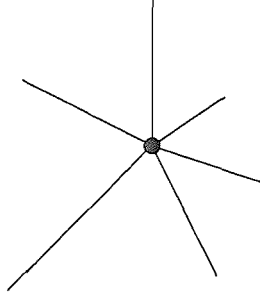
Figure 6.1: The *hydra*, a star graph composed of a central vertex from which all other bonds emanate.

and hence we can study the eigenvalue statistics of the system by using the two point correlation factor [58]

$$R_2(x) = \frac{1}{\overline{d}^2} \left\langle \rho(k), \rho\left(k + \frac{x}{\overline{d}}\right) \right\rangle - \delta(x) \qquad (6.8)$$

where the mean density $\overline{d} = < \rho(k) >$, which defines average spacing of the eigenvalues of the system.

6.3.2   Plate Equation Governed Graph

While the quantum star graph described the behavior under Schrödinger's equation, in the case presented here we are studying the effects of modeling a star graph where the governing factor on the bonds is the plate equation and shall extend the method as necessary, which shall be referred to as the *elastic star graph*. This allows the effects of both flexural and rotational motion within the beams to be studied. We will now outline the model that we shall be applying this technique to in order to further investigate the effects of using the star graph to extract statistical properties. Assume a wavefunction along the beams of

$$\Psi_{ij} \quad = \quad A_{ij}\sin(kx_{ij}) + B_{ij}\sinh(kx_{ij}) + C_{ij}\cos(kx_{ij}) + D_{ij}\cosh(kx_{ij})$$

$$(6.9)$$

that is a solution of

$$\frac{d^4}{dx^4}\Psi_{ij}(x) = k^4\Psi_{ij}(x), \qquad x \in [0, L_{ij}]. \tag{6.10}$$

The clamped boundary conditions at the center vertex and all external vertices are given by

$$\Psi_{ij}(0) = \phi_i, \qquad \Psi'_{ij}(0) = \phi'_i$$
$$\Psi_{ij}(L_j) = \phi_j, \qquad \Psi'_{ij}(L_j) = \phi'_j. \tag{6.11}$$

By considering these boundary conditions, (6.9) can then be expressed in terms of the boundary variables rather than the original coefficients. In the case of of forced vibrations, the shear force F is related to the third derivative of the wavefunction

$$F = -EI\frac{d^3\psi}{dx^3}. \tag{6.12}$$

The fact that due to forced vibration, this force across the beam is discontinuous can be written in the quantum graph terminology as the condition

$$\sum_{j<i} C_{ij}\left(-\Psi'''_{ji}(x_{ij})\big|_{x=L_j}\right) + \sum_{j>i} C_{ij}\left(\Psi'''_{ij}(x_{ij})\big|_{x=0}\right) = \lambda_i\phi_i. \tag{6.13}$$

This states that the graph can be modeled by denoting the connecting vertex as i, then all bonds where $j < i$ are separated from all bonds where $j > i$ by a discontinuity of size $\lambda_i\phi_i$, with λ an arbitrary constant to be determined at a later point.
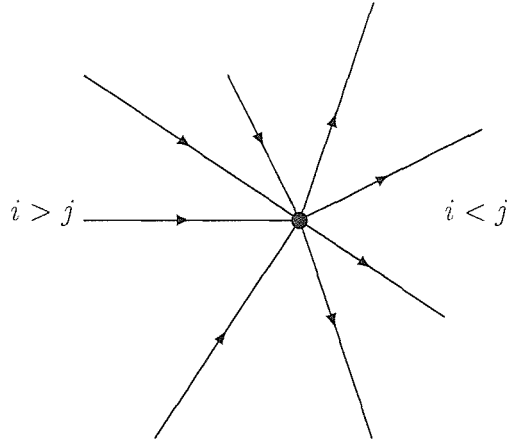
Figure 6.2: Star graph points modeled as $i < j$ on the left and $i > j$ on the right, with the the central vertex i.

6.4 Quantization

6.4.1 Quantum Star Graph

In order to understand later comparisons to the quantum star graph case, we shall present a method used to calculate its quantization condition [53]. From (6.5) we apply the conservation conditions (6.4) to obtain a solution for Ψ

$$\Psi_{ij}(x) = \frac{1}{\sin(kL_{ij})} \left(\phi_i \sin(k(L_{ij} - x)) + \phi_j \sin(kx) \right) C_{ij} \qquad (6.14)$$

Now substitute this into the continuity condition (6.3), using the fact that $C_{ij} = C_{ji} = (C_{ij})^2$ to obtain

$$\sum_{j<i} -C_{ij} \left(-\frac{\phi_j k}{\sin(kL_{ij})} + \phi_i k \cot(kL_{ij}) \right)$$

$$+ \sum_{j>i} \left(-\phi_i \cot(kL_{ij}) + \frac{k\phi_j}{\sin(kL_{ij})} \right) = \lambda_i \phi_i \qquad (6.15)$$

106

where λ_i is a constant determining the strength of the discontinuity. We can write (6.15) as

$$\phi_i \left(\sum_{i \neq m} C_{im} \cot(kL_{im}) - \frac{\lambda_i}{k} \right) + \sum_{i \neq j} \frac{C_{ij}\phi_j}{\sin(kL_{ij})} = 0. \qquad (6.16)$$

Using the conditions established in (6.2) and that fact we are only considering a system of one singularity we get

$$\phi_0 \left(-\sum_{m \neq 0} \cot(kL_m) - \frac{\lambda_0}{k} + \sum_{j \neq 0} \frac{1}{\cos(kL_j)\sin(kL_j)} \right) = 0 \qquad (6.17)$$

which leads to

$$\sum_{m \neq 0} \left(\frac{1}{\cos(kL_j)\sin(kL_j)} - \frac{\cos(kL_m)}{\sin(kL_m)} \right) = \frac{\lambda_0}{k}$$

$$\sum_{m \neq 0} \frac{1 - \cos^2(kL_m)}{\cos(kL_j)\sin(kL_j)} = \frac{\lambda_0}{k}$$

$$\sum_{m \neq 0} \tan(kL_m) = \frac{\lambda_0}{k} \qquad (6.18)$$

giving the quantization condition for the quantum star graph system. This gives us an explicit condition that defines when k can be considered an eigenvalue for this problem. With this in mind we can then calculate the same condition for the graph governed by the plate equation.

6.4.2 Elastic Star Graph

We shall now apply the presented method to the elastic star graph model. From this will then be able to determine the appropriate quantization condition and use this for further analysis of the system. By calculating the third derivative of (6.9) and applying the boundary conditions (6.11) we can write the relevant terms in (6.13) as

$$\Psi_{ji}'''(x_{ij}) = \phi_i \gamma - \phi_i' \beta - \phi_j \overline{\gamma} - \phi_j' \overline{\beta} \qquad (6.19)$$

$$\Psi_{ij}'''(x_{ij}) = \phi_i \gamma + \phi_i' \beta - \phi_j \overline{\gamma} + \phi_j' \overline{\beta} \qquad (6.20)$$

107

using the terms

$$\alpha = \frac{\sin(kL_j)\cosh(kL_j) - \cos(kL_j)\sinh(kL_j)}{1 - \cos(kL_j)\cosh(kL_j)}k, \quad (6.21)$$

$$\overline{\alpha} = \frac{\sinh(kL_j) - \sin(kL_j)}{1 - \cos(kL_j)\cosh(kL_j)}k, \quad (6.22)$$

$$\beta = \frac{\sin(kL_j)\sinh(kL_j)}{1 - \cos(kL_j)\cosh(kL_j)}k^2, \quad (6.23)$$

$$\overline{\beta} = \frac{\cosh(kL_j) - \cos(kL_j)}{1 - \cos(k_jL)\cosh(kL_j)}k^2, \quad (6.24)$$

$$\gamma = \frac{\sin(kL_j)\cosh(kL_j) + \cos(kL_j)\sinh(kL_j)}{1 - \cos(kL_j)\cosh(kL_j)}k^3, \quad (6.25)$$

and $$\overline{\alpha} = \frac{\sinh(kL_j) + \sin(kL_j)}{1 - \cos(kL_j)\cosh(kL_j)}k^3. \quad (6.26)$$

Hence we can write (6.13) as

$$\sum_{j<i} C_{ij}\left(\phi_i\gamma - \phi_i'\beta - \phi_j\overline{\gamma} - \phi_j'\overline{\beta}\right)$$
$$+ \sum_{j>i} C_{ij}\left(\phi_i\gamma + \phi_i'\beta - \phi_j\overline{\gamma} + \phi_j'\overline{\beta}\right) = \lambda_i\phi_i. \quad (6.27)$$

Now consider the case when $i = 0$, this gives

$$\sum_{j<0}\left(\phi_0\gamma - \phi_0'\beta - \phi_j\overline{\gamma} - \phi_j'\overline{\beta}\right)$$
$$+ \sum_{j>0}\left(\phi_0\gamma + \phi_0'\beta - \phi_j\overline{\gamma} + \phi_j'\overline{\beta}\right) = \lambda_0\phi_0, \quad (6.28)$$

this gives us

$$\sum_{j\neq 0}\left(\phi_0\gamma - \phi_j\overline{\gamma}\right) = \frac{\lambda_0\phi_0}{2}. \quad (6.29)$$

Then due to the fact that the external vertices are clamped, the boundary conditions can be set with $\phi_j = 0$ and hence

$$\sum_{j\neq 0}\gamma = \lambda_0 \quad (6.30)$$

108

where the factor of two has been absorbed into λ_0. By substituting the original equation for γ this gives

$$\sum_{j \neq 0} \frac{\sin(kL_j)\cosh(kL_j) + \cos(kL_j)\sinh(kL_j)}{1 - \cos(kL_j)\cosh(kL_j)} = \frac{\lambda_0}{k^3} \qquad (6.31)$$

as the quantization condition for this example. Taking this quantization condition, k is an eigenvalue of the unclamped system if and only if this condition is equal to zero, hence

$$\sum_{j \neq 0} \frac{\sin(kL_j)\cosh(kL_j) + \cos(kL_j)\sinh(kL_j)}{1 - \cos(kL_j)\cosh(kL_j)} = 0 \qquad (6.32)$$

This will be the case when $\sin(kL_j)\cosh(kL_j) + \cos(kL_j)\sinh(kL_j) = 0$, except when $1 - \cos(kL_j)\cosh(kL_j) = 0$, that is the case when $kL = 0$ and can be neglected due to the fact that $kL_j = 0$ only in the case of bond lengths $L_j = 0$ which we shall not be considering. By rearranging the terms, the special case of (6.32) can be written as

$$F(k) = \sum_{j=1}^{v} \eta(kL) = 0, \qquad (6.33)$$

where

$$\eta(kL_j) = \tan(kL_j) + \tanh(kL_j) \qquad (6.34)$$

allows the density $d(k)$ to be written as

$$d(k) = \frac{1}{2\pi} \int |F'(k)| \, e^{izF(k)} \, dz. \qquad (6.35)$$

With these elastic variations defined, the quantum calculation in [53] can be followed for this case.

6.5   Statistical Properties

The statistical properties of star graphs governed by Schrödinger were investigated in [58], relating the eigenvalues on a star graph via an exact trace

109

formula. In deriving a formula for the form factor $K(\tau)$, it was demonstrated that this model is not Poissonian nor governed by RMT, fitting into an intermediate ensemble. This strongly suggests that using a similar approach to a graph governed by the plate equation and hence graph edges with behavior determined by a different operator will give similar results. Returning to previously calculated properties, in a star graph consisting of v bonds with a length distribution of independent uniform random variables in the range $[L_j, L_j + \Delta L_j]$, the mean density $\overline{d}$ is defined as

$$\lim_{\Delta L \to 0, k \to \infty} \langle d(k) \rangle_{L_j}, \tag{6.36}$$

with the averaging calculated using

$$< \cdot >_{L_j} = \int_{L_0}^{L_0 + \Delta L} \cdots \int_{L_0}^{L_0 + \Delta L_j} \cdot \frac{dL_1}{\Delta L_j} \cdots \frac{dL_v}{\Delta L_j}. \tag{6.37}$$

This gives

$$\langle d(k) \rangle_{L_j} = \frac{v}{2\pi} \int_{-\infty}^{\infty} \tilde{f}^{v-1}(z) \tilde{g}(z) \, dz \tag{6.38}$$

with

$$\tilde{f}(z) = \int_{L_0}^{L_0 + \Delta L_j} e^{iz\eta(kL_j)} \frac{dL_j}{\Delta L_j} \tag{6.39}$$

$$\tilde{g}(z) = \int_{L_0}^{L_0 + \Delta L_j} |F'(k)| \, e^{iz\eta(kL_j)} \frac{dL_j}{\Delta L_j}. \tag{6.40}$$

By changing the integration variable

$$F'(k) \frac{dL_j}{\Delta L_j} = \frac{d\eta(kL_j)}{d(kL_j)} \frac{d(kL_j)}{dk} \frac{dL_j}{\Delta L_j} \tag{6.41}$$

$$= \frac{L_j}{k} \frac{d\eta}{d(kL_j)} \frac{d(kL_j)}{\Delta L_j} \tag{6.42}$$

$$= \frac{L_j}{k \Delta L_j} d\eta \tag{6.43}$$

we can then write $\tilde{g}(z)$ as

$$\tilde{g}(z) = \frac{L_0}{k \Delta L_j} \int_{\eta(kL_0)}^{\eta(k(L_0 + \Delta L_j))} e^{iz\eta(kL_j)} \, d\eta \tag{6.44}$$
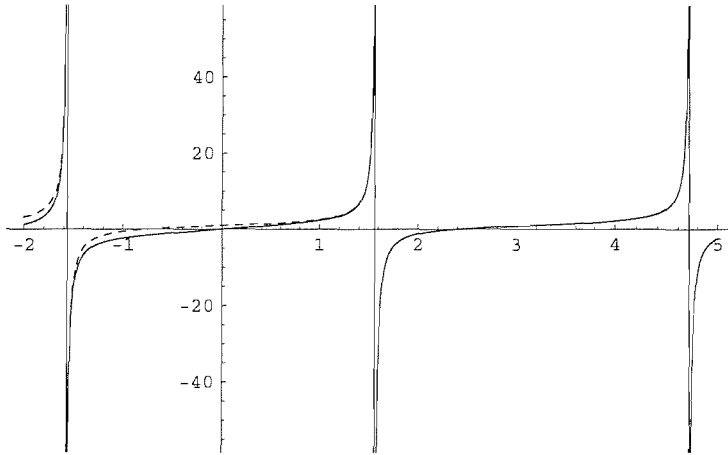
Figure 6.3: Discrepancy between $\tan(x) + \tanh(x)$ (full line) and $\tan(x) + 1$ (dashed line).

In this case L_j can be approximated by L_0 since it is slowly varying in comparison to $\eta(kL_j)$. We shall now consider this while approaching the expanded model.

6.5.1 Near Zero Behavior

It is known that $\tan(kL_j)$ is a periodic function with period $\frac{\pi}{k}$. Since the function $\eta(kL_j) = \tan(kL_j) + \tanh(kL_j)$ is also periodic, although containing a $\tanh(kL_j)$ component, we shall investigate its behavior in order to determine if the periodic behavior of $\tan(kL_j)$ will also be applicable in the case being studied. It is this periodicity that is vital to the calculation and hence what we shall focus on in this section. The function $\tanh(x)$ can be written in terms of exponential functions

$$\tanh(x) \;=\; \frac{e^x - e^{-x}}{e^x + e^{-x}} \tag{6.45}$$

111
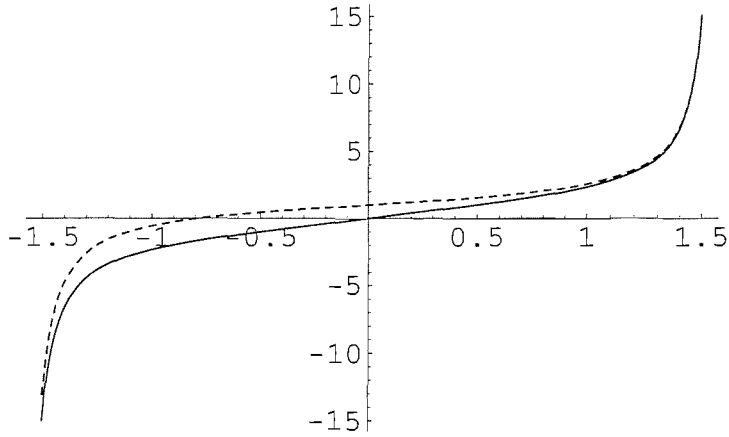
Figure 6.4: Discrepancy between $\tan(x) + \tanh(x)$ (full line) and $\tan(x) + 1$ (dashed line) in the region of $x = 0$.

This can then be expressed as

$$\tanh(x) \quad = \quad 1 - 2e^{-2kL_j} + O(e^{-4k}) \tag{6.46}$$

and the value of η can then be written as

$$\eta(kL_j) \quad = \quad \tan(kL_j) + 1 - 2e^{-2kL_j} + O(e^{-4k}). \tag{6.47}$$

We have already assumed that k is tending toward infinity, so the behavior of $\eta(kL)$ can now be approximated as

$$\eta(kL_j) = \tan(kL_j) + 1. \tag{6.48}$$

This will only be invalid in the region $kL_j \sim 0$. As $k \to \infty$, this is only true in the case where $L_0 = 0$ (see figure 6.4). However this is the case of a non-connected beam and is not included in this case, allowing the approximation $\eta(kL_j) = \tan(kL_j) + 1$ to be used in this case. As stated earlier, neglecting the cases where bond length is equal to zero allows us to note that the period

of the two arguments for both the quantum star graph and for the elastic star graph are identical. It is this fact that means we can approximate the behavior of (6.34) to (6.48) and use this in subsequent calculations.

While we have shown that the in both the original quantum star graph and in the elastic star graph the periodic behavior is the same when terms past $O(\frac{1}{k})$ are neglected, it is still possible that such terms could affect the system. In previous chapters we have shown that lower order terms are vital in calculating corrections to quantum techniques so why are we neglecting the lower order terms in this calculation?

The terms that we have neglected in the periodicity argument were $O(e^{-2kl})$ and as we stated above, it is only when $k = O(\frac{1}{L})$ that this will produce any effect as the terms neglected are of lower order even than those considered in previous chapters. It is thought that inclusion of this term in subsequent calculations would produce an extra integral term from the use of

$$\eta(kL_j) \quad = \quad \tan(kL_j) + 1 - 2e^{-2kL_j} \tag{6.49}$$

as opposed to

$$\eta(kL_j) = \tan(kL_j) + 1. \tag{6.50}$$

The effects of including such a term however would be exponentially small and its contribution will be neglected at this stage in order to first establish if there is a first order correspondence between the two studied models. Taking the periodicity argument into consideration in order to simplify further calculations we will now derive the statistical properties of the elastic star graph in parallel to those in [53].

6.5.2 Mean Density

In the calculation of the quantum star graph, the fact that $\tan kL_j$ was periodic over $\frac{\pi}{k}$ was used in the calculation of the mean density for the graph. In this case, we determined that in the quantization condition, instead of $\tan kL_j$ we use (6.34). Although this is an alternative function, its periodic behavior is still the same, meaning that the assumption of altering the domain of integration (6.48) is still valid in this case. With this assumption, η is then taken to be a periodic function with period $\frac{\pi}{k}$. The integration in $\tilde{g}(z)$ is performed over the interval $[\eta(kL_0), \eta(k(L_0 + \Delta))]$. This contains approximately $\frac{\Delta L_j k}{\pi}$ periods, and so the integral (6.44) can now be written as

$$
\begin{aligned}
\tilde{g}(z) &= \frac{L_0}{k\Delta L_j} \left[\frac{k\Delta L_j}{\pi} \int_{-\infty}^{\infty} e^{iz\eta} \, d\eta + O(1) \right] \\
&= \frac{L_0}{k\Delta L_j} \left[\frac{k\Delta L}{\pi} \int_{-\infty}^{\infty} e^{iz(\tan(kL_j)+1)} \, d(\tan(kL_j) + 1) + O(1) \right] \\
&\approx 2L_0\delta(z).
\end{aligned}
\tag{6.51}
$$

In order to calculate $\tilde{f}(z)$ we can use this alternative approach, giving

$$
\tilde{f}(z) \simeq \frac{L_0}{k\Delta L_j} \int_{\tan(kL_0)}^{\tan(k(L_0+\Delta L_j))} \frac{e^{iz\tan(kL_j)}}{1 + \tan^2(kL)} \, d(\tan(kL_j)).
\tag{6.52}
$$

Using similar periodicity arguments yields

$$
\tilde{f}(z) \simeq \frac{1}{\pi} \int_{-\infty}^{\infty} \frac{e^{iz\alpha}}{1 + \alpha^2} \, d\alpha
\tag{6.53}
$$

$$
= e^{-|z|},
\tag{6.54}
$$

so we have obtained

$$
\tilde{f}(z) \simeq e^{-|z|}
\tag{6.55}
$$

$$
\tilde{g}(z) \simeq 2L_0\delta(z).
\tag{6.56}
$$

114

Substituting these back into (6.38) gives

$$\bar{d} = \frac{v}{2\pi}2L_0 \int_{-\infty}^{\infty} e^{(v-1)|z|}\delta(z)\,dz$$

$$= \frac{L_0 v}{\pi}. \tag{6.57}$$

Comparing this to the quantum star graph calculation shows that even with the additional factor from the more complicated quantization condition, appropriate approximations due to $k \to \infty$ behavior show that the mean density of the two systems are the same under the assumption of the two functions have quantization conditions with similar periodicity. This is to be expected, the Fourier transform performed in this calculation will yield the same result independent of z and so we retrieve the above value.

6.5.3   Two Point Correlation Function

In order to proceed to calculating a form factor, we would first need to calculate the two point correlation function of the system. In this section we perform this calculation for the elastic star graph model. A similar calculation for the quantum star graph can be found in [53], the results of which we are hoping to duplicate in order to display a correspondence between the two cases. The two point correlation function $R_2(x)$ is given by

$$R_2(x) = \lim_{\Delta L_j \to 0, k \to \infty} \frac{1}{\bar{d}^2} R\left(k, k + \frac{x}{\bar{d}}\right), \tag{6.58}$$

Again we take the limit such that $k\Delta L_j \to \infty$ and use

$$R(k_1, k_2) = \langle d(k_1), d(k_2)\rangle_{L_j}$$

$$= \left\langle \int_{-\infty}^{\infty} \sum_{r,s=1} \frac{d\eta_1(k_1 L_j)}{dk_1} \frac{d\eta_2(k_1 L_j)}{dk_2} e^{i(z_1 F_1(z_1) + z_2 F_2(z_2))} \frac{dz}{4\pi^2} \right\rangle_{L_j}$$

$$\tag{6.59}$$

115

Analogous to the mean density calculation, this can be written as

$$R(k_1, k_2) = \frac{1}{4\pi^2} \int_{-\infty}^{\infty} \left\{ vg(z)f^{v-1}(z) + v(v-1)\Phi_1(z)\Phi_2(z)f^{v-2}(z) \right\} dz \tag{6.60}$$

Where

$$g(z) = \int_{L_0}^{L_0+\Delta L} \frac{d\eta_1}{dk_1} \frac{d\eta_2}{dk_2} e^{i(z_1\eta_1+z_2\eta_2)} \frac{dL_j}{\Delta L_j} \tag{6.61}$$

$$f(z) = \int_{L_0}^{L_0+\Delta L} e^{i(z_1\eta_1+z_2\eta_2)} \frac{dL_j}{\Delta L_j} \tag{6.62}$$

$$\Phi_1(z) = \int_{L_0}^{L_0+\Delta L_j} \frac{d\eta_1}{dk_1} e^{i(z_1\eta_1+z_2\eta_2)} \frac{dL_j}{\Delta L_j} \tag{6.63}$$

$$\Phi_2(z) = \int_{L_0}^{L_0+\Delta L_j} \frac{d\eta_2}{dk_2} e^{i(z_1\eta_1+z_2\eta_2)} \frac{dL_j}{\Delta L_j} \tag{6.64}$$

Noting the form of (6.58), we set $k_1 = k$, $k_2 = k + \frac{x}{d} = k + \frac{\pi x}{vL_0}$. So for $f(z)$

$$f(z) = \frac{1}{\Delta L_j} \int_{L_0}^{L_0+\Delta L_j} e^{i\left(z_1\eta(kL_j)+z_2\eta\left(kL_j+\frac{\pi xL_j}{vL_0}\right)\right)} dL$$

as $k \to \infty$

$$= \frac{\gamma(z_1, z_2)}{\Delta L_j} \int_{L_0}^{L_0+\Delta L_j} e^{i\left(z_1 \tan(kL_j)+z_2 \tan\left(kL_j+\frac{\pi xL_j}{vL_0}\right)\right)} dL_j$$

$$= \frac{\gamma(z_1, z_2)}{\pi} \int_{-\frac{\pi}{2}}^{\frac{\pi}{2}} e^{i\left(z_1 \tan(\psi)+z_2 \tan\left(\psi+\frac{\pi x}{v}\right)\right)} d\psi \tag{6.65}$$

where we have used the fact that $\frac{L_j}{L_0} \approx 1$. So in the elastic star graph there is an extra factor to be considered in the calculation of R_2. This factor is the result of the addition of the $\tanh(kL_j)$ terms, and written in full, is given by

$$\gamma = e^{i\left(z_1 \tanh(kL_j)+z_2 \tanh\left(kL_j+\frac{\pi xL_j}{vL_0}\right)\right)}. \tag{6.66}$$

However, as we are considering the case of large k, keeping in mind behavior of $\tanh(kL)$, this can be reduced to

$$\gamma(z_1, z_2) = e^{i(z_1+z_2)}. \tag{6.67}$$

116

As this is assuming $k \to \infty$ we have also been able to approximate f by the integral over one period. By manipulating the properties of tan and taking

$$
\begin{aligned}
\beta &= \left(\tan \left(\frac{\pi x}{v} \right) \right)^{-1} \\
&\propto \frac{v}{\pi x} \qquad \text{as } v \to \infty & (6.68) \\
\alpha &= \tan \psi - \beta & (6.69)
\end{aligned}
$$

we can now write f as

$$
f(z) \simeq \gamma(z_1, z_2) \frac{e^{i\beta(z_1 - z_2)}}{\pi} \int_{-\infty}^{\infty} e^{iz_1 - iz_2 \left(\frac{\beta^2 + 1}{\alpha} \right)} \frac{d\alpha}{(\alpha + \beta)^2 + 1}. \qquad (6.70)
$$

Differentiate this with respect to z_1 and z_2 to get

$$
\begin{aligned}
\frac{\partial f}{\partial z_1} - \frac{\partial f}{\partial z_2} &= \gamma(z_1, z_2) \frac{i e^{i\beta(z_1 - z_2)}}{\pi} \int_{-\infty}^{\infty} (2\beta + \alpha + \lambda) e^{iz_1 - iz_2 \lambda} \frac{d\alpha}{(\alpha + \beta)^2 + 1} \\
&= \gamma(z_1, z_2) \frac{i e^{i\beta(z_1 - z_2)}}{\pi} \int_{-\infty}^{\infty} e^{iz_1 \alpha - iz_2 \lambda} \frac{d\alpha}{\alpha} \\
&= -\gamma(z_1, z_2) e^{i\beta(z_1 - z_2)} \Theta(z_1, z_2), & (6.71)
\end{aligned}
$$

with

$$
\Theta(z_1, z_2) = -\frac{i}{\pi} \int_{-\infty}^{\infty} e^{iz_2 \alpha - iz_2 \lambda} \frac{d\alpha}{\alpha} \qquad (6.72)
$$

and

$$
\lambda = \frac{\beta^2 + 1}{\alpha}. \qquad (6.73)
$$

By applying the method of characteristics to (6.71), we obtain the solution

$$
f(z) \simeq \gamma(z_1, z_2) \left(e^{-|z_1 + z_2|} - \int_0^{z_1} e^{i\beta(2y - z_1 - z_2)} \Theta(y, z_1 + z_2 - y) \, dy \right). \qquad (6.74)
$$

Applying a similar methods for the other functions in (6.60) yields

$$
g(z) \simeq \gamma(z_1, z_2) L_0^2 (\beta^2 + 1) \left(\frac{\partial}{\partial z_1} - \frac{\partial}{\partial z_2} \right) \left(e^{i\beta(z_1 - z_2)} \Theta(z_1, z_2) \right), \qquad (6.75)
$$

$$
\Phi_1(z) \simeq \gamma(z_1, z_2) L_0 e^{i\beta(z_1 - z_2)} \frac{\partial}{\partial z_1} \Theta(z_1, z_2), \qquad (6.76)
$$

$$
\Phi_2(z) \simeq -\gamma(z_1, z_2) L_0 e^{i\beta(z_1 - z_2)} \frac{\partial}{\partial z_2} \Theta(z_1, z_2). \qquad (6.77)
$$

117

These can now be substituted back into (6.60), begin with just using $g(z)$ and manipulating to give

$$R_2(x) = \frac{v(v-1)L_0^2}{\overline{d}^2} \int \frac{dz}{4\pi^2} f^{v-2} \gamma^2(z_1, z_2) e^{2i\beta(z_1 - z_2)} \left((\beta^2 + 1)\Theta^2 - \frac{\partial\Theta}{\partial z_1} \frac{\partial\Theta}{\partial z_2} \right)$$

(6.78)

Taking the case as $v \to \infty$, write $f^{v-2}(z) = e^{(v-2)\ln f}$ and rescale $f(z)$ to $f(\frac{u}{\beta})$. By taking $v \to \infty$ ($\beta \to \infty$), $\gamma\left(\frac{u}{\beta}\right) = e^{\frac{u_1 + u_2}{\beta}} \to 1$ and hence is removed. The calculation then proceeds as in [53], yielding the same result, an exact formula for the two point correlation function for star graphs when the number of bonds tends to infinity. This result is the same as obtained in [53] for Seba billiards, with the additional factor involved in the calculation not affecting the final result.

$$R_2(x) = 1 + \int_D e^{-\pi x M(u) + 2i(u_1 + u_2)} \left[J_0^2 \left(2\sqrt{u_1 u_2} \right) + J_1^2 \left(2\sqrt{u_1 u_2} \right) \right] d\mathbf{u}, \quad (6.79)$$

with

$$M(u) = |u_1| + |u_2| - 2i \, \text{sign}\,(u_1) \sum_{r,s=1}^{\infty} \frac{(iu_1)^r (iu_2)^s (r+s-2)!}{r! s! (r-1)! (s-1)!}. \quad (6.80)$$

As this calculation has yielded the same two point correlation function as in our comparison model, we can assume that further calculations would also retrieve the same form factor $K(\tau)$. Hence it is noted that calculation of statistical properties for the elastic star graph displays very close links to its quantum star graph counterpart as was expected.

6.6 Comparison and Conclusions

Having shown the correspondence with the quantum star graph, what does this tell us about the eigenvalue statistics of the model we have been study-
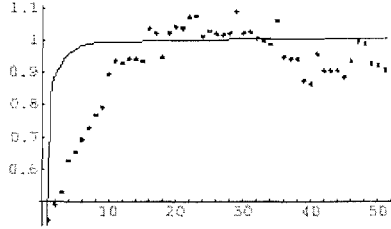
Figure 6.5: Two point correlation function predicted from [58] for the hydra compared to elastic star graph eigenvalue statistics

ing? In the cases of large and small x, $R_2(x)$ can be respectively approximated [58] for the quantum star graph by

$$R_2(x) \sim 1 + 2\Re \left[\frac{1}{x^2 \pi^2} + \frac{2i}{x^3 \pi^3} - \frac{1}{x^4 \pi^5} + \mathrm{O}\left(\frac{1}{x^5}\right) \right], \qquad (6.81)$$

$$R_2(x) \sim \frac{\pi \sqrt{3}}{2} x + \mathrm{O}\left(x^2\right). \qquad (6.82)$$

It was an initial goal of this chapter that we would be attempting to model the elastic plate using an alternative approach based on the star graph model which used beam behavior. How do the results we that we have found compare with those taken from the previous model which looked at a similar plate? By taking a small star graph composed of five bonds ($v = 5$) where bond lengths are given by a uniform random distribution over $[0, 1]$ and determining an array of eigenvalues we can plot the spectral statistics for the elastic plate. A comparison of the predicted behavior of $R_2(X)$ to those of the quantum star graph is shown in figure 6.5. Here we see that despite few results the overall trend of the calculated results is toward that of the predicted behavior. While for complete results a large number of graphs averaged over a variety of bond lengths would be required, here we looked at one case in order to show the emergent behavior of the system. An important facet of this work is showing that despite a low number of bonds

119

and a relatively small number of eigenvalues, a reasonably accurate set of results can be produced, in this case the distribution has been calculated using only the first 150 eigenvalues. By considering an ensemble of graphs with such a random distribution of bond lengths a set of results with greatly increased accuracy could be retrieved. It is not necessary to do this however, as the exact correspondence between (6.79) and published results will mean that this elastic star graph will have the same statistical distribution and hence be part of the same intermediate ensemble. We conclude that in both cases, both the elastic and quantum star graph, the statistical behavior is the same under this approach. This tells us that at first approximation there are no additional terms introduced by considering the elastic plate and that further study into lower contributions would be necessary to see any such contributions.

Chapter 7

Summary and Conclusions

We began this thesis by outlining the semiclassical methods we would be using to apply to elastic plates. It was our aim to apply these methods and establish in which cases such uses would be viable in describing the behavior of these plates. In chapter 2 we saw that there are several approaches to solving the basic problems presented by looking at integrable systems. The EBK quantization method, useful while investigating integrable systems, is no longer of use when any such system is extended into a chaotic case. We didn't look further at such cases as the aim of this thesis was to develop existing approaches to be more accurate in cases of more complicated boundaries, and so looking at the chaotic directly is not necessary for use of the trace formula. It is important to note however that the methods we were developing can be applied to chaotic systems with relevant alterations, and any accuracy improvements would then be carried through. It is the comparison with EBK and other existing methods on which initial results were based; the integrability of the problems we tackled allowed us to have a sound basis on which to compare any changes and determine their usefulness.

7.1 Elastic Plates

It was our intention to determine the important factors that should be considered when applying the semiclassical methods to elastic plates and in doing so we found that there was an important factor to be be investigated. This factor was the effect of the boundary of the plate and led us to study the behavior of the plate under various boundary conditions in order to determine which cases provided a suitable model and which would need changing in the transition.

7.1.1 Semiclassical Analysis of Elastic Plates

Looking back to the boundary conditions quoted in [32], if we were to have used these conditions instead in the trace formula what would the effect have been? Ultimately, since in determining the phase term we have neglected all but the highest order terms in the first approximation, using these boundary conditions would produce the same result. It would however neglect any additional contributions dependent on the curvature, and for a more complicated boundary this could have an effect that we have not seen in the case studied in this chapter due to its simplistic structure.

Adding the phase terms to the trace formula provided accurate eigenvalues in the small k region, although deviations emerged with use of the free edge boundary condition. When this analysis was extended to the rectangular plate we noticed the same behavior, leading us to conclude that there was some element of this boundary condition that made obtaining results at low k difficult. By also retrieving eigenvalues through the Poisson summation approach this view was reinforced. Calculating the eigenvalues with this method was found to be ultimately of the same level of accuracy as that of

the trace formula with the additional phase terms. This did confirm that the application of quantum processes was valid for elastic plate problems though improvement would be necessary to describe all but the simplest of systems with an increase in accuracy.

7.1.2 Lower Order Phase Contributions

Having determined that investigation of the free edge boundary condition was necessary we rederived this condition in a general coordinate system, finding that the general conditions were in fact incorrect as stated and neglecting additional lower order terms and care must be taken in its application to include these additional curvature terms that could affect results. The curvature was also a factor in our derivation of the trace formula phase correction, these corrections are vital in applying semiclassical techniques to elastic systems and we found that previous derivations had neglected order $1/k$ and curvature terms. This previously went unnoticed as at higher k the terms have a negligible effect, but this could not immediately be assumed where k was small. For the phase term

$$\phi_f = -2\arctan\left(\frac{\sin\theta}{\sqrt{1+\cos^2\theta}}\frac{C}{D}\right),$$

we state that

$$
\begin{aligned}
C &= (1+(1-\sigma)\cos^2\theta)^2 k^4 \\
&\quad + \kappa\left[\frac{3\cos^2\theta}{\sin^2\theta}(1-(1-\sigma)\cos^2\theta)+\sigma\sqrt{1+\cos^2\theta}(1+2\cos^2\theta)\right]k^3 \\
D &= (1-(1-\sigma)\cos^2\theta)^2 k^4 - \kappa\left[\frac{2\cos^2\theta}{\sqrt{1+\cos^2\theta}}(1+(1-\sigma)\cos^2\theta)\right]k^3.
\end{aligned}
$$

Although in the case studied there are no angular regions where specular reflection is suspect, this cannot be obviously stated for all curvatures, with

effects at low k in boundaries of variable curvature being possible cases where these phase terms would need to include terms of lower order than in simple cases for obvious reasons. Generating eigenvalues for the elastic plate using this new phase correction term for the circular plate allowed us to improve upon the original result, producing a flattened cumulative frequency distribution. Our goal of applying quantum processes to elastic systems was here shown to be valid one, and with calculated corrections we were able to use this for a simple case, with the expectation that further work would be able to extend this to more complicated boundaries.

Why have these methods still not been able to increase the accuracy of the free edged disk eigenvalues at low k? Even after taking all orders into consideration in section 4.4 we were still left with eigenvalues that were only a fraction better than the original trace formula. The answer appears to lie in the original assumption made in the process of obtaining the phase term. It is as0sumed that where the periodic orbits intersect with the boundary of the disk, and because $k \to \infty$, the interaction can be thought of as happening with a straight line. As $k \to 0$ this assumption clearly becomes less and less valid, with the results becoming more and more inaccurate. In order to fully explore the behavior in this region, it is thought that a lower order correction term would need to be added to the terms taken from this interaction. While this would not be completely correct, it would provide another improvement in accuracy, just as the inclusion of the lower order term made a slight improvement to the original phase term.

An alternative case for consideration would have been that of the boundary described by $x^{2p} + y^{2p} = 1$. This boundary in the limit of $p \to \infty$ provides a smooth transition between the circular and rectangular plates and hence would allow the introduction of diffractive effects from corners to be observed

124

as a limiting process. Although this was not investigated in this thesis it is thought that such a problem would provide additional insight into diffractive behavior.

7.2 Diffractive Effects

After looking at the effects of the free edge boundary condition we turned our attention to looking at the effects of diffraction on the elastic plate, we tackled this in two ways; looking at the diffraction directly applied to the elastic plate and also by studying how we could use star graphs as a model.

7.2.1 Diffractive Effects in the Circular Billiard

In comparing the behavior of the pinched plate Green function solution under several boundary condition with that of the EBK solution, we found that both methods ultimately yielded the same results, showing us that for the case of the pinched circular billiard that we were studying these methods were both equally valid. In doing so it was noted that there existed a disparity between the results expected and those found in that the calculation of the eigenvalues under the plate equation which suggested that the problem was not confined to only affecting axisymmetric orbits. This suggestion that the problem is not as local as originally thought and that the addition of a center diffractive point has a wide reaching effect is similar to the idea in [8] that adding a diffractive point to an integrable system will convert it into a system intermediate between fully integrable and fully chaotic, this was further studied in the subsequent chapter.

We then proceeded to calculate an addition to the semiclassical trace

formula that gave the corrected trace formula

$$\delta\rho_{cor}(k) = \delta\rho(k) + 2\sum_{r=1}^{\infty} \cos(2kr)\left[\cos(\pi r) - 1\right]$$

and allowed us to extract the eigenvalues generated from the addition of the diffractive point, noting that pre-existing eigenvalues were not affected. These extra eigenvalues corresponded to results calculated using alternative methods and suggest that such a method is valid in its aim of modeling a diffractive point in a circular billiard and that it could be extended to include additional diffractive points given further investigation.

One thing that needs to be considered in the diffractive problem is that the behavior of ka is very much dependent on which order the limits $k \to \infty$ and $a \to 0$ are taken, the approach detailed in section 5.1 considers the case of $k \to \infty$ first while keeping the internal radius a small but fixed. In chapter 5 this was also the order in which we took the limits in order to allow comparison to this problem. In that chapter we took the plate equation as the defining equation rather than the Helmholtz equation in order to expand the problem to include thin plates rather than just two dimensional billiards.

The investigation of a diffraction coefficient for an annulus billiard scattering system gave us

$$d = -8i\left\{1 - \frac{\pi\cos\phi}{2i\left[\ln\left(\frac{ka}{2}\right) + \gamma - \frac{i\pi}{4}\right]}\right\}.$$

This coefficient was calculated by having to include an unsatisfactory number of assumptions and neglections to reach a workable form. From this we saw that such a system governed by the plate equation is more complicated than simply adding an additional condition as in the trace formula case. This does in turn though correspond with our observation in the first section of the chapter that further work would be needed in modeling this system in order

to take into account the extra effects brought into being by the diffractive conditions.

7.2.2 Star Graphs

In this chapter we saw that the statistical properties of the elastic star graph correspond to the those of the elastic star graph. From this we noted that the elastic star graph also displays the properties of an intermediate ensemble. In terms of modeling vibrational systems using this method means that the addition of the center point via the star graph model confirms the disruption of the phase tori of the integrable system without being fully chaotic and being described by RMT. This suggests as thought that the star graph is a valid model for describing the behavior of the plate in this case. Considering the statistical properties, the mean level spacing, similar to the mean density we have used in this chapter, is known to decrease as $\hbar^d$, while semiclassical approximations are believed to only provide accuracy to an order of $\hbar^2$. This could restrict models such as the star graph to two dimensions, and bearing this in mind, investigations into the accuracy measures involved in higher dimensional calculations have been undertaken in more detail [59], attempting to show that the semiclassical methods can be used in these cases.

The data found from the statistical properties show that under the plate equation, there is no significant change from the star graph under Schrödinger, marked only by a constant term that becomes irrelevant once the two point correlation factor and form factor are calculated. While this is not a surprise as such a pattern has been seen throughout the thesis, it does leave us with the question of why we did not observe the influence of additional lower order terms as in the cases looked at in chapters 3 and 5. One reason for this is likely to be that our studies of this method contained a number

of assumptions that neglected some lower order terms in order to establish a basic correspondence to the followed model. While this did confirm the validity of using such a model, further work would focus on possible lower order effects.

The use of star graphs to describe plates is hence reinforced as they can be shown to reproduce the behavior of quantum systems as studied using other methods, and while we have only considered one case here, such a method could be extended to more complicated such as plates with additional scattering centers or diffractive effects. Similar work on the statistical energy analysis [60] has found that such models can provide a direct comparison to physical systems [61] and as looking toward the application of graphs to more complicated systems was part of our initial motivation in studying them, it is reasonable to believe that such application would be viable.

7.3 Overall Conclusions

The original aim of this study was to investigate the use of semiclassical methods in order to model vibroacoustic systems. We found that the semiclassical trace formula provided an accurate means to derive eigenvalues from simple billiard systems, but that altering boundary conditions to include higher order terms such as in the free edge case leads to inaccuracies resulting from neglecting terms in order to simplify the calculation. By modeling boundary interactions with the free edge using Bogomolny's transfer matrix method we deduced that including extra terms that we previously neglected past the original assumption of a locally straight boundary gave a small improvement in overall accuracy.

Looking at diffractive effects yielded mixed results. The addition of an

extra term to the semiclassical trace formula provided accurate eigenvalues and the use of an elastic star graph model provided statistical properties that corresponded to those of the quantum star graph as thought. However calculating a useful diffraction coefficient for a similar system was not possible within the bounds of this thesis due to a large number of assumptions and extra terms that were introduced by looking at the system governed by the plate equation. This diffraction coefficient model is however more suited to complex systems as it includes angular dependent terms which means it could be adapted to model more general boundaries.

In accordance with our initial aim to investigate the application of semi-classical methods to elastic plate problems we looked at several methods of doing this. In the process of these investigations we noted that the free edge boundary condition produced numerical errors that we then further studied and found that the additional lower order terms from this condition could be included in the semiclassical methods and improve upon them. Our study of diffraction that also presented itself as a relevant factor in applying such methods did not produce such useful results, instead showing that further study would be needed to obtain any significant results. In both situations however we showed that existing quantum mechanical methods could be applied to elastic plate problems in simple cases with extensions of these methods noted as areas of viable further study.

Appendix A

Trace Formula Results Tables

Results tables from earlier chapters are presented in this appendix as reference to earlier calculations.

k_{ex}	k_{tf}	$\Delta\%$)
1.031	1.691	-63.96
2.284	1.947	14.76
3.101	2.661	14.18
3.485	3.149	9.63
4.575	3.839	16.08
4.6741	4.639	0.76
5.858	4.980	14.99
5.922	5.481	7.45
6.263	6.097	2.65
7.040	6.366	9.58
7.212	7.355	-1.98
7.773	7.806	-0.43
8.469	8.270	2.35
9.193	8.636	6.05
9.411	9.241	1.81
9.706	9.576	1.33
10.556	9.888	6.33
10.929	10.632	2.72
10.938	10.962	-0.22
11.880	11.475	3.41
12.394	11.981	3.33
12.556	12.427	1.03
13.178	12.695	3.66
13.801	13.531	1.95
14.093	13.849	1.73
14.454	14.111	2.37
15.170	14.594	3.80
15.571	14.880	4.44
15.700	15.234	2.97
16.512	15.863	3.93
17.006	16.595	2.41
17.242	17.041	1.17
17.830	17.926	-0.54
18.407	18.451	-0.24
18.736	18.762	-0.14
18.843	19.238	-2.10
19.780	19.836	-0.29
20.191	20.215	-0.12
20.390	20.477	-0.43

k_{ex}	k_{tf}	$\Delta\%$	k_{ex}	k_{tf}	$\Delta\%$
3.1961	3.1445	1.62	2.2317	2.3584	-5.68
4.6109	4.5752	0.77	3.7330	3.7964	-1.70
5.4563	5.0977	6.57	5.0645	5.1025	-0.75
5.9059	5.8716	0.58	5.4548	5.5005	-0.84
6.3064	6.2866	0.31	6.3239	6.3477	-0.38
7.1442	7.1094	0.49	6.9651	6.9995	-0.49
7.7987	7.7808	0.23	7.5416	7.5537	-0.16
8.3467	8.3105	0.43	8.3756	7.9395	5.21
9.1967	9.1798	0.19	8.6133	8.4009	2.47
9.4395	9.4946	-0.58	8.7313	8.7354	-0.05
10.5361	10.5225	0.13	9.7253	9.7461	-0.21
10.6870	10.6010	0.80	10.1393	10.1023	0.36
10.9581	10.9448	0.12	11.0333	11.0498	-0.15
11.8367	11.2061	5.33	11.7622	11.6089	1.30
12.4020	11.8140	4.74	12.3106	12.3218	-0.09
12.5771	12.3901	1.49	12.9887	13.0054	-0.13
13.1074	13.0933	0.11	13.2979	13.3154	-0.13
13.7949	13.7842	0.08	14.0100	13.5767	3.09
14.0982	14.0942	0.03	14.3486	14.3579	-0.06
14.1089	14.3457	-1.68	14.9079	14.7949	0.76
14.3552	14.6216	-1.86	15.6783	15.6909	-0.08
15.1499	15.1465	0.02	16.2783	16.0205	1.58
15.5792	15.5688	0.07	16.4498	16.4648	-0.09
15.7164	15.7611	-0.28	16.7836	16.9922	-1.24
16.4751	16.4673	0.05	17.2019	17.2437	-0.24
17.0050	16.9995	0.03	17.5966	17.6099	-0.08
17.2560	17.2510	0.03	17.9411	17.9517	-0.06
17.7764	17.7661	0.06	18.0522	18.2739	-1.23
18.0001	18.0176	-0.10	18.9621	18.9722	-0.05
18.3960	18.3887	0.04	19.6000	19.6094	-0.05

Figure A.1: Eigenvalue results comparison for known exact solution and the trace formula method for a disk plate with free, simply supported and clamped edges respectively, with difference expressed as a percentage of the mean density Δ.

k_{ex}	k_{tf}	$\Delta\%$
3.1416	3.1434	0.05
4.4429	4.4431	0.01
6.2832	6.2855	0.07
7.0248	7.0249	0.00
8.8858	8.8860	0.01
9.4248	9.4265	0.05
9.9346	9.9349	0.01
11.3272	11.3280	0.02
12.5664	15.666	0.01
12.9531	12.9540	0.03
13.3286	13.3230	-0.16
14.0496	14.0501	0.01
15.7080	15.7077	-0.01
16.0190	16.0198	0.02
16.9180	16.9170	0.03
18.3185	18.3184	0.00
18.8496	18.8511	0.05
19.1096	19.1088	-0.02
19.8691	19.8695	0.01
20.1160	20.1166	0.02

k_{ex}	k_{tf}	$\Delta\%$
3.1416	3.1456	0.2
5.3759	5.4201	2.21
6.2832	6.2500	-1.66
7.4027	7.4402	1.87
8.3187	8.3510	1.62
9.4248	9.4386	0.69
9.7263	9.7627	1.82
10.1094	10.1245	0.75
11.3622	11.3757	0.67
11.8406	11.8701	1.47
12.4419	12.4585	0.83
12.5664	12.5854	0.95
13.0499	13.0591	0.46
14.1385	14.1577	0.96
14.3736	14.4067	1.66
14.4430	14.4580	0.75
15.3134	15.3309	0.87
15.7080	15.7190	0.55
16.0780	16.0901	0.61
16.2849	16.3062	1.06

k_{ex}	k_{tf}	$\Delta\%$
1.779	1.571	11.7
3.793	3.512	7.4
4.914	4.712	4.1
5.218	5.664	-8.54
6.434	6.47	-0.66
7.669	7.854	-2.41
8.22	8.459	-2.91
9.455	9.555	-1.06
10.139	10.058	0.80
10.614	10.537	0.73
11.013	10.996	0.15
11.374	11.436	-0.55
12.172	12.268	-0.79
12.609	12.664	-0.44
13.350	13.421	-0.53
13.863	14.137	-1.98
14.547	14.482	0.45
15.117	14.819	1.97
15.535	15.471	0.41
15.744	15.786	-0.27
16.371	16.400	-0.18

Figure A.2: Eigenvalue results comparison for known exact solutions and the trace formula method of the rectangular plate in cases A and B and C (figure 3.1.2), with difference expressed as a percentage of the mean density Δ.

k_{ex}	$k_{tf}(1)$	$\Delta\%$	$k_{tf}(+\text{cor})$	$\Delta\%$ (cor)
1.031	1.691	-63.96	1.599	-55.08
2.284	1.947	14.76	2.362	-3.41
3.101	2.661	14.18	2.808	9.46
3.485	3.149	9.63	3.064	12.09
4.575	3.839	16.08	3.802	16.88
4.6741	4.639	0.76	4.193	10.29
5.858	4.980	14.99	5.103	12.90
5.922	5.481	7.45	5.505	7.04
6.263	6.097	2.65	6.348	-1.35
7.040	6.366	9.58	7.001	0.56
7.212	7.355	-1.98	7.556	-4.77
7.773	7.806	-0.43	7.941	-2.15
8.469	8.270	2.35	8.405	0.76
9.193	8.636	6.05	8.740	4.92
9.411	9.241	1.81	9.210	2.14
9.706	9.576	1.33	9.747	-0.43
10.556	9.888	6.33	10.162	3.7 3
10.929	10.632	2.72	10.702	2.08
10.938	10.962	-0.22	11.053	-1.05
11.880	11.475	3.41	11.615	2.23
12.394	11.981	3.33	12.323	0.58
12.556	12.427	1.03	13.007	-3.59
13.178	12.695	13.318	3.66	-1.06
13.801	13.531	1.95	13.580	1.60
14.093	13.849	1.73	14.362	-1.91
14.454	14.111	2.37	14.801	-2.40
15.170	14.594	3.80	15.692	-3.44
15.571	14.880	4.44	16.022	-2.89
15.700	15.234	2.97	16.467	-4.89
16.512	15.863	3.93	16.998	-2.95
17.006	16.595	2.41	17.255	-1.46
17.242	17.041	1.17	17.615	-2.16
17.830	17.926	-0.54	17.957	-0.71
18.407	18.451	-0.24	18.280	0.69
18.736	18.762	-0.14	18.976	-1.28
18.843	19.238	-2.10	19.611	-4.07
19.780	19.836	-0.29	19.958	-0.90

Figure A.3: Eigenvalues and errors for original phase term and phase term including lower order correction under the Boundary Integral Method

135

Appendix B

Straight Line Integrals and Derivatives at Leading Order

With the boundary integral representations for the components of the boundary conditions found, we need to consider the integrals over the straight line. However, if indeed we are considering a straight line case then it is evident that curvature of the line will be equal to zero, as will the derivative with respect to s. This removes several elements leaving us with the equivalent boundary conditions for the straight line

$$\frac{\partial^3 G^\pm}{\partial n^3} + (2 - \sigma)\frac{\partial^3 G^\pm}{\partial s^2 \partial n} = 0 \tag{B.1}$$

$$\frac{\partial^2 G^\pm}{\partial n^2} + \sigma\frac{\partial^2 G^\pm}{\partial s^2} = 0. \tag{B.2}$$

Of the remaining terms, the derivatives on the straight line that are present in (B.1), using the near-boundary function for the Green function (2.87) and taking $s \to x$ and $n \to y$, are given by

$$\left.\frac{\partial^3 G^\pm}{\partial n^3}\right|_{SL} = -\frac{5}{2\pi}\frac{(y - y')}{((x - x')^2 + (y - y')^2)^2} + \frac{4}{\pi}\frac{(y - y')^2}{((x - x')^2 + (y - y')^2)^3} \tag{B.3}$$

$$\left.\frac{\partial^3 G^\pm}{\partial s^2 \partial n}\right|_{SL} = -\frac{1}{\pi}\frac{(y - y')}{((x - x')^2 + (y - y')^2)^2} + \frac{4}{\pi}\frac{(x - x')(y - y')}{((x - x')^2 + (y - y')^2)^3}. \tag{B.4}$$
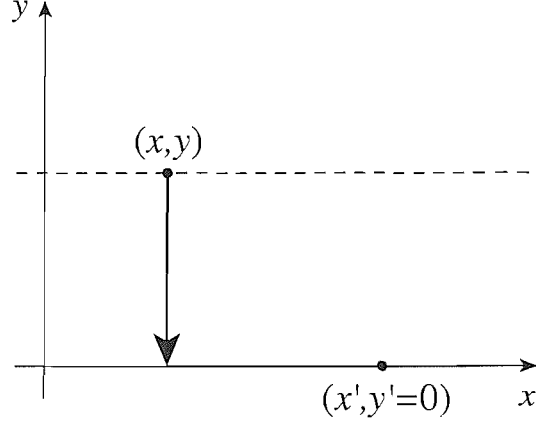
136

Figure B.1: Straight line approximation to boundary interaction

Since on the straight line $y \to y'$ then

$$\frac{\partial^3 G^\pm}{\partial n^3}\bigg|_{SL} = -\frac{5}{2\pi}\frac{0}{(x-x')^4} + \frac{4}{\pi}\frac{0}{(x-x')^6} = 0 \qquad (B.5)$$

$$\frac{\partial^3 G^\pm}{\partial s^2 \partial n}\bigg|_{SL} = -\frac{1}{\pi}\frac{0}{(x-x')^4} + \frac{4}{\pi}\frac{0}{(x-x')^5} = 0. \qquad (B.6)$$

This leaves us with only the non-zero derivatives

$$\frac{\partial^2 G^\pm}{\partial n^2} + \sigma\frac{\partial^2 G^\pm}{\partial s^2} = 0 \qquad (B.7)$$

to be calculated over the straight line for (B.2). We can then use the reduction of the two dimensional Green functions

$$G^+ = \int \frac{e^{ipx}}{4\pi}\frac{e^{iq|y|}}{iq}\,dp \qquad (B.8)$$

$$G^- = \int -\frac{e^{ipx}}{4\pi}\frac{e^{-Qy}}{Q}\,dp \qquad (B.9)$$

to evaluate the straight line factors in the same manner as in the clamped case. Doing so we receive to first order in the semiclassical expansion

$$\frac{\partial^2 G^+}{\partial n^2} \sim i\int q\frac{dp}{4\pi}e^{ipx}e^{iq|y|}, \qquad (B.10)$$

137

$$\frac{\partial^2 G^+}{\partial s^2} \sim i \int \frac{p^2}{q} \frac{dp}{4\pi} e^{ipx} e^{iq|y|}, \tag{B.11}$$

$$\frac{\partial^2 G^-}{\partial n^2} \sim -\int Q \frac{dp}{4\pi} e^{ipx} e^{-Q|y|}, \tag{B.12}$$

$$\frac{\partial^2 G^-}{\partial s^2} \sim \int \frac{p^2}{Q} \frac{dp}{4\pi} e^{ipx} e^{-Q|y|}. \tag{B.13}$$

We also note in addition to (2.107),(2.108), at leading order of the semiclassical approximation the values of

$$\frac{\partial G^{\pm}(\beta, \alpha)}{\partial s_{\beta}} \sim i \int \int p G^{\pm}_{p,p'} e^{ip\beta - ip'\alpha} \, dp \, dp', \tag{B.14}$$

$$\frac{\partial^2 G^+(\beta, \alpha)}{\partial n_{\beta}^2} \sim -\int \int q^2 G^+_{p,p'} e^{ip\beta - ip'\alpha} \, dp \, dp', \tag{B.15}$$

$$\frac{\partial^2 G^-(\beta, \alpha)}{\partial n_{\beta}^2} \sim \int \int Q^2 G^-_{p,p'} e^{ip\beta - ip'\alpha} \, dp \, dp', \tag{B.16}$$

$$\frac{\partial^2 G^{\pm}(\beta, \alpha)}{\partial s_{\beta}^2} \sim -\int \int p^2 G^{\pm}_{p,p'} e^{ip\beta - ip'\alpha} \, dp \, dp', \tag{B.17}$$

$$\frac{\partial^3 G^+(\beta, \alpha)}{\partial n_{\beta}^3} \sim i \int \int q^3 G^+_{p,p'} e^{ip\beta - ip'\alpha} \, dp \, dp', \tag{B.18}$$

$$\frac{\partial^3 G^-(\beta, \alpha)}{\partial n_{\beta}^3} \sim -\int \int Q^3 G^-_{p,p'} e^{ip\beta - ip'\alpha} \, dp \, dp', \tag{B.19}$$

$$\frac{\partial^3 G^+(\beta, \alpha)}{\partial s_{\beta}^2 \partial n_{\beta}} \sim i \int \int q p^2 G^+_{p,p'} e^{ip\beta - ip'\alpha} \, dp \, dp', \tag{B.20}$$

$$\frac{\partial^3 G^-(\beta, \alpha)}{\partial s_{\beta}^2 \partial n_{\beta}} \sim -\int \int Q p^2 G^-_{p,p'} e^{ip\beta - ip'\alpha} \, dp \, dp'. \tag{B.21}$$

By considering the originally assumed values for μ (2.104) and ν (2.105) the derivatives of the distribution functions are given by

$$\frac{\partial \mu}{\partial s}(\alpha) = ip \int \mu_p e^{ip\alpha} \, dp \tag{B.22}$$

$$\frac{\partial^2 \mu}{\partial s^2}\mu(\alpha) = -p^2 \int \mu_p e^{ip\alpha} \, dp \tag{B.23}$$

$$\frac{\partial \nu}{\partial s}\nu(\alpha) = ip \int \nu_p e^{ip\alpha} \, dp \tag{B.24}$$

$$\frac{\partial^2 \nu}{\partial s^2}\nu(\alpha) = -p^2 \int \nu_p e^{ip\alpha} \, dp. \tag{B.25}$$

In the clamped case it the functions $\mu(\alpha)$ and $\nu(\alpha)$ were defined solely on the boundary and as such did not deal with the dependency on the normal derivative that has now been introduced with the new boundary condition other than to suggest that they were equal to zero. Instead of accepting this, we assume an analytic continuation away from the boundary that will introduce an additional factor dependent on the distance from the boundary.

$$\mu(\alpha) = \int_{-\infty}^{\infty} e^{i(p\alpha} e^{iqn_\alpha)} \mu_p \, dp \tag{B.26}$$

$$\nu(\alpha) = \int_{-\infty}^{\infty} e^{i(p\alpha} e^{-Qn_\alpha)} \nu_p \, dp. \tag{B.27}$$

The value n_α is taken to be the same as used in (4.6) and so on the boundary the added factor will disappear to leave us with the original values. As all of the term used in this calculated are taken on the boundary, this term will only be visible in the case where the normal derivative of μ or ν is taken. The functions (B.22-B.25) are unchanged, with the normal derivatives now taken as

$$\frac{\partial\mu}{\partial n}(\alpha) = -iq \int \mu_p e^{ip\alpha} \, dp \tag{B.28}$$

$$\frac{\partial^2\mu}{\partial n^2}\mu(\alpha) = -q^2 \int \mu_p e^{ip\alpha} \, dp \tag{B.29}$$

$$\frac{\partial\nu}{\partial n}\nu(\alpha) = Q \int \nu_p e^{ip\alpha} \, dp \tag{B.30}$$

$$\frac{\partial^2\nu}{\partial n^2}\nu(\alpha) = -Q^2 \int \nu_p e^{ip\alpha} \, dp. \tag{B.31}$$

Appendix C

Calculation of Green Function Coefficients

In order to satisfy equation (5.102), the following values are chosen

$$(A - E) = \alpha H^- \tag{C.1}$$

$$B = -\alpha H^+ \tag{C.2}$$

$$C = \beta K \tag{C.3}$$

$$(D - F) = -\beta I. \tag{C.4}$$

Equations (5.99) and (5.100) can be seen to be equivalent which gives

$$(A - E)H_m^{+''}(kr') + BH_m^{-''}(kr') + CI_m''(kr') + (D - F)K_m''(kr') = 0 \tag{C.5}$$

Using the substitutions [46]

$$H^{\pm''} = -\frac{1}{r}H^{\pm'} - \left(k^2 - \frac{m^2}{r^2}\right)H^{\pm}, \tag{C.6}$$

$$K'' = -\frac{1}{r}K' + \left(k^2 + \frac{m^2}{r^2}\right)K, \tag{C.7}$$

$$I'' = -\frac{1}{r}I' + \left(k^2 + \frac{m^2}{r^2}\right)I, \tag{C.8}$$

in (5.100), this will then reduce to equation (5.99). We now introduce the values (C.1-C.4) into equation (C.5)

$$\alpha H^{+\prime} H^{-} - \alpha H^{+} H^{-\prime} + \beta I' K - \beta I K' = 0$$

$$\Rightarrow \alpha \left(H^{-} H^{+\prime} - H^{-\prime} H^{+} \right) + \beta \left(K I' - K' I \right) = 0. \qquad (C.9)$$

Noting the Wronskians

$$W(H^{+}, H^{-}) = H^{-} H^{+\prime} - H^{-\prime} H^{+} = -\frac{4i}{\pi k r'}, \qquad (C.10)$$

$$W(I, K) = K I' - K' I = -\frac{1}{k r'}, \qquad (C.11)$$

we can write

$$\alpha W(H^{-}, H^{+}) = -\beta W(K, I)$$

$$\Rightarrow \alpha = -\beta \frac{W(K, I)}{W(H^{+}, H^{-})}$$

$$\alpha = -\beta \frac{\left(-\frac{1}{kr} \right)}{\left(-\frac{4i}{\pi kr} \right)}$$

$$\alpha = -\beta \frac{\pi}{4i}. \qquad (C.12)$$

This value can now be used in (5.101). Note that

$$H^{\pm\prime\prime\prime} = -\frac{1}{r} H^{\pm\prime\prime} + \left(\frac{1}{kr^2} - \left(k^2 - \frac{m^2}{r^2} \right) \right) H^{\pm\prime} - \frac{2m^2}{r^3} H^{\pm} \quad (C.13)$$

$$K''' = -\frac{1}{r} K'' + \left(\frac{1}{kr^2} + \left(k^2 + \frac{m^2}{r^2} \right) \right) K' - \frac{2m^2}{r^3} K \qquad (C.14)$$

$$I''' = -\frac{1}{r} I'' + \left(\frac{1}{kr^2} + \left(k^2 + \frac{m^2}{r^2} \right) \right) I' - \frac{2m^2}{r^3} I \qquad (C.15)$$

gives

$$\alpha H^{-} \left[-\frac{1}{r} H^{+\prime\prime} + \left(\frac{1}{kr^2} - \left(k^2 - \frac{m^2}{r^2} \right) \right) H^{+\prime} - \frac{2m^2}{r^3} H^{+} \right]$$

$$-\alpha H^{+} \left[-\frac{1}{r} H^{-\prime\prime} + \left(\frac{1}{kr^2} - \left(k^2 - \frac{m^2}{r^2} \right) \right) H^{-\prime} - \frac{2m^2}{r^3} H^{-} \right]$$

$$+\beta K \left[-\frac{1}{r} I'' + \left(\frac{1}{kr^2} + \left(k^2 + \frac{m^2}{r^2} \right) \right) I' - \frac{2m^2}{r^3} I \right]$$

$$\beta I \left[-\frac{1}{r} K'' + \left(\frac{1}{kr^2} + \left(k^2 + \frac{m^2}{r^2} \right) \right) K' - \frac{2m^2}{r^3} K \right] = -\frac{1}{2\pi r k^2} \qquad (C.16)$$

$\Rightarrow$

$$\alpha \left[\frac{k}{r} \left(H^+ H^{-\prime\prime} - H^{+\prime\prime} H^- \right) + \left(\frac{1}{r^2} - k^3 + \frac{m^2 k}{r^2} \right) W(H^-, H^+) \right]$$
$$+ \beta \left[\frac{k}{r} \left(I K^{\prime\prime} - I^{\prime\prime} K \right) + \left(\frac{1}{r^2} + k^3 + \frac{m^2 k}{r^2} \right) W(K, I) \right] = \frac{-1}{2\pi r k^2} \tag{C.17}$$

Using the fact that $\alpha W(H^-, H^+) = -\beta W(K, I)$ we can now write

$$-\frac{1}{2\pi r k^2} = \beta W(I, K) \left[\left(\frac{1}{r^2} - k^3 + \frac{m^2 k}{r^2} \right) - \left(\frac{1}{r^2} + k^3 + \frac{m^2 k}{r^2} \right) \right]$$
$$= -2k^3 \beta W(I, K). \tag{C.18}$$

This gives us

$$\beta = -\frac{1}{4\pi k^4}, \tag{C.19}$$

$$\alpha = \frac{1}{16 i k^4}, \tag{C.20}$$

so that we can now write

$$(A - E) = \frac{1}{16 i k^4} H^-, \tag{C.21}$$

$$B = -\frac{1}{16 i k^4} H^+, \tag{C.22}$$

$$C = -\frac{1}{4\pi k^4} K, \tag{C.23}$$

$$(D - F) = \frac{1}{4\pi k^4} I. \tag{C.24}$$

Now use conditions (5.96) and (5.97) at $r = a$ to determine the values of A, D, E and F,

$$A H^+(ka) - \frac{1}{16 i} H^+(kr') H^-(ka) - \frac{1}{4\pi} K(kr') I(ka) + D K(ka) = 0 \tag{C.25}$$

$$A H^{+\prime}(ka) - \frac{1}{16 i} H^+(kr') H^{-\prime}(ka) - \frac{1}{4\pi} K(kr') I'(ka) + D K'(ka) = 0 \tag{C.26}$$

Rearrange (C.25) to give

$$D = \frac{1}{16i}\frac{H^+(kr')H^-(ka)}{K(ka)} + \frac{1}{4\pi}\frac{K(kr')I(ka)}{K(ka)} - A\frac{H^+(ka)}{K(ka)}, \qquad \text{(C.27)}$$

substitute this into (C.26) in order to extract a value for A

$$A = \frac{1}{16i}\frac{W_a(K, H^-)}{W_a(K, H^+)}H^+(kr') + \frac{1}{4\pi}\frac{W_a(K, I)}{W_a(K, H^+)}K(kr'). \qquad \text{(C.28)}$$

With $W_a(K, H^-) = W(K(ka), H^-(ka))$ and other W_a segments accordingly. Similarly for D

$$D = \frac{1}{16i}\frac{W_a(H^-, H^+)}{W_a(K, H^+)}H^+(kr') + \frac{1}{4\pi}\frac{W_a(I, H^+)}{W_a(K, H^+)}K(kr'). \qquad \text{(C.29)}$$

This means that we can obtain values for all six coefficients.

$$A = \frac{1}{16i}\frac{W_a(K, H^-)}{W_a(K, H^+)}H^+(kr') + \frac{1}{4\pi}\frac{W_a(K, I)}{W_a(K, H^+)}K(kr'), \qquad \text{(C.30)}$$

$$B = -\frac{1}{16ik^4}H^+(kr'), \qquad \text{(C.31)}$$

$$C = -\frac{1}{4\pi k^4}K(kr'), \qquad \text{(C.32)}$$

$$D = \frac{1}{16i}\frac{W_a(H^-, H^+)}{W_a(K, H^+)}H^+(kr') + \frac{1}{4\pi}\frac{W_a(I, H^+)}{W_a(K, H^+)}K(kr'), \qquad \text{(C.33)}$$

$$E = \frac{1}{16i}\frac{W_a(K, H^-)}{W_a(K, H^+)}H^+(kr') + \frac{1}{4\pi}\frac{W_a(K, I)}{W_a(K, H^+)}K(kr') - \frac{1}{16i}H^-(kr'),$$
$$\text{(C.34)}$$

$$F = \frac{1}{16i}\frac{W_a(H^-, H^+)}{W_a(K, H^+)}H^+(kr') + \frac{1}{4\pi}\frac{W_a(I, H^+)}{W_a(K, H^+)}K(kr'). \qquad \text{(C.35)}$$

We can now use these constants in the initially investigated equation in an effort to determine the diffraction coefficient of the plate with scattering from an annulus.

143

Bibliography

[1] B. Hu, B. Li and D.C. Rouben. *J. Phys. A* **32** (1999) 5419-5433

[2] T. Prosen and M. Robnik. *J. Phys. A* **26** (1993) L37-L44

[3] P.A. Boasman. *Nonlinearity* **7** (1994) 485-537

[4] B.R. Levy and J.B. Keller. *Comm. Pure and Appl. Math.*. **12**, 159 (1959)

[5] J.B. Keller, *J. Opt. Soc. Am.* **52**, (1962) 116

[6] G. Vattay, A. Wirzba and P.E. Rosenqvist, *Phys. Rev. Lett.* **73** (1994) 2304

[7] N. Pavloff and C. Schmit, *Phys. Rev. Lett.* **75** (1995) 61

[8] P. Šeba. *Phys. Rev. Lett.* **64** (1990) 1855-1858

[9] S. M. Reimann *et al*, *Phys. Rev. A* **53** (1996) 39

[10] M. Brack *et al*. *Chaos* **5** (1995) 317

[11] N. Sondergaard. *Periodic Orbit Theory Applied to Acoustics* (1996)

[12] P. Bertlesen, C. Ellegaard and E. Hughes. *Eur. Phys. J. B.* **15** (2000) 87-96

[13] K.Schaadt. *The Quantum Chaology of Acoustic Resonators* (1997)

[14] E. Vergini and G. Carlo. *J. Phys. A* **33** (2000)

[15] K. Schaadt, G. Simon and C. Ellegaard. *Physica Scripta* **90**, (2001) 231-237

[16] J. Marsden. *Applications of Global Analysis in Mathematical Physics.* (1974)

[17] E. Schrödinger, *Ann. Phys. (Leipzig)* **79** (1926) 362

[18] A. Messiah. *Quantum Mechanics, Vol. 1* North-Holland Amsterdam (1961)

[19] M.V. Berry and K. E. Mount. *Reps. Prog. Phys* **35** (1972) 315-397

[20] J. B. Keller and S. I. Rubinow, *Ann. Phys. (NY)* **9**, 24 (1960)

[21] J. B. Keller. *Ann. Phys. (N.Y.)* **4** (1958), 1451

[22] M. Berry and M. Tabor. *J. Phys. A* **10** (1977) 375

[23] R. P. Feynman and A.R. Hibbs, *Quantum Mechanics and Path Integrals.* (1965), McGraw-Hill New York

[24] M. Brack and R. Bhaduri. *Semiclassical Physics.* (1997), Addison-Wesley.

[25] M.C. Gutzwiller. *Chaos in Classical and Quantum Mechanics.* (1990), Springer-Verlag

[26] M.C. Gutzwiller. *J. Math. Phys* **8** (1967), 1979

[27] M. Berry and M. Tabor, *Proc. R. Soc. Lond* **A 349** (1976) 101

[28] E. N. Bogachek and G. A. Gogadze, *Sov. Phys/ JETP* **36**, 973 (1973)

[29] L. D. Landau and E. M. Lifshitz, *Theory of Elasticity*. (1959), Pergamon Press New York

[30] E. Bogomolny and E. Hughes. *Phys. Rev. E* **57** (1998) 5404-5424

[31] A. Leissa. *Vibration of Plates*. (1969)

[32] A. E. H. Love. *A Treatise on the mathematical theory of elasticity* (1944), Dover

[33] D. G. Vasil'ev. *Trans. Mosc. Math. Soc.* **49** (1987), 173

[34] E.B. Bogomolny, *Nonlinearity* **5** (1992) 805

[35] J. Airey. *Proc. Phys. Soc* **23** (1911) 225-232

[36] M.C.M.Wright, C.J.Howls, B.A. Welch, *Periodic orbit calculations of modecount functions for elastic plates, Proceedings of Eight International Conference on Recent Advances in Structural Dynamics, ISVR, Southampton, 14-16 July 2003*, (University of Southampton Institute of Sound and Vibration Research, Southampton, UK) ISBN 0854327894

[37] R.L. Weaver, *J. Acoust. Soc. Am.* (1989) **85** 1005.

[38] C. Ellegaard et al *Phys. Rev. Lett.* (1995) **75** 1546.

[39] O. Legrand, C. Schmit, D. Sornette, *Europhys. Lett.* (1992) **18** 101.

[40] A. Andersen, C. Ellegaard et al., *Phys. Rev. E* (2001) **63** R066204.

[41] P. Bertelsen et al *Phys. Rev. Lett* (1999) **83** 2171-2174

[42] E. Doran and U. Smilansky, *Nonlinearity* **5**, 1055 (1992)

[43] C. Rouvinez and U. Smilansky, *J. Phys. A* **28**, 77 (1995)

[44] P. Rosenqvist, N.D. Whelan and A. Wirzba, *J. Phys. A.* **29** (1996) 5441

[45] H. Bruus and N.D. Whelan, *Nonlinearity* **9** (1996) 1

[46] M. Abramowitz and I. A. Stegun. *Handbook of mathematical functions* (1964)

[47] M.V. Berry and M. Tabor. *Proc. Roy. Soc.* (1977) **356** 375

[48] O. Bohigas, M. J. Giannoni and C. Schmit *Phys. Rev. Lett.* **52** (1984), 1

[49] M.L. Mehta. *Random Matrix Theory.* (1990), New York: Springer

[50] E. Bogomolny and O. Giraud. *Nonlinearity* **15** (2002), 993-1018

[51] E. Bogomolny, U. Gerland and C. Schmidt. *Singular Statistics* (2000)

[52] T. Kottos and U. Smilansky. *J. Phys. A* **36** (2003), 3501–3524

[53] G. Berkolaiko, E. B. Bogomolny and J. P. Keating. *J. Phys. A* **34** (2001) 335-350.

[54] M.V. Berry. *Proc. Roy. Soc.* (1985) **400** 229-251

[55] T. Kottos and U. Smilansky. *Annals of Physics* **274** (1999) 76-124

[56] P. Exner and K. Nemcova *J. Phys. A* (2001) **34** 7783-7794

[57] M. Hellmund and W. Janke, *Phys. Rev. E* (2003) **67** 026118

[58] G. Berkolaiko and J. P. Keating. *J. Phys. A* **32** (1999), 7827-7841.

[59] H. Primack and U. Smilansky. *On the accuracy of the semiclassical trace formula* (1998)

[60] R. S. Langley, *J. Sound and Vibration* **135**, 499 (1989)

[61] R. S. Langley, *J. Sound and Vibration* **201**, 235 (1997)

[62] M.C. Gutzwiller. *J. Math. Phys* **12** (1971), 343

[63] C. E. Porter. *Statistical theory of spectra: Fluctuations* Academic Press New York (1965)

[64] R. Balian and C. Bloch. *Ann. Phys. (N.Y.)* **60** (1970), 401

[65] E. B. Bogomolny, U. Gerland and C. Schmit. *Phys. Rev. E* **63** (2001) 036206

[66] T. Kottos and H. Schanz. *Physica E* **9** (2001) 523-530

[67] J. M. Bosson. *Helmholtz equation and the natural frequencies of flat panel loudspeakers* (2001)

[68] M. Sieber. *J. Phys. A* **32** (1999) 7679-7689

[69] R. Colwell and H. Hardy. *Phil. Mag. S.* **24** (1937) 1041-1055

[70] P. Bertlesen. *Quantum Chaos and Vibration of Elastic Plates* (1997)

[71] N. Whelan. *Phys. Rev. Lett.* **76** (1996) 2605-2608

[72] H.J. Stockmann. *Quantum Chaos - An Introduction.* (1999), Cambridge University Press

[73] E. Bogomolny, P. Leboeuf, and C. Schmit. *Phys. Rev. Lett.* **85**, (2000) 2486

[74] N. C. Snaith and D. A. Goodings. *Phys. Rev. E* **55**, 5212 (1997)